

CELLULOSE BASED ELECTROSPUN SCAFFOLDS  
FOR TISSUE ENGINEERING APPLICATIONS

A THESIS SUBMITTED TO  
THE GRADUATE SCHOOL OF NATURAL AND APPLIED SCIENCES  
OF  
MIDDLE EAST TECHNICAL UNIVERSITY

BY

DENİZ HAZAL ATİLA

IN PARTIAL FULFILLMENT OF THE REQUIREMENTS  
FOR  
THE DEGREE OF MASTER OF SCIENCE  
IN  
ENGINEERING SCIENCES

SEPTEMBER 2014



Approval of the thesis:

**CELLULOSE-BASED ELECTROSPUN SCAFFOLDS FOR  
TISSUE ENGINEERING APPLICATIONS**

submitted by **DENİZ HAZAL ATİLA** in partial fulfillment of the requirements for  
the degree of **Master of Science In Engineering Sciences Department, Middle  
East Technical University** by,

Prof. Dr. Canan Özgen  
Dean, Graduate School of **Natural and Applied Sciences**

\_\_\_\_\_

Prof. Dr. Murat Dicleli  
Head of Department, **Engineering Sciences**

\_\_\_\_\_

Assoc. Prof. Dr. Ayşen Tezcaner  
Supervisor, **Engineering Sciences Dept., METU**

\_\_\_\_\_

Prof. Dr. Ayten Yazgan Karataş  
Co-Supervisor, **Molecular Biology and Genetics Dept., ITU**

\_\_\_\_\_

**Examining Committee Members:**

Assoc. Prof. Dr. Şükrü Talaş  
Metallurgical and Materials Dept., Afyon Kocatepe University

\_\_\_\_\_

Assoc. Prof. Dr. Ayşen Tezcaner  
Engineering Sciences Dept., METU

\_\_\_\_\_

Assoc. Prof. Dr. Dilek Keskin  
Engineering Sciences Dept., METU

\_\_\_\_\_

Assoc. Prof. Dr. Erkan Türker Baran  
Center of Excellence in Biomaterials in Tissue Eng., METU

\_\_\_\_\_

Assist. Prof. Dr. Irem Erel Göktepe  
Chemistry Dept., METU

\_\_\_\_\_

**Date:** \_\_\_\_\_

**I hereby declare that all information in this document has been obtained and presented in accordance with academic rules and ethical conduct. I also declare that, as required by these rules and conduct, I have fully cited and referenced all material and results that are not original to this work.**

Name, Last name: Deniz Hazal, Atila

Signature :

## ABSTRACT

### CELLULOSE-BASED ELECTROSPUN SCAFFOLDS FOR TISSUE ENGINEERING APPLICATIONS

Atila, Deniz Hazal

M. S., Department of Engineering Sciences

Supervisor: Assoc. Prof. Dr. Ayşen Tezcaner

Co-Supervisor: Prof. Dr. Ayten Yazgan Karataş

September 2014, 101 pages

With the use of a scaffold as support material, adequate number of cells, and bioactive molecules, tissue engineering applications intend to promote the regeneration of tissues or to replace failing or malfunctioning tissues/organs. In this study, electrospun 2D and 3D cellulose-based scaffolds were aimed to be produced with pullulan (PULL). Cellulose acetate (CA) and PULL powders in various ratios (80/20, 50/50, and 80/20) were dissolved in DMAc/DMSO solvent system and electrospun as either 2D or 3D forms. Scaffolds were modified by crosslinking or sacrificial fiber removal and characterized. When the electrospun scaffolds were crosslinked with STMP, a crosslinker for PULL, weight loss was so high and this crosslinking demolished fiber morphology. Therefore, for plant origin cellulose based scaffolds instead of crosslinking, PULL fibers were used as sacrificial fibers to increase porosity and produce 3D scaffolds.

After sacrificial fibers of PULL were removed, cell viability tests were conducted via Alamar Blue Assay using CA/PULL with 50/50 ratio having  $82.90 \pm 6.77\%$  porosity,  $14.19 \mu\text{m}$  mean fiber diameter and  $146.9 \pm 9.24 \text{ MPa}$  compressive strength by seeding human osteogenic sarcoma cell line (Saos-2) and mouse fibroblastic cell line (L929) cell line. Cell culture studies showed that electrospun scaffolds were biocompatible.

Bacterial cellulose (BC) pellicles synthesized by bacteria species *Glucanoacetobacter xylinum*, were modified in order to be electrospun with the addition of PULL or/and gelatin. Acetylation, powder size reduction by mixer milling and autoclave treatments, and sulfuric acid exposure of BC were performed. However, crystalline BC was not easily processable for electrospinning due to poor solubility in the solvent systems suitable for plant origin cellulose. FTIR-ATR showed that these modifications altered the physicochemical characteristics of BC however they could not be sufficient for complete dissolution.

**Keywords:** tissue engineering, electrospinning, cellulose, pullulan

## ÖZ

### DOKU MÜHENDİSLİĞİ UYGULAMARINA YÖNELİK ELEKTRO-EĞİRİLMİŞ SELÜLOZ TEMELLİ HÜCRE TAŞIYICILAR

Atila, Deniz Hazal

Yüksek Lisans, Mühendislik Bilimleri Bölümü

Tez Yöneticisi: Doç. Dr. Ayşen Tezcaner

Ortak Tez Yöneticisi: Prof. Dr. Ayten Yazgan Karataş

Eylül 2014, 101 sayfa

Hücre taşıyıcı destek malzemeleri yeterli sayıda hücre ve biyoaktif molekül ile birlikte doku mühendisliği uygulamaları doku rejenrasyonunu ve doku/organ kayıplarının yerine konmasını hedeflemektedir. Bu çalışmada, pullulan (PULL) ile birlikte elektro-eğirilmiş 2 ve 3 boyutlu selüloz temelli hücre taşıyıcılar üretmek amaç edinilmiştir. Çeşitli oranlarda karıştırılmış selüloz asetat (SA) ve PULL tozları (80/20, 50/50, 80/20) DMAc/DMSO çözücü sistemlerinde çözülmüştür ve 2 yada 3 boyutlu şekillerde elektro-eğirme yapılmıştır. Hücre taşıyıcılar çapraz-bağlama ve fiber geri çekme yöntemleri ile modifiye edilmiş ve karakterizasyonları yapılmıştır. Elektro-eğirilmiş taşıyıcılar PULL'un çapraz bağlayıcısı STMP ile çapraz bağlandığında kütle kaybının yüksek oranda olduğu tespit edilmiş ve çapraz bağlama işleminin fiber morfolojisini tahrip ettiği görülmüştür. Bitki kökenli selüloz ve PULL ile üretilen yapılar için PULL fiberler 3-boyut sağlamak için kullanılmış ve gözenekliliği arttırmak için geri çekilmiştir.

Çözünen PULL fiberler uzaklaştırıldıktan sonra hücre canlılık testleri Alamar Blue yöntemi ile insan osteojenik sarcoma hücre hattı (Saos-2) ve fare fibroblastik hücre hattı (L929) ekilmiş SA/PULL 50/50 oranındaki %82.90±6.77 gözenekliliğe ve 14.19 µm ortalama çap kalınlığına ve 146.9±9.24 MPa basma kuvvetine sahip taşıyıcılar için yapılmıştır. Hücre kültürü çalışmaları taşıyıcı yapıların biyoyumlu olduğunu göstermiştir.

*Glucanoacetobacter xylinum* bakteri türü tarafından sentezlenen bakteriyel selüloz (BS), PULL ve/veya gelatin ile birlikte elektro-eğirme işlemine tabi tutulabilmesi için modifiye edilmiştir. Asetilasyon, mekanik öğütücü ile toz haline getirme, otoklavlama ve sülfurik asit ile muamele etme yöntemleri uygulanmıştır ancak kristallin BS bikti kökenli selüloz için uygun çözücü sistemlerinde az çözüldüğünden elektro-eğirme için kolay işlenebilir bir malzeme değildir. FTIR-ATR modifikasyonların BS'nin fizikokimyasal karakteristiklerini değiştirdiğini göstermiştir fakat bu tamamen çözünme için yeterli olamamıştır.

**Anahtar Kelimeler:** Doku mühendisliği, elektoreğirme, selüloz, pullulan

*To all my teachers,*

## ACKNOWLEDGMENTS

I would like to thank to my advisor Assoc. Prof. Dr. Ayşen Tezcaner for her dynamic guidance and endless care throughout my studies, co-advisor Prof. Dr. Ayten Yazgan Karataş for her constant supportive attitude during my research, and Assoc. Prof. Dr. Dilek Keskin for her cooperative academic advisory. I would like to thank to my inspirational teachers: Assoc. Prof. Dr. Senih Gürses for his curious approach to Biomechanics and Assist. Prof. Dr. İrem Erel-Göktepe for her brilliant sessions on Polymer Chemistry. Special thanks to other committee members of my thesis, Assoc. Prof. Dr. Şükrü Talaş and Assoc. Prof. Dr. Erkan Türker Baran for their valuable contribution to finalize my thesis.

I wish to thank to BIOMATEN for allowing me to use their laboratory for my FTIR studies, Personnel team of the Department of Chemistry and Engineering Sciences in METU for their supports about any requirements during my analysis, and The Scientific and Technological Research Council of Turkey for the support to the study they provided (1002 Project no: TUBITAK 112T749).

I have to thank to my lab mates. They were all great. In particular, thanks to my seniors and friends: Ayşegül Kavas for her tenderness and kind share of experiences, Nur Merve Kazaroğlu for her teaching on electrospinning, Ömer Aktürk for his continuous information exchange, Özge Erdemli for all her contributions combined with both logic and craziness, Ali Deniz Dalgiç for his infinite enthusiasm for every single thing we wanted to do, Alişan Kayabölen for his late-at-night-lab-mate friendship, Aydın Tahmasebifar for his gentle support, Bengi Yılmaz for her innovative thinking and graceful sharing, Engin Pazarçeviren for his helpful presence, Hazal Aydoğdu for her evermore positive and energetic attitude, Merve Güldiken for her extra-colorful and intimate companionship, Nil Göl for her sympathetic and relaxing motivation, Sibel Ataol for her collaborative approach to any study and future projects, Reza Moonesirad for his conversational motivation all the time, Zeynep Barçın for her never-ending effort for support and care, and my other lab mates Bora Onat, Burcu Orhan, Serap Güngör, Yağmur Çalışkan, Sina Khoshsima, and Şeyma Akseki for their contributions.

I also have to thank to my roommates Buşra Çiftçi for her problem-solving attitude and everlasting smile, Ekin Varlı for her lively-lovely nature and expressiveness, Dilge Varlı for her frequent reinforcement, Yasemin Öztermur for her exclusive existence in my life and valuable assists whenever I need.

I would like also to thank to my mother Şükran Öz and my father Yüksel Oğuz Atila for their endless encouragement, freedom to hold, receive, and disseminate ideas without restriction, together with all my other great family members they were always stable sources of support, love, and compassion for me.

## TABLE OF CONTENTS

<b>ABSTRACT .....</b>	<b>v</b>
<b>ÖZ.....</b>	<b>vi</b>
<b>ACKNOWLEDGMENTS .....</b>	<b>viii</b>
<b>TABLE OF CONTENTS.....</b>	<b>ix</b>
<b>LIST OF TABLES .....</b>	<b>xiii</b>
<b>LIST OF FIGURES .....</b>	<b>xiv</b>
<b>LIST OF ABBREVIATIONS .....</b>	<b>xviii</b>
<b>CHAPTERS.....</b>	<b>1</b>
<b>1. INTRODUCTION.....</b>	<b>1</b>
1.1. Tissue Engineering .....	1
1.2. Scaffold Guided Tissue Engineering Technologies for Different Tissues.....	1
1.2.1. Bone Tissue Engineering.....	3
1.2.1.1. Bone Tissue and Its Properties .....	3
1.2.1.2. Bone Tissue Defects .....	4
1.2.1.3. Bone Tissue Engineering Approaches.....	5
1.2.2. Skin Tissue Engineering.....	6
1.2.2.1. Skin Tissue and Its Properties .....	6
1.2.2.2. Skin Tissue Defects .....	8
1.2.2.3. Skin Tissue Engineering Approaches.....	9
1.3. Scaffold Fabrication Methods .....	9

1.3.1. Electrospinning .....	10
1.4. Biomaterials for Scaffolding .....	12
1.4.1. Pullulan .....	12
1.4.2. Cellulose .....	14
1.5. Modifications of Electrospun Scaffolds .....	17
1.6. Aim of the Study.....	17
<b>2. MATERIALS &amp; METHODS .....</b>	<b>19</b>
2.1. Materials .....	19
2.2. Methods .....	19
2.2.1. Production and Purification of Bacterial Cellulose .....	19
2.2.2. Pre-treatments .....	21
2.2.2.1. Pre-treatments of Bacterial Cellulose (BC) .....	21
2.2.2.2. Pre-treatments on Pullulan (PULL) .....	23
2.2.3. Preparation of Polymer Solutions for Electrospinning.....	23
2.2.3.1. CA/PULL Solutions .....	23
2.2.2.3. BC/PULL Solutions.....	24
2.2.4. Electrospinning of Three Dimensional (3D) Scaffolds .....	24
2.2.5. Crosslinking of Scaffolds .....	27
2.2.6. Sacrificial Fiber Removal.....	29
2.2.6. Characterization of Fibrous Scaffolds .....	29
2.2.6.1. Scanning Electron Microscopy (SEM).....	29
2.2.6.2. Fourier Transform Infrared Spectroscopy - Attenuated Total Reflectance (FTIR-ATR) Analyses .....	30
2.2.6.3. Degradation Study .....	30
2.2.6.4. Mechanical Tests .....	31
2.2.6.5. Porosity Measurements.....	31

2.2.7. Cell Culture Studies.....	32
2.2.7.1. Cell Viability Assays.....	32
2.2.7.2. Cell Morphology Analyses.....	33
2.2.7.3. Cell Migration Analyses through 3D Scaffolds .....	34
<b>3. RESULTS &amp; DISCUSSIONS .....</b>	<b>35</b>
3.1. Part I: Cellulose Acetate – Based Scaffolds.....	35
3.1.1. Electrospinning of CA/PULL .....	35
3.1.1.1. Conventional Electrospinning of CA/PULL .....	35
3.1.1.2. Wet Electrospinning of CA/PULL.....	38
3.1.2. Characterization of Conventionally Electrospun CA/PULL Scaffolds.....	41
3.1.2.1. Scanning Electron Microscopy (SEM).....	41
Effect of Applied Electrical Voltage .....	41
Effect of Total Polymer Concentration.....	42
Effect of Solvent System .....	43
Effect of Collector Geometry .....	45
3.1.2.2. Degradation Analyses.....	49
3.1.3. Characterization of Wet-Electrospun CA/PULL Scaffolds .....	49
3.1.3.1. Fourier Transform Infrared Spectroscopy - Attenuated Total Reflectance (FTIR-ATR) Analyses.....	49
3.1.3.2. Scanning Electron Microscopy (SEM).....	52
Effect of CA/PULL Blend Weight Ratio.....	52
Effect of Degradation.....	56
Effect of Cross-linking.....	60
3.1.3.3. Porosity Measurements .....	63
3.1.3.4. Mechanical Testing .....	65
3.1.4. Cell Culture Studies .....	70

3.1.4.1. Cell Viability Measurements .....	70
3.1.4.2. Cell Morphology Analysis.....	73
3.1.4.3. Cell Migration Analyses through 3D Scaffolds .....	74
3.2. Part II: Bacterial Cellulose – Based Scaffolds.....	76
3.2.1. BC Production.....	76
3.2.2. Pretreatments on BC .....	76
3.2.3. Electrospinning of BC/PULL .....	78
3.2.4. Characterization of BC/PULL Scaffolds .....	81
3.2.4.1. Scanning Electron Microscopy (SEM).....	81
<b>4. CONCLUSION.....</b>	<b>83</b>
<b>REFERENCES.....</b>	<b>85</b>

## LIST OF TABLES

### TABLES

Table 1. Effects of electrospinning parameters on fiber morphology (Sill & von Recum, 2008; Pham et al., 2006). .....	11
Table 2. Solubility of CA/PULL in different solvents or combinations of them.....	36
Table 3. Mechanical properties of CA/PULL scaffolds.....	69
Table 4. Electrospinning behavior of BC/PULL (1/1 w/w %) solutions. ....	79
Table 5. Electrospinning behavior of BC/PULL/GEL polymer solutions in NMMO/DMAc/DMSO 2/1/1 (volume ratio).....	80

## LIST OF FIGURES

### FIGURES

Figure 1. Influences of the length scales on cell organization on scaffold (Li et al., 2009).....	2
Figure 2. Renewal of natural bone tissue (Coxon et al., 2004). .....	4
Figure 3. Schematic representations of different bone tissue engineering approaches; (a) osteo-conductive and –inductive scaffold implants and (b) cell seeded scaffolds cultured in vitro and implanted in vivo (Engel et al., 2008). .....	6
Figure 4. Structure of skin (Metcalf & Ferguson, 2007). .....	7
Figure 5. Scar formation after a loss in dermal layer (Spector et al., 2004). .....	9
Figure 6. Chemical structure of PULL (Mano et al., 2007). .....	13
Figure 7. Chemical structure of cellulose.....	15
Figure 8. Chemical structure of cellulose acetate. ....	16
Figure 9. <i>G. xylium</i> colonies on HS solid agar.....	20
Figure 10. <i>G. xylium</i> colonies and BC layer in HS liquid culture medium.....	20
Figure 11. Purified BC before freeze drying.....	21
Figure 12. Dried BC (a) before and (b) after sulfuric acid treatment.....	23
Figure 13. Conventional electrospinning set-up and its schematic drawing showing mesh formation with electrospinning (insert). .....	25
Figure 14. Diagrammatic illustration of modified electrospinning set-up for 3-dimensionality. ....	26
Figure 15. Wet electrospinning set-up and its schematic drawing (insert). .....	26
Figure 16. Proposed mechanism for the cross-linking reaction of PULL with STMP (Dulong et al., 2011). .....	28
Figure 17. Schematic presentation of GTA cross-linking with oxidized polysaccharides (BC or PULL) and proteins (GEL) (Asma et al., 2014). .....	29
Figure 18. 2D-electrospun CA/PULL scaffolds top (a) and crosssection (b) views..	37

Figure 19. 3D-electrospun CA/PULL scaffolds at the initial (a) and final (b) formation steps.....	37
Figure 20. 3D-electrospun CA/PULL scaffolds produced with altered collector geometry on the aluminum surface (a) and disc form obtained with a skin puncher (b).....	38
Figure 21. Electrospun CA/PULL scaffolds with 80/20 and 20/80 (w/w)% ratios before (a) & (b) and after (c) & (d) freeze-drying, respectively. ....	39
Figure 22. (a) Side view of CA/PULL 50/50 (w/w) % scaffold and (b) Top views of all CA/PULL ratio scaffolds (80/20 and 20/80 w/w %). ....	40
Figure 23. SEM images of CA/PULL (80/20 w/w%) scaffolds electrospun with (a) 12 and (b) 14 kV electrical voltage (15wt% total polymer concentration, 1 ml/hr flow rate, and 25 cm distance).....	42
Figure 24. SEM images of CA/PULL (80/20 w/w%) scaffolds electrospun with 16 kV electrical voltage, 1 ml/hr flow rate, 25 cm distance, and total polymer concentrations; (a) 15 and (b) 20 wt %.....	43
Figure 25. SEM images of CA/PULL (80/20 w/w%) scaffolds electrospun in DMAc/DMSO at v/v% ratios of; (a) 50/50 and (b) 55/45 (other parameters were set as 20 wt% total polymer concentration, 1 ml/hr flow rate, 25 cm distance, electrical voltage 15 kV).....	44
Figure 26. SEM images of electrospun CA/PULL (80/20 w/w %) scaffolds collected on (a) unmodified-flat and (b) modified-curved collectors. (Parameters: 20 wt% total polymer concentration, 1.5 ml/hr flow rate, 25 cm distance, and 15 kV voltage).....	45
Figure 27. SEM images of aligned 3D CA/PULL (80/20 w/w%) scaffolds electrospun with 20 wt% total polymer concentration, 1 ml/hr flow rate, 30 cm distance, and electrical voltage 14 kV by using set-ups with angles 90° (right) and 45° (left) of aluminum curves to the horizontal axis of the collector base. Histogram for fiber diameter distributions is given as an insert figure. ....	48
Figure 28. Cumulative weight losses of the scaffolds in PBS (0.1 M, pH 7.2) at 37°C in water bath for 1., 2., and 3. day of incubation with their standard deviations. ....	49
Figure 29. FTIR-ATR spectra of CA/PULL scaffolds a) 50/50, b) 20/80, c) 80/20, d) 50/50, cross-linked, e) 20/80, cross-linked, f) 80/20, cross-linked. *One of the	

characteristic bonds of the native PULL. **Sodium tripolyphosphate forming after the crosslinking treatment with STMP.....	50
Figure 30. FTIR-ATR spectra of CA/PULL (50/50) scaffolds (red) before and (blue) after removal of sacrificial fibers. Arrows: Characteristic peaks of PULL. ....	51
Figure 31. SEM images of CA/PULL (a) 80/20, (b) 50/50, and (c) 20/80 w/w% scaffolds electrospun with 20 wt% total polymer concentration, 8 ml/hr flow rate, 20 cm distance, and 15 kV electrical voltage.....	53
Figure 32. Fiber diameter distribution histograms of CA/PULL scaffolds; (a) 80/20, (b) 50/50, and (c) 20/80 w/w % constructed from 100 fiber measurements from SEM images.....	55
Figure 33. Cumulative percentages of weight loss of CA/PULL (50/50) scaffolds crosslinked with STMP using different reaction times (2 and 10 minutes) and PULL/STMP ratios (10:5, 10:3, 10:1). ....	57
Figure 34. SEM images of CA/PULL scaffolds (50/50) (a) before degradation, (b) after degradation without crosslinking, and (c) with crosslinking. Right hand side show high magnification images of single fibers.....	59
Figure 35. SEM images of CA/PULL 80/20 w/w% scaffolds after crosslinking with STMP (Arrows: thicker PULL fibers). ....	60
Figure 36. SEM images of CA/PULL 50/50 w/w% after crosslinking (Arrows: deformed fibers due to cross-linking). ....	61
Figure 37. SEM images of cross-section view of CA/PULL 20/80 w/w% after crosslinking (Arrows: deformed fibers due to water and cross-linker contact). ....	62
Figure 38. Histograms of pore size distributions of CA/PULL (a) 80/20, (b) 50/50, and (c) 20/80 (w/w %) scaffolds obtained by using mercury porosimeter and helium pycnometer results.....	64
Figure 39. Histograms of pore size distributions of CA/PULL (a) 80/20 and (b) 50/50 (w/w%) scaffolds after sacrificial fiber removal in PBS at 37°C. ....	65
Figure 40. Compression test diagrams of CA/PULL scaffolds illustrating stress-strain curves before and after cross-linking. ....	66
Figure 41. Tension test diagrams of CA/PULL scaffolds illustrating stress-strain curves before and after cross-linking. ....	67

Figure 42. (a) Compression and (b) Tension test diagrams of CA/PULL scaffolds illustrating stress-strain curves before and after cross-linking.....	68
Figure 43. Alamar Blue-reduction levels of CA/PULL 50/50 w/w % scaffolds with cells of (a) L929 and (b) Saos-2 for specific incubation times (n=3). .....	71
Figure 44. Cell viability levels of CA/PULL 50/50 (w/w) scaffolds with cells of L929 and Saos-2 for specific incubation times (Control groups: 100%).....	73
Figure 45. SEM images of (a) unmodified and (b) cross-linked CA/PULL 50/50 scaffolds at 1 <sup>st</sup> day after Saos-2 cell seeding. Arrows: Cells extending from one fiber to another fiber. ....	74
Figure 46. Confocal Laser Scanning Microscope images of cross-linked CA/PULL (50/50) scaffolds with Saos-2 cells 35-day after cell seeding (Arrows: Cells adhere to fibers). RED: Cell nuclei stained with PI. GREEN: Fibers of scaffold counter stained with FITC.....	75
Figure 47. DS values of acetylated BC groups treated with different amounts of acetic anhydride. ....	77
Figure 48. FTIR-ATR spectra of native BC and BC acetylated with 2 ml, 4 ml, and 6 ml acetic anhydride (*carbonyl stretching, **methyl in plane bending, and ***acetyl group stretching). ....	78
Figure 49. Electrospun BC/PULL scaffolds (a) collected in etOH bath and (b) after freeze-drying. ....	79
Figure 50. SEM images of electrospun BC/PULL (50/50 w/w %) scaffolds with (a) 10, (b) 12, and (c) 14 % of polymer concentrations. Scale bars: 10 $\mu$ m (left) and 50 $\mu$ m (right). ....	82

## LIST OF ABBREVIATIONS

<b>A</b>	Absorbance of test wells
<b>A'</b>	Absorbance of negative control well
<b>ALP</b>	Alkaline Phosphatase
<b>ANOVA</b>	Analysis of Variance
<b>ATCC</b>	American Type Culture Collection
<b>ATR</b>	Attenuated Total Reflectance
<b>BA</b>	Bacterial Cellulose
<b>BCA</b>	Bicinchoninic Acid
<b>BSA</b>	Bovine Serum Albumin
<b>CA</b>	Cellulose Acetate
<b>DMAc</b>	Dimethyl acetamide
<b>DMF</b>	Dimethyl formamide
<b>DMEM</b>	Dulbecco's Modified Eagle Medium
<b>DMSO</b>	Dimethyl Sulfoxide
<b>DS</b>	Average number of acetyl groups per anhydro-D-glucose unit of cellulose
<b>DSC</b>	Differential Scanning Calorimetry
<b>ELISA</b>	Enzyme-Linked Immunosorbent Assay
$\epsilon_{\text{red}}$	Molar extinction coefficient of AlamarBlue reduced form (Red)
$\epsilon_{\text{ox}}$	Molar extinction coefficient of AlamarBlue oxidized form (Blue)
<b>FBS</b>	Fetal Bovine Serum
<b>FITC</b>	Fluorescein Isothiocyanate
<b>FT-IR</b>	Fourier Transform Infrared
<b>GEL</b>	Gelatin
<b>GTA</b>	Glutaraldehyde
<b>HS</b>	Hestrin-Schramm (standard solid culture medium)

$\lambda_1$	570 nm
$\lambda_2$	600 nm
<b>L929</b>	Mouse Fibroblastic Cell Line
$N_B$	Normality of the base solution (NaOH)
$N_A$	Normality of the acid solution (HCL)
<b>NMMO</b>	4-Methylmorpholine <i>N</i> -oxide solution 50 wt. % in H <sub>2</sub> O
<b>UV</b>	Ultra Violet
<b>PBS</b>	Phosphate Buffered Saline
<b>PI</b>	Propidium Iodide
<b>pNPP</b>	p-Nitrophenyl Phosphate
<b>PMMA</b>	Poly(methyl methacrylate)
<b>PULL</b>	Pullulan
<b>Saos-2</b>	Human Osteogenic Sarcoma Cell Line
<b>SEM</b>	Scanning Electron Microscopy
<b>STMP</b>	Trisodium Trimetaphosphate
<b>TCPS</b>	Cells seeded on polystyrene tissue culture wells
$T_d$	Decomposition Temperature
$T_g$	Glass Transition Temperature
$T_m$	Melting Temperature
$V_{Ab}$	Volume of acid solution added to the blank (mL)
$V_{As}$	Volume of acid solution added to the sample (mL)
$V_{Bb}$	Volume of base solution added to the blank (mL)
$V_{Bs}$	Volume of base solution added to the sample (mL)
<b>W</b>	Weight of the sample (g)



# CHAPTER 1

## INTRODUCTION

### 1.1. Tissue Engineering

Tissue engineering is an interdisciplinary field that involves the use of living cells, biomaterials and/or biomolecules in a diverse array of ways to restore, maintain, or regenerate tissues and organs in the body, from skin substitutes, artificial nerves to heart tissues with varying degrees of success (Griffith & Naughton, 2002; Priya et al., 2008). It aims to develop strategies using the benefits of nanoscience, which provides (i) larger surface area for cell attachment, (ii) proper porosity for cell colonization and cell to cell interaction, and (iii) 3-dimensionality on a macroscopic scale (Horner et al., 2010; Subbiah et al., 2005; Yang et al., 2013). Various approaches have been introduced to treat diseased or injured tissues in patients; (i) implantation of freshly isolated or cultured cells; (ii) implantation of tissues assembled *in vitro* with cell seeded scaffolds; and (iii) *in situ* tissue regeneration (Griffith & Naughton, 2002).

### 1.2. Scaffold Guided Tissue Engineering Technologies for Different Tissues

Biological substitutes that restore, maintain, or improve tissue function consist of two main components, i.e. cells and their carriers, and the cell carrier is often referred to as “scaffold” (Bačáková et al., 2014). The concept of tissue engineering involves the development of a scaffold that has the appropriate physical, chemical, and mechanical properties to enable cell penetration and tissue formation in three dimensions (Karp et al., 2003). Scaffolds mimicking native ECM of tissues more precisely at nanoscale can be fabricated and it is known that cellular response

towards ECM-like architectures in scaffolds differs at different length scales (Yang et al., 2005; Li et al., 2009). These structural features have influences on cell morphology and organization in a scaffold (Figure 1). In brief, micrometer based lengths induce more 2D, i.e. planar, geometries, while cells are more spatially interactive on 3D nanoscaled meshes (Li et al., 2009).

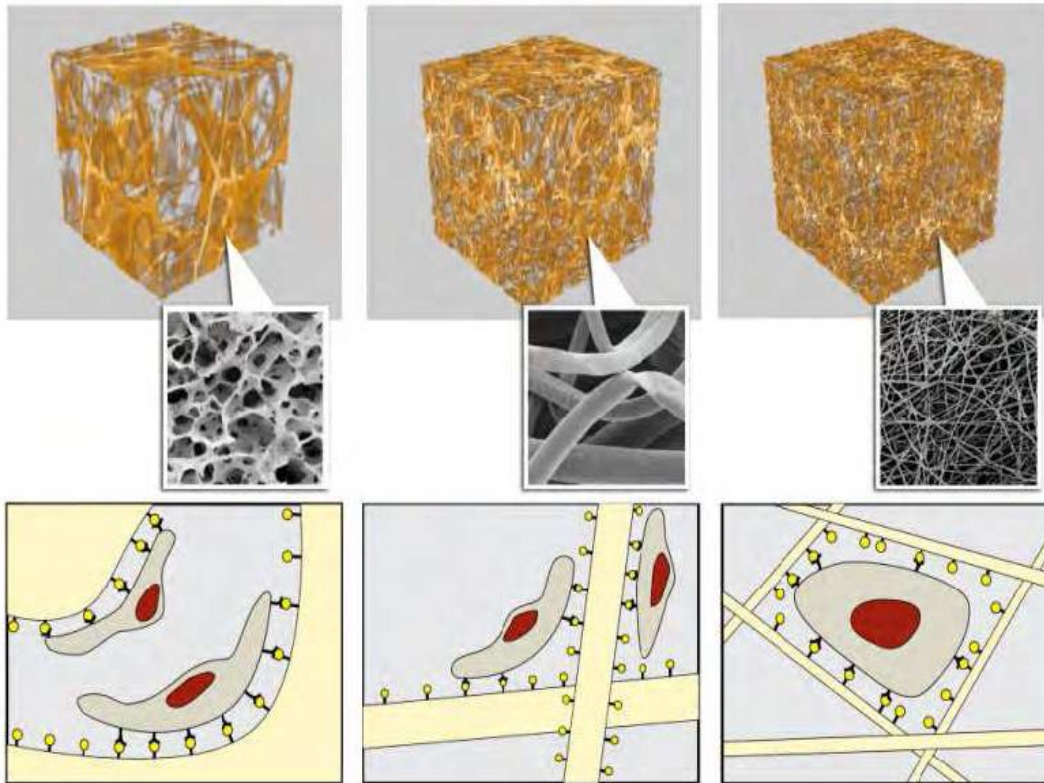


Figure 1. Influences of the length scales on cell organization on scaffold (Li et al., 2009).

A successful tissue engineering strategy includes designing a scaffold competent to support regeneration (Mano et al., 2007). Furthermore, the desired scaffold should closely imitate the natural three dimensional ECM of the engineered tissue and provide sufficient surface area for cells to adhere and proliferate that allows cell colonization (Holzwarth & Ma, 2011). In addition, the scaffold should serve as a temporary support for the regeneration of the tissue thereby the rate of scaffold degradation should match the rate of the new natural ECM formation (Mano et al., 2007; Melchels et al., 2010).

## **1.2.1. Bone Tissue Engineering**

### **1.2.1.1. Bone Tissue and Its Properties**

Bone tissue comprises most of the connective tissue in the body (Rosen et al., 2009). Bone acquires;

- (i) Structural functions such as providing support for organs, muscles, and soft tissues,
- (ii) Mechanical functions such as endurance against compressive & tensile forces and also movement of the body,
- (iii) Protective functions such as covering vital organs,
- (iv) Biological functions such as maintaining hematopoiesis i.e. formation of blood cells, and
- (v) Chemical functions such as ensuring homeostasis i.e. organizing bone cells and serving as an ion source for electrolyte balance (Aubin & Triffitt, 2002; Jang et al., 2009; Stevens, 2008).

Apart from the other connective tissues, bone matrix is mineralized matrix and it is remodeled dynamically during lifetime (Rosen et al., 2009). This process is unique for bone and achieved by well-tuned collaboration of two kinds of bone cells functioning antagonistically, namely osteoclasts destroying the bone tissue, and osteoblasts forming it (Figure 2) (Coxon et al., 2004). During bone formation, some of the osteoblasts are buried into a mineralized matrix and turns into osteocytes (Kerschnitzki et al., 2011).

Extra-cellular matrix (ECM) of bone tissue consists of organic and inorganic phases (Shekaran & García, 2011). The organic phase, also called osteoid phase, comprises 20% of the total bone ECM and is crucial for templating the architecture of the inorganic part (Palmer et al, 2008; Shekaran & García, 2011). Moreover, 90% of the organic phase is made up of type I collagen and these collagen helix structures are aligned in a regular quarter-staggered pattern (Olszta et al., 2007; Shekaran & García, 2011). This arrangement is responsible for the tensile strength of bone (Pettersson et al., 2004). Neighboring cells communicate to each other during the osteoid formation while the osteocyte network creates spaces and holes systematically in order to provide osteo-conduction through ECM (Kerschnitzki et al., 2011). On the other hand, the inorganic phase comprises 70% of the total bone

ECM and is made up of hydroxyapatite ( $\text{Ca}_{10}(\text{OH})_2(\text{PO}_4)_6$ ) crystals (Shekaran & García, 2011; Zhou & Lee, 2011). These crystals fill the spaces remained from collagen fibrils and are responsible for compressive strength of bone (Shekaran & García, 2011).

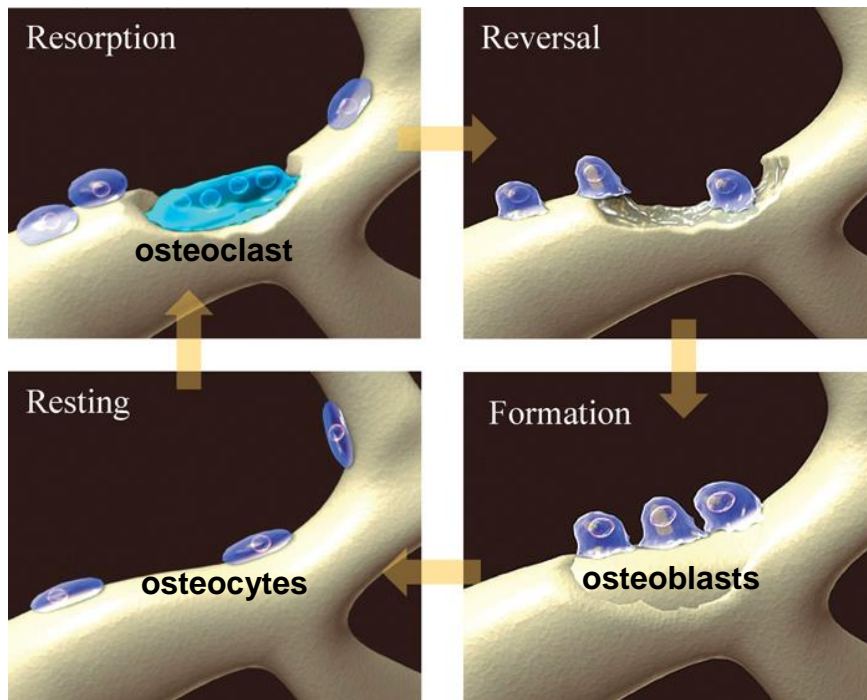


Figure 2. Renewal of natural bone tissue (Coxon et al., 2004).

### 1.2.1.2. Bone Tissue Defects

Nowadays many people need bone regeneration in some way due to bone defects emerged from trauma, tumor, or another bone related diseases and some has died because of insufficient treatments (Swetha et al., 2011; Wei & Ma, 2004). Traumatic bone defects are repaired in a natural way by complex and coordinated signals produced by different kinds of cells. Self-healing of the bone may not be achieved in some cases such as age, inadequate nourishment, injection, inflammation, preexisting diseases, drug use, anemia, smoking, etc. (Horner et al., 2010). Furthermore, factors like the location of defect site, shape of the fracture, excessive space between bone surfaces, and insufficient exposure to daily biomechanical forces influence surrounding tissue damage, preferred type and permanence of therapy (Horner et al., 2010).

There are different options for treating bone defects (Swetha et al., 2011). Although autografts and allografts are being used for treatments in some cases, limited number of donors, risk of transmitted diseases, and immune reactions are among the main drawbacks (Swetha et al., 2011; Wei & Ma, 2004). Therefore, alternative approaches are being sought by the researchers.

### **1.2.1.3. Bone Tissue Engineering Approaches**

Engineering of bone tissue with tissue engineering approach is among the most widely studied. Generally this approach aims to develop a 3D scaffold with suitable porosity, good mechanical properties, and regulatory functions that enhance tissue formation (Swetha et al., 2011). The ideal scaffold should be biodegradable and resistant to the mechanical stresses at the same time (Stevens, 2008).

Figure 3 shows the steps of development of a bioengineered scaffold; (i) porous scaffold production, (ii) untreated defect site, (iii) placed scaffold within the defect site, migration of osteoblasts through the pores, and mechanical support period of scaffold during tissue formation, and (iv) biodegradation of scaffold and formation of a new tissue (Silva et al., 2012) (Figure 3).

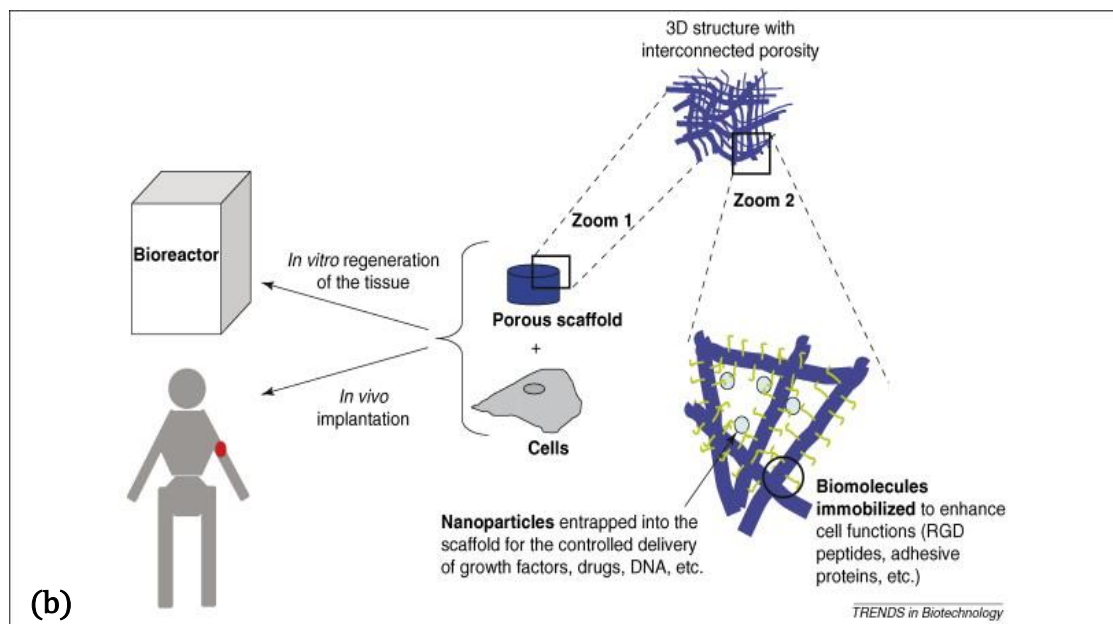
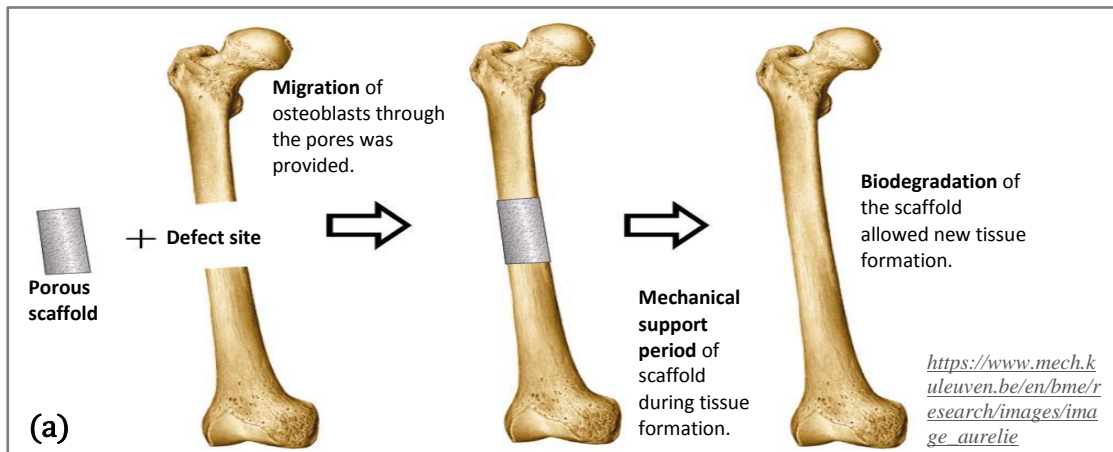


Figure 3. Schematic representations of different bone tissue engineering approaches; (a) osteo-conductive and -inductive scaffold implants and (b) cell seeded scaffolds cultured in vitro and implanted in vivo (Engel et al., 2008).

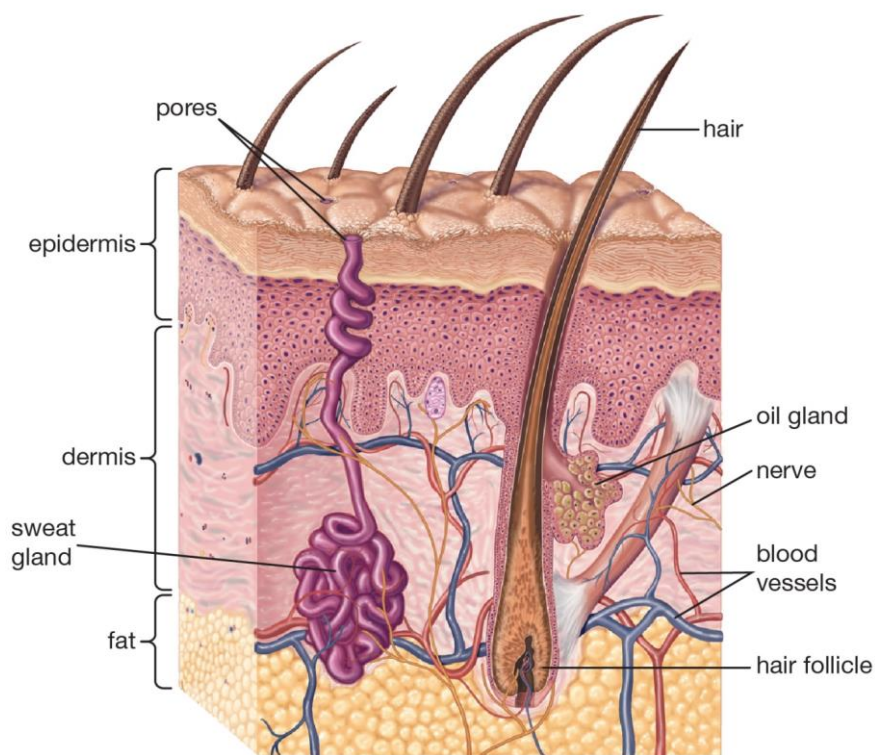
## 1.2.2. Skin Tissue Engineering

### 1.2.2.1. Skin Tissue and Its Properties

In human, skin represents approximately one-tenth of the body mass and is the largest organ in vertebrates (Metcalf & Ferguson, 2007). Skin has (i) protective roles such as guarding underlying organs and the body against the external effects, pathogens and microorganisms, (ii) chemical functions such as sensation with

various nerve endings, (iii) thermal functions such as thermoregulation with sweat glands and vasodilatation, (iv) a control of evaporation reducing loss of fluids, (v) synthesis and storage functions for lipids and water, (vi) an absorption role for oxygen, nitrogen, and carbon dioxide, and (vii) water resistance (Groeber et al., 2011; Priya et al., 2008).

The skin consists of two types of structural layers, the epidermis and dermis with a complex nerve and blood supply which protects the body from any mechanical damage such as wounding (Figure 4) (Priya et al., 2008; Metcalfe & Ferguson, 2007).



© 2013 Encyclopædia Britannica, Inc.

Figure 4. Structure of skin (Metcalfe & Ferguson, 2007).

Despite its thin and cellular structure, the stratified epidermis has sufficient thickness to provide vital barrier function (Priya et al., 2008; Metcalfe & Ferguson, 2007). Different types of cells constitute epidermal layer of the skin. Keratinocytes are the most common cell type in the epidermis and form the surface barrier layer. Melanocytes are found in the lower layer of the epidermis and provide skin color (MacNeil, 2007). Mammalian epidermis and its appendages (hair, nail, sweat, and

sebaceous glands) maintain homeostasis by constant recycling of the basal cell layer and provide a barrier to keep harmful elements out and essential body fluids in (Alonso & Fuchs, 2003; Metcalfe & Ferguson, 2007). The epidermis is also exposed to ultraviolet radiation, and the resulting damage is one of the factors contributing to the constant shedding of cells from the stratum corneum, which are replaced by migrating cells from the basal layers (Alonso & Fuchs, 2003).

An underlying thick layer of collagen-rich dermal connective tissue below the epidermis constitutes the bulk part of the skin and is composed of collagen with some elastin and glycosaminoglycans (Priya et al., 2008; Metcalfe & Ferguson, 2007). The major cell type present in the dermis is fibroblast, which is capable of producing remodeling enzymes such as proteases and collagenases, which play an important role in the wound healing process (Metcalfe & Ferguson, 2007). A third layer, the hypodermis, is located beneath the dermis and composed mainly of fat and a layer of loose connective tissue, contributing to both the mechanical and the thermoregulatory properties of the skin (Metcalfe & Ferguson, 2007). The hypodermis contains a considerable amount of adipose tissue that is well vascularized (Metcalfe & Ferguson, 2007).

#### **1.2.2.2. Skin Tissue Defects**

Large full-thickness skin defects can form due to burns, soft tissue trauma, and disease leading to skin necrosis (Böttcher-Haberzeth et al., 2010). Loss of integrity of large portions of the skin due to injury or illness may result in significant disability or even death (Priya et al., 2008). There is donor site shortage for autologous skin transplantation when the defect exceeds 60% of the total body surface area such as in massive deep burn (Loss et al., 2000). A burn wound is a dynamic process that can deepen in time, and thereby increase the total tissue damage and the risk of complications such as hypertrophic scarring (Liu et al., 2008). Most conventional skin grafting techniques used to provide autologous defect coverage are based on transplanting split-thickness skin (the today's gold standard). Split-thickness skin contains all of the epidermis but only part of the dermis, and that frequently leads to scarring (Böttcher-Haberzeth et al., 2010). Xenografts, tissues from other species, are more accessible for allografting but they do not lead to permanent revascularization (Priya et al., 2008).

### 1.2.2.3. Skin Tissue Engineering Approaches

In adult human, the dermis is a non-regenerative tissue. When injured, it does not regenerate spontaneously, but closes with contraction and scar formation (Figure 5) (Spector et al., 2004).

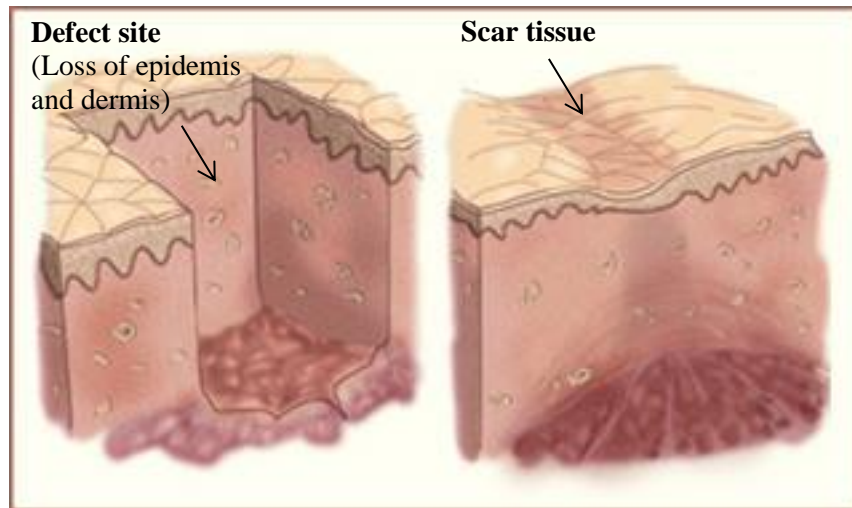


Figure 5. Scar formation after a loss in dermal layer (Spector et al., 2004).

Skin substitutes should have some essential characteristics like; (i) being easy to handle and apply to the wound site, (ii) providing vital barrier function with appropriate water flux, (iii) being readily adherent, (iv) having appropriate physical and mechanical properties, (v) undergoing controlled degradation, (vi) being sterile, non-toxic, non-antigenic, and (vii) evoking minimal inflammatory reactivity. Additionally, they should incorporate into the host with minimal scarring & pain and facilitate angiogenesis, while still being cost effective (Metcalf & Ferguson, 2007).

### 1.3. Scaffold Fabrication Methods

Methods for scaffold production include a variety of ways such as solution casting, salt leaching, freeze drying, phase separation, gas foaming, fiber bonding, melt molding, 3D printing, stereolithography, fused deposition modelling, selective laser sintering, and electrospinning (Li et al., 2009; Melchels et al., 2010; Sachlos & Czernuszka, 2003).

### 1.3.1. Electrospinning

Electrospinning is a simple, applicable, and cheap technique for manufacturing very fine fibers by using electrostatic forces; thus it has been widely preferred around the world (Subbiah et al., 2005). Furthermore, this multi-functional method allows producing fibrous meshes with smaller pores and larger surface area, making it a suitable choice for 3D engineered-structures (Blackwood et al., 2008; Canton et al., 2010; Subbiah et al., 2005). Small pore sizes increase the tendency for cell proliferation, while large pore sizes benefit the formation of ECM (Izadifar et al., 2012). According to new findings, such 3D electrospun networks support osteogenic, hematogenous, neurogenic, and chondrogenic differentiation of cells (Dawson et al., 2008).

Electrospinning is basically creating electrified jets of polymer solutions or molten polymers depending on the complex interplay of polymeric surfaces, shapes of molecules, rheology of solutions, and electrostatic charge profiles (Reneker & Yarin, 2008). During electrospinning, polymer chains under high electrical voltage entangle to each other and form stable fibers while the solvent evaporates (Bognitzki et al., 2001). Principle behind this phenomenon is based on the Coulomb repulsion between the charged ions favoring the creation of shapes such as a jet for a fixed quantity of fluid, while the surface tension of the fluid favors sphere-like shapes with smaller surface area per unit mass (Reneker & Yarin, 2008).

Despite the relative simplicity of the method, parameters concerned with set-up and experimental conditions should be well-tuned in order to realize electrospinning and reach intended fiber size and morphology (Sill & von Recum, 2008). Primary electrospinning parameters and their influences on fiber morphology are listed in Table 1. Apart from the parameters mentioned, there are also environmental conditions such as surrounding air, relative moisture, blowing, vapor pressure, and pre-existing gases affecting fiber diameter and texture (Megelski et al., 2002).

Table 1. Effects of electrospinning parameters on fiber morphology (Sill & von Recum, 2008; Pham et al., 2006).

Parameter	Effect on fiber diameter and structure
Viscosity/concentration	<ul style="list-style-type: none"> <li>✓ Low concentrations/viscosities yield defects in the form of beads and junctions; increasing concentration/viscosity reduces these defects.</li> <li>✓ Fiber diameters increase with increasing concentration/viscosity (not monotonic).</li> </ul>
Conductivity/solution charge density	<ul style="list-style-type: none"> <li>✓ Increasing the conductivity aids in the production of uniform bead-free fibers.</li> <li>✓ Higher conductivities in general yield smaller fibers (except PAA and polyamide-6)</li> </ul>
Surface tension	<ul style="list-style-type: none"> <li>✓ No conclusive link is established between surface tension and fiber morphology.</li> </ul>
Polymer molecular weight	<ul style="list-style-type: none"> <li>✓ Increasing molecular weight reduces the number of beads and droplets.</li> </ul>
Dipole moment and dielectric constant	<ul style="list-style-type: none"> <li>✓ Successful spinning occurs in solvents with a high dielectric constant.</li> </ul>
Solvent volatility	<ul style="list-style-type: none"> <li>✓ High volatility cause pore formation on fibers, leading to increased surface area.</li> </ul>
Flow rate	<ul style="list-style-type: none"> <li>✓ Lower flow rates yield fibers with smaller diameters.</li> <li>✓ High flow rates produce fibers that do not dry upon reaching the collector.</li> </ul>
Field strength/voltage	<ul style="list-style-type: none"> <li>✓ Beading occurs at too high voltage.</li> <li>✓ Correlation between voltage and fiber diameter is ambiguous.</li> </ul>
Distance between tip and collector	<ul style="list-style-type: none"> <li>✓ A minimum distance is required to obtain dried fibers.</li> <li>✓ At distances either too close or too far, beading is observed.</li> </ul>
Needle tip design	<ul style="list-style-type: none"> <li>✓ Using a coaxial, 2-capillary spinneret, hollow fibers are produced.</li> <li>✓ Multiple needle tips are employed to increase output.</li> </ul>
Collector composition and geometry	<ul style="list-style-type: none"> <li>✓ Smoother fibers are formed on metal collectors; more porous fiber structure was obtained using porous collectors.</li> <li>✓ Aligned fibers are obtained using a conductive frame, rotating drum, or a wheel-like bobbin collector.</li> <li>✓ Yarns and braided fibers.</li> </ul>
Ambient parameters	<ul style="list-style-type: none"> <li>✓ Increased temperature decreases solution viscosity, resulting in smaller fibers.</li> <li>✓ Increasing humidity causes circular pore formation on the fibers.</li> </ul>

A successful experimental electrospinning process acquires three properties of solvent system;

- (i) Semi-conductivity with an average charge capacity within an optimum range,
- (ii) High volatility of solvent for ensuring fast solidification of polymeric fibers, and
- (iii) Sufficient solubility that prevents the inter- and intra-molecular interactions among polymer chains (Ohkawa et al., 2009).

#### **1.4. Biomaterials for Scaffolding**

Success in tissue engineering studies highly depends on properties of materials used as well as parameters of the method chosen (Sill & von Recum, 2008). Materials used in bone tissue engineering, for example, require high resistance to mechanical stress and biodegradability (Stevens, 2008). Moreover, biocompatibility is another requirement which is closely related with the surface chemistry of material used, bulk material properties, and also degradation products (Dammachke et al., 2005; Höglund et al., 2012; Subbiah et al., 2005). Polymers can be classified into two groups: synthetic and natural. They offer a variety of options for reaching desired biological and mechanical properties and mimicking natural ECM (Lee & Atala, 2013). For instance, synthetic polymers such as poly L-lactic acids, poly L-lactic-co-D-lactic acids, poly L-lactic-co-glycolic acids are considered to have good mechanical properties whereas their biodegradability level is low during tissue regeneration (Cooper et al., 2011; Hutmacher, 2000). On the other hand, natural polymers namely alginate, silk fibroin, collagen etc. satisfy biodegradability and biocompatibility criteria, while they may not compensate the required mechanical requirements (Bhardwaj & Kundu, 2011; Sakai et al., 2013).

##### **1.4.1. Pullulan**

Pullulan (PULL), a natural polysaccharide, is synthesized by an omnivorous yeast *Aureobasidium pullulans* that attaches to woody surfaces (Figure 6) (Leathers, 2003; Mishra et al., 2011; Singh et al., 2008). Hence, it holds the promise due to its capability of forming coherent structures with the cellulose-based polymers. In

addition, PULL is being used as an adhesive for wound dressing applications and as tooth coverage material world wide (Leathers, 2003).

Polysaccharides are divided into three groups in terms of their electrospinning behaviors; (i) being capable of forming jet and fiber, (ii) forming jet but not fiber, and (iii) forming neither jet nor fiber (Stijnman et al., 2011). PULL is in the first class of polysaccharides with respect to recent findings besides its other favorable properties for tissue engineering applications, namely, non-toxicity, non-immunogenicity, non-carcinogenicity, and non-mutagenicity (Mishra et al., 2011; Stijnman et al., 2011).

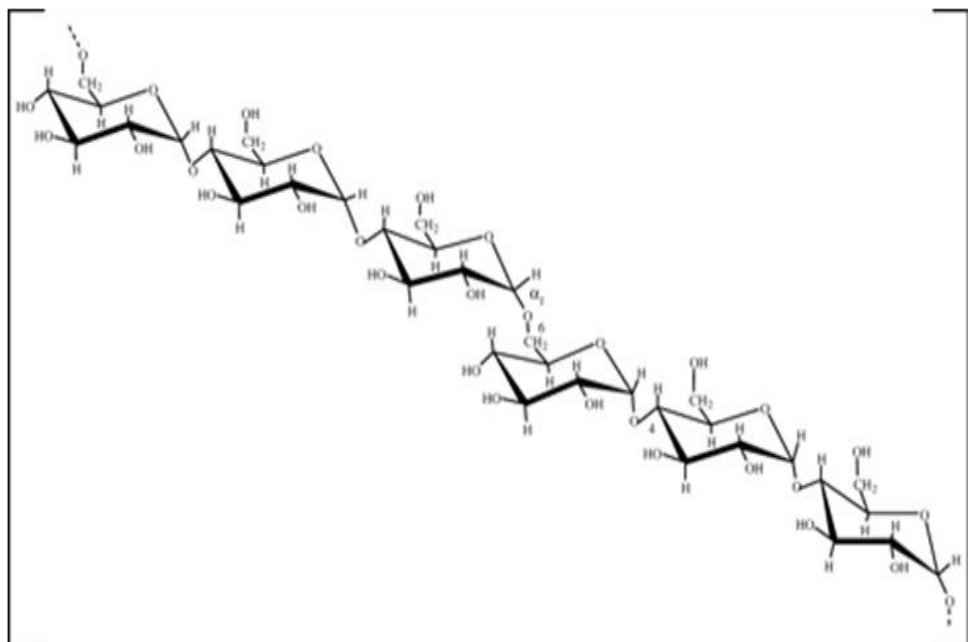


Figure 6. Chemical structure of PULL (Mano et al., 2007).

Osteogenic differentiation of human adipose derived stem cells *in vitro* has been reported for PULL-based scaffolds (Lalande et al., 2011). Furthermore, nano-hydroxyapatite loaded PULL scaffolds were shown to induce bone formation *in vivo* (Fricain et al., 2013; Lalande et al., 2011). Ideally, scaffolds should be degradable for new tissue formation and osteo-conduction; otherwise, nondegradable scaffolds allow tissue formation only on the surface of the scaffold (Burg et al., 2000; Chan & Mooney, 2008). In literature, the biodegradability index of PULL is stated as 0.7,

which is quite high value compared to other similar polysaccharides (i.e., index for dextran is 0.05) (Rekha & Sharma, 2007).

With regard to skin tissue engineering, PULL has been considered as a promising biomaterial for dermal hydrogel fabrication owing to its water retention capabilities. This polymer is ideal for hydrogel-based delivery of both cells and biomolecules, and its multiple functional groups permit crosslinking (Wong et al., 2011). Various concentrations of PULL and combinations of it with versatile biomaterials can be used and adjusted according to requirement of desired end product.

#### **1.4.2. Cellulose**

Cellulose, a linear glucosic homopolymer, is represented as  $(C_6H_{12}O_6)_n$ , where n number varies between 500 and 5000 in different derivatives of cellulosic materials in nature (Figure 4) (Müller et al., 2006). Enzymatically degraded cellulose has different solubility properties in water according to its n number (Mårtson et al., 1999; Müller et al., 2006). Cellulose and its derivatives exhibit osteogenic features that make them ideal for bone tissue engineering applications and have been used in a range of tissue engineering studies (Ekholm et al., 2005; Fang et al., 2009). Although inter- and intra-molecular hydrogen bonds among hydroxyl groups within glucose units (Figure 7) give excellent mechanical properties to cellulose, i.e. modulus of the cellulose microcrystal >130 GPa, however this property also limits their application range (Murakami et al., 2007; Malmström & Carlmark, 2012). For instance, stiffness arising from hydrogen bonds among polymer chains represses the solubility of cellulose in water and most of common organic solvents (Murakami et al., 2007).

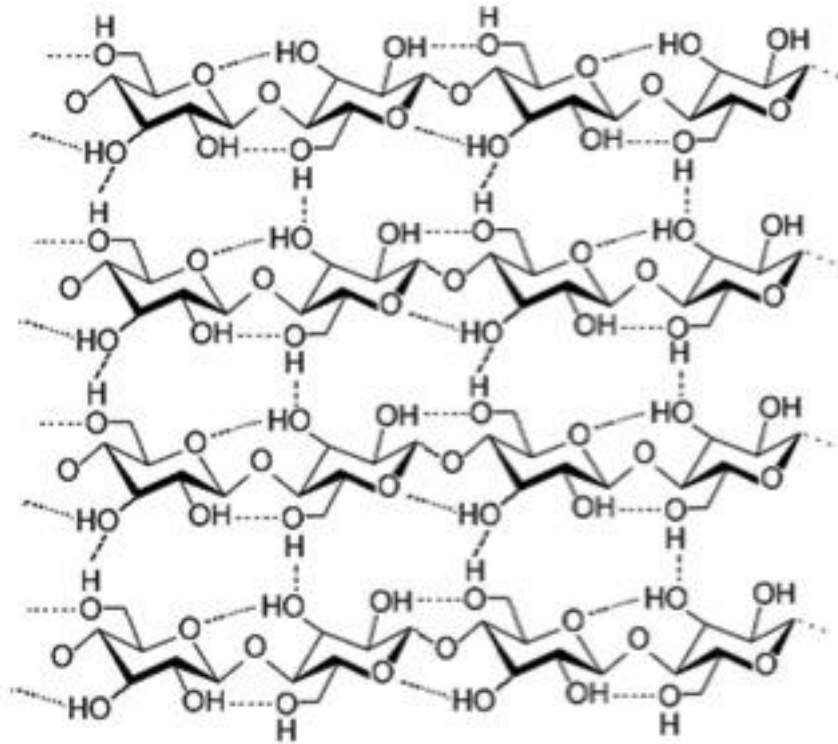


Figure 7. Chemical structure of cellulose.

To overcome these processability problems of cellulose, various chemical modifications such as phosphorylation and acetylation are being used (Oshima et al., 2011). Among these methods, optimum level of acetylation of cellulose is a suitable technique for the removal of the crystalline regions and moving polymeric chains apart from each other (Figure 8) (Jonoobi et al., 2009). Additionally, polymer blends, grafts, and derivatives of cellulose are used for enhancing the mechanical properties as well as processability (Ikada & Tsuji, 2000).

Cellulose may be extracted from plants cell walls or obtained by growing bacteria colonies synthesizing it naturally (Fatimi et al., 2008; Svensson et al., 2005). *Acetobacter xylinum* bacteria produce bacterial cellulose (BC) which has quite higher fracture strength and Young's modulus than processed BC' with its amorphous regions (Mano et al., 2007; Svensson et al., 2005). Furthermore, BC after acetylation has been found to have similar mechanical strength as the natural bone tissue matrix. This modification made cellulose electrospinnable (Liu et al., 2011; Zhou & Lee, 2011). Moreover, BS based scaffold satisfies other criteria of tissue engineered scaffolds, namely sufficient porosity to support cell growth, sustained mechanical

resistance, 3D network structure in micro- and nano-scale, high water retention capacity, and biocompatibility (Wan et al., 2007).

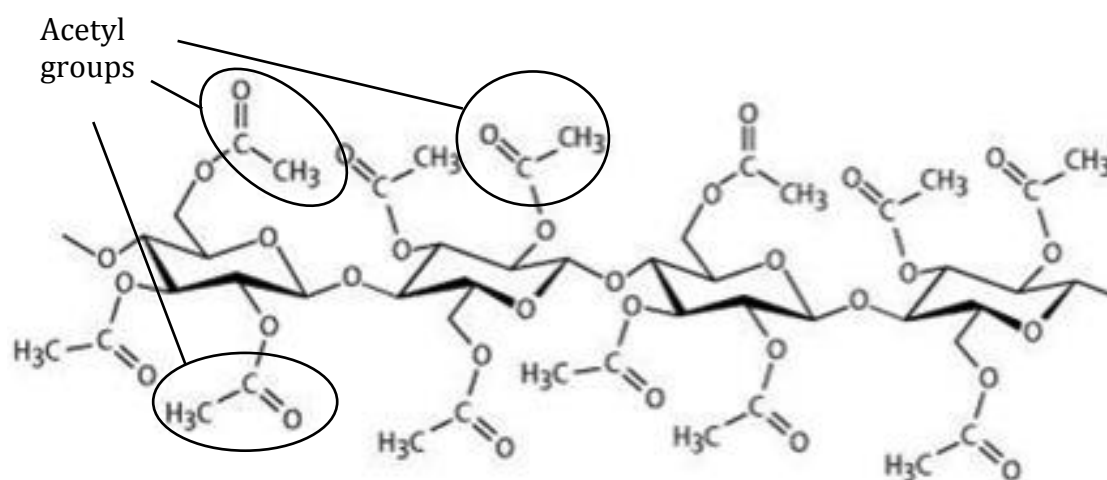


Figure 8. Chemical structure of cellulose acetate.

Another criterion that should be considered is the degradation products (Chen, 2009). BC and its degradation products are found as non-toxic and it has been shown that they enhance cell proliferation (Helenius et al., 2006; Chen, 2009). In addition, it was reported that BC-based scaffolds when implanted did not cause any chronic inflammation and integrated with the host tissue (Chan & Mooney, 2008). Moreover, BC is more likely to be preferred than polymers with animal origins since it does not cause any infections (Wan et al., 2007).

Owing to its economic advantages, due to easy production & accessibility, and safe work conditions, BC has been preferred by many researchers in the recent years (Jhon & Thomas, 2008). Moreover, electrospun cellulose structures were reported as suitable for wound repair applications (Miao et al., 2011). Water retention capability of electrospun porous CA membranes showed ten times higher performance per unit fiber mass than commercial CA fibers having similar degrees of wettability (Callegari et al., 2011). Cellulosic fibers have been used for bandages since they neither dissolve nor become gel when they are in contact with the liquid environments (Miao et al., 2011).

Cellulose has been used for bone tissue engineering applications. Viscous sponge-like cellulose structures were reported to be ideal carriers for bone

regeneration (Burg et al., 2000). In addition, starch containing constructs when combined with cellulose nano and microfibers have supported and oriented cells with its own architecture as well as inducing cell matrix deposition and organization (Tuzlakoglu et al., 2005). Moreover, these scaffolds when implanted in distal femurs proximal to the epiphyseal plate were induced new bone formation in rats without any inflammatory reactions (Salgado et al., 2006). Furthermore, it has been observed that bone formation was predominantly on cellulose sponges enhancing osteoconduction (Burg et al., 2000). In another study, CA scaffolds reinforced with nano-hydroxyapatite crystals promoted proliferation of SaOS-2 cells *in vitro* (Gouma et al., 2012). Apart for bone tissue engineering applications cellulose films were also applied for periodontal tissue regeneration (Rambo et al., 2008).

Cellulose and its derivatives can also be considered as an ideal scaffold material for skin tissue engineering applications. Non-porous cellulose membranes are used as stent coatings, for dura-mater substitution in tumor or trauma cases or as skin protection in cases of burn and deep wounds, pointing out its compatibility with skin tissue (Rambo et al., 2008).

To sum up, cellulose and its derivatives can be considered as favorable material for soft and hard tissue engineering applications by its tunable properties (Wan et al., 2006).

### **1.5. Modifications of Electrospun Scaffolds**

Polymeric scaffolds are cross-linked to modify their mechanical, thermal, chemical, and degradation properties (Costa-Júnior et al., 2009). On the other hand, scaffolds can be intentionally produced using mixture of different types of materials, which differ in solubility. The fibrous scaffolds can be modified by selective removal of sacrificial fibers after being electrospun. This method is used for increasing porosity and accelerating cell infiltration (Baker et al., 2008).

### **1.6. Aim of the Study**

In this study, we aimed to develop cellulose (of plant or bacterial origins) and PULL based scaffolds in the form of electrospun sheets in 2D and 3D architectural constructs with adjustable thickness via electrospinning technique and characterize

for skin and bone tissue engineering applications. The main purpose was to satisfy mechanical needs of the tissue by using cellulosic materials (BC or CA) while acquiring adequate biodegradability by using PULL and/or GEL. Crosslinking of PULL portion of the scaffolds were aimed to increase mechanical strength and decrease biodegradability of the scaffolds. On the other hand, PULL was used as sacrificial fibers for obtaining 3-dimensional electrospun porous scaffolds of CA with an increased porosity. For BC based scaffolds, gelatin (GEL), an electrospinnable and osteo-conductive-inductive protein, was included to crosslink PULL in the preparation of electrospun scaffolds.

## CHAPTER 2

### MATERIALS & METHODS

#### 2.1. Materials

Commercial cellulose acetate (CA; Mw 30 kDa) was purchased from Aldrich (Missouri, U.S.A.). Pullulan (PULL, Mw, 200 kDa), a product of Hayashibara Inc. (Okayama, Japan) was kindly provided by Kale Kimya Group the distributor of Turkey. Electrospinning solvents *N,N*-Dimethyl acetamide (DMAc), Dimethyl sulfoxide (DMSO) puriss. p.a.,  $\geq 99.5\%$  (GC), and 4-Methylmorpholine *N*-oxide solution 50 wt% in H<sub>2</sub>O (NMMO) were purchased from Sigma-Aldrich (Missouri, U.S.A.). Cellulose producing bacterial strain *Glucanoacetobacter xylinum* was commercially obtained from the American Type Culture Collection (ATCC 10245, U.K.). All other chemicals were purchased from Sigma and Merck (New Jersey, U.S.A.).

#### 2.2. Methods

##### 2.2.1. Production and Purification of Bacterial Cellulose

*G. xylinum* bacteria colonies were seeded into Hestrin-Schramm (HS) standard solid culture medium containing 1.5 % agar, 1% glucose, 0.5% peptone, 0.5% yeast extract, 0.27% disodium phosphate, and 0.127% citric acid, at pH 6 and incubated at 30°C for 48-72 hours (Figure 9). Then, the colonies were transferred to HS liquid medium containing 1% glucose, 0.5 % peptone, 0.5 % yeast extract, 0.27

% disodium phosphate, and 0.127 % citric acid, and incubated for 7 days in erlenmeyer flask in dark (Figure 10).



Figure 9. *G. xylium* colonies on HS solid agar.



Figure 10. *G. xylium* colonies and BC layer in HS liquid culture medium.

BC pellicles were washed with distilled and were incubated in 1% NaOH at 90°C for 15 minutes to kill the bacteria. After washing with water and cooling down, BC sheets were awaited in acetic acid (1%) for 15 minutes. Before filtering, BC layers were washed with distilled water for several times to ensure that the acid was completely removed (Figure 11). After purification, BC sheets were freeze dried at -48°C for 48 hours.



Figure 11. Purified BC before freeze drying.

## **2.2.2. Pre-treatments**

### **2.2.2.1. Pre-treatments of Bacterial Cellulose (BC)**

Prior to electrospinning, BC needs further modification because of its crystalline regions in the polymeric chains. This structure renders BC highly resistant to dissolution by preventing necessary chemical interactions such as solvent-polymer interactions. Therefore, several treatments, namely acetylation, powder size reduction by mixer milling and autoclave treatments, and sulfuric acid exposure of BC were performed.

First, acetylation of BC was attempted and degree of acetylation was determined with a back titration method (Kim et al., 2002; Samios et al., 1997). In acetylation procedure, BC pellicles were placed in a glass bottle containing a mixture of acetic acid, toluene, and 60% perchloric acid having the ratios; 200:250:1. Next, the mixture was shaken vigorously for about 1 min. Then, acetic anhydride was added at 1/10, 2/10, 3/10, 4/10, and 5/10 partitions with acetic acid, and the mixtures were shaken vigorously for about 1 min. The mixtures were allowed to stand for 1 h at room temperature. The BC sample pieces were squeezed and washed thoroughly with methanol and water sequentially. For the final product, a back titration procedure was applied and degree of acetylation was calculated as described below. In addition, FTIR-ATR analysis was conducted on verification of acetylation (Hu et al., 2011; Freger et al., 2005).

$$\% \text{ acetylation} = [(V_{Bs} - V_{Bb})xN_b - (V_{As} - V_{Ab})N_a]x4.3/W$$

$$n = \frac{3.86 \times \% \text{ acetylation}}{102.4 - \% \text{ acetylation}}$$

$N_B$ ; Normality of the base solution (NaOH),

$V_{Bs}$ ; Volume of base solution added to the sample (mL),

$V_{Bb}$ ; Volume of base solution added to the blank (mL),

$N_A$ ; Normality of the acid solution (HCL),

$V_{As}$ ; Volume of acid solution added to the sample (mL),

$V_{Ab}$ ; Volume of acid solution added to the blank (mL),

$W$ ; Weight of the sample (g),

4.3; A factor to calculate the % acetyl groups and,

$n = DS$ ; Average number of acetyl groups per anhydro-D-glucose unit of cellulose.

As another way to improve processability of BC, pellicles were autoclaved, washed several times, and freeze dried via Freeze Dryer (Labconco, Kansas City, USA) for extra purification and softening. Then, mixer mills (Retsch MM200, Haan, Germany) were used for powdering dry BC. Next, sulfuric acid treatment was carried out with 65, 50, and 40 wt% sulfuric acid solutions by stirring for 6, 12, 24, 48, 72, and 120 hours at room temperature. All treatments were finalized with washing and filtering cycles. For batches with more exposure-time and higher acid percentages, centrifugation at 6000 rpm for 15 min for several times (Sigma 3-30 K centrifuge, Germany) was used for removal of acidic residues. Finally, treated BC was freeze dried and powdered again via mixer mill (Figure 12) (Chen et al., 2008; Martínez-Sanz et al., 2010; Park et al., 2007).



Figure 12. Dried BC (a) before and (b) after sulfuric acid treatment.

#### **2.2.2.2. Pre-treatments on Pullulan (PULL)**

To prevent the fast loss of PULL due to its high water solubility, gelatin was added to the composition of BC based scaffolds. Sodium periodate oxidation of PULL was carried out to form aldehyde groups on PULL chains which eventually can be cross-linked with gelatin by using a cross-linker, gluteraldehyde. In this reaction it is assumed that the periodate ion attacks one of the hydroxyl groups of the vicinal C2–C3 diol of the anhydroglucose unit, breaking the C–C bond and forming aldehyde groups (Gómez-Mascaraque et al., 2014).

PULL (1 g) was dissolved in 8 ml distilled water (total volume). The solution was placed in a light protected glass vessel and 0.125 mL of sodium iodate (10 mg/mL) was added per mL of PULL solution. After incubating at room temperature for 30 min under slow magnetic stirring, glycerin (0.1 mL/mL solution) was added and stirred for additional 10 min. The solution was transferred into a dialysis tube and dialyzed against distilled water for 2 days with several daily changes. The oxidized PULL solution was stored at 4°C in a light protected glass vessel until being freeze-dried for further use (Hermanson, 1997; Balmayor et al, 2012).

#### **2.2.3. Preparation of Polymer Solutions for Electrospinning**

##### **2.2.3.1. CA/PULL Solutions**

During optimization studies, various solvents including distilled water, acetone, acetonitrile, acetic acid, dimethyl formamide (DMF), 1,1,1,3,3,3-

hexafluoro-2-propanol, dimethyl acetamide (DMAc), and dimethyl sulfoxide (DMSO) were tested in several combinations. For finding the best solvent system for electrospinning DMAc/DMSO was selected as the solvent system. Different DMAc/DMSO ratios ranging from 90/10 to 40/60 (v/v) and different polymer concentrations were used during optimization studies. Eventually, the ratio of DMAc/DMSO was set to 55/45 (v/v) and 20 wt% polymer concentration was chosen as the polymer concentration for 80/20, 50/50, and 20/80 (w/w)% CA/PULL during electrospinning.

### **2.2.2.3. BC/PULL Solutions**

Due to presence of crystalline regions in BC electrospinnability BC/PULL solutions was difficult to prepare. Different ratios of BC/PULL solutions were prepared for electrospinning. When high percentage of PULL (highly electrospinnable) was used, collapse of the scaffolds in aqueous media even after cross-linking with STMP occurred. Therefore, gelatin (GEL) was added to the polymer composition oxidized-BC/oxidized-PULL/GEL at different ratios were used as polymer composition.

The solvents for dissolving both gelatin (GEL) and oxidized PULL (ox-PULL) were chosen as dimethyl acetamide (DMAc), dimethyl sulfoxide (DMSO), and 4-Methylmorpholine *N*-oxide solution 50 wt% in H<sub>2</sub>O (NMMO). Apart from ox-PULL and GEL, solubility of ox-BC was not considered during making a choice for the solvent because ox-BC powders were found as suspension.

First, 5-10% ox-PULL/GEL 50/50 (w/w) solutions in NMMO/DMAc/DMSO (2:1:1, volume ratio) were used for optimization of electrospinning parameters (electrical voltage, flow rate, and distance into ethanol bath). Then, the solutions of ox-BC/ox-PULL/GEL (1/10/10, volume ratios) at different polymer concentrations (5-10%) in NMMO/DMAc/DMSO (2:1:1, volume ratio) were electrospun using different electrical voltages, flow rates, and distances to ethanol bath.

### **2.2.4. Electrospinning of Three Dimensional (3D) Scaffolds**

The experimental set-up for wet and conventional electrospinning experiments consisted of NE-1000 syringe pump (New Era Pump Systems, Inc., New York, USA), Gamma High Voltage Source ES30 (Gamma High Voltage

Research, Inc., Florida, USA), static metal collector, rotational collector stand (Gözeler Elektronik, Ankara, Turkey), and plexiglass cabinet (Kesit Pleksi, Ankara, Turkey) made up of PMMA.

During conventional electrospinning, the system was set up at horizontal axis so that jet formation was influenced by the gravitational forces equally along its way. Aluminium plate was placed on the surface of the static metal collector, and then all components of the system were positioned in the cabinet according to the specified configuration, distance, and angle (Figure 13). Finally, the solution loaded to the syringe pump was electrospun at adjusted flow rates and electrical voltages supplied, by the connected power supply for manufacturing the fibrous meshes. After careful removal of the collected scaffolds from ethanol bath and freeze drying, they were characterized.

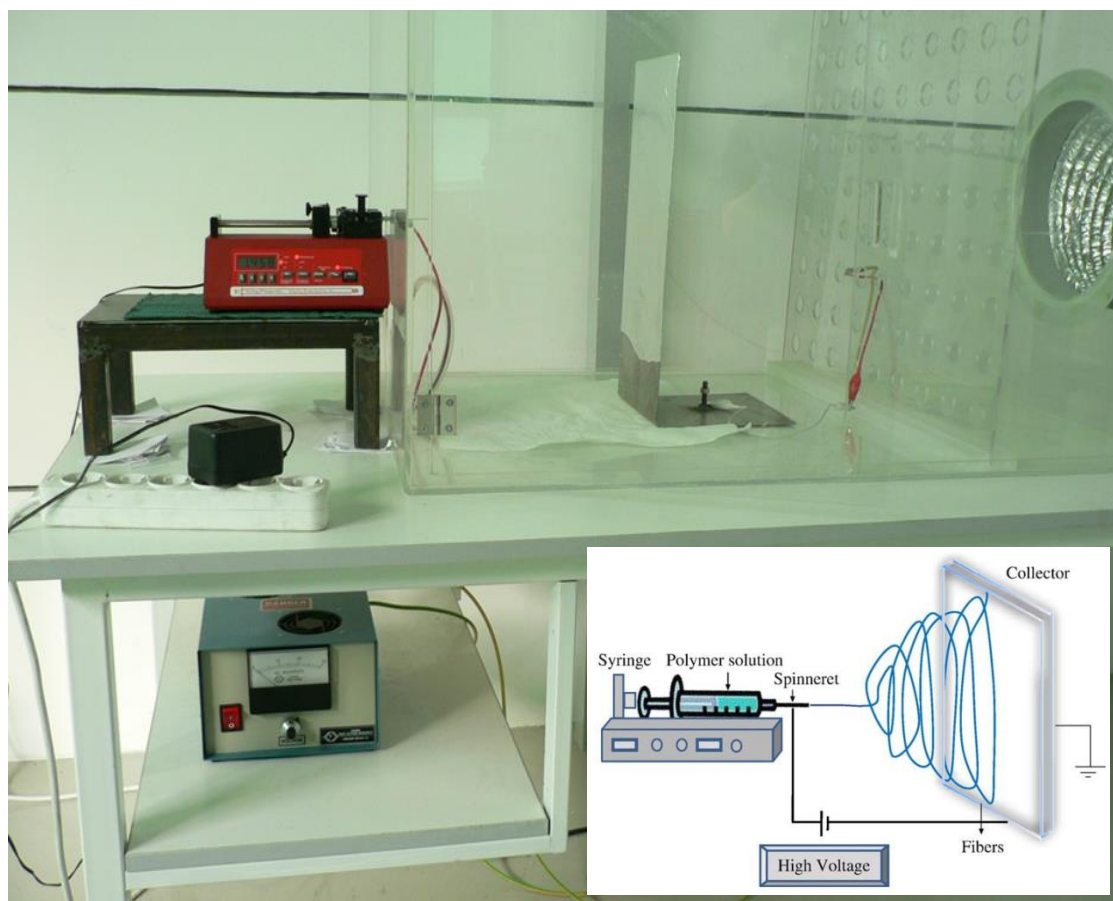


Figure 13. Conventional electrospinning set-up and its schematic drawing showing mesh formation with electrospinning (insert).

During conventional electrospinning studies, the geometry and configuration of the aluminum collector surface was altered and 3D-scaffold production was achieved to some extent. Schematic illustration of one of the various collector modifications was placed in Figure 14 to give an idea.

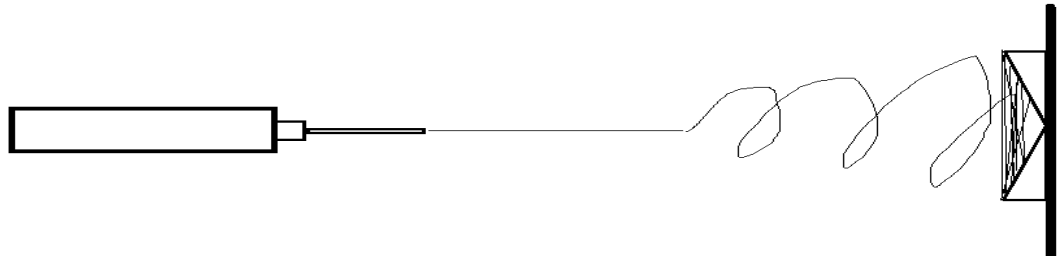


Figure 14. Diagrammatic illustration of modified electrospinning set-up for 3-dimensionality.

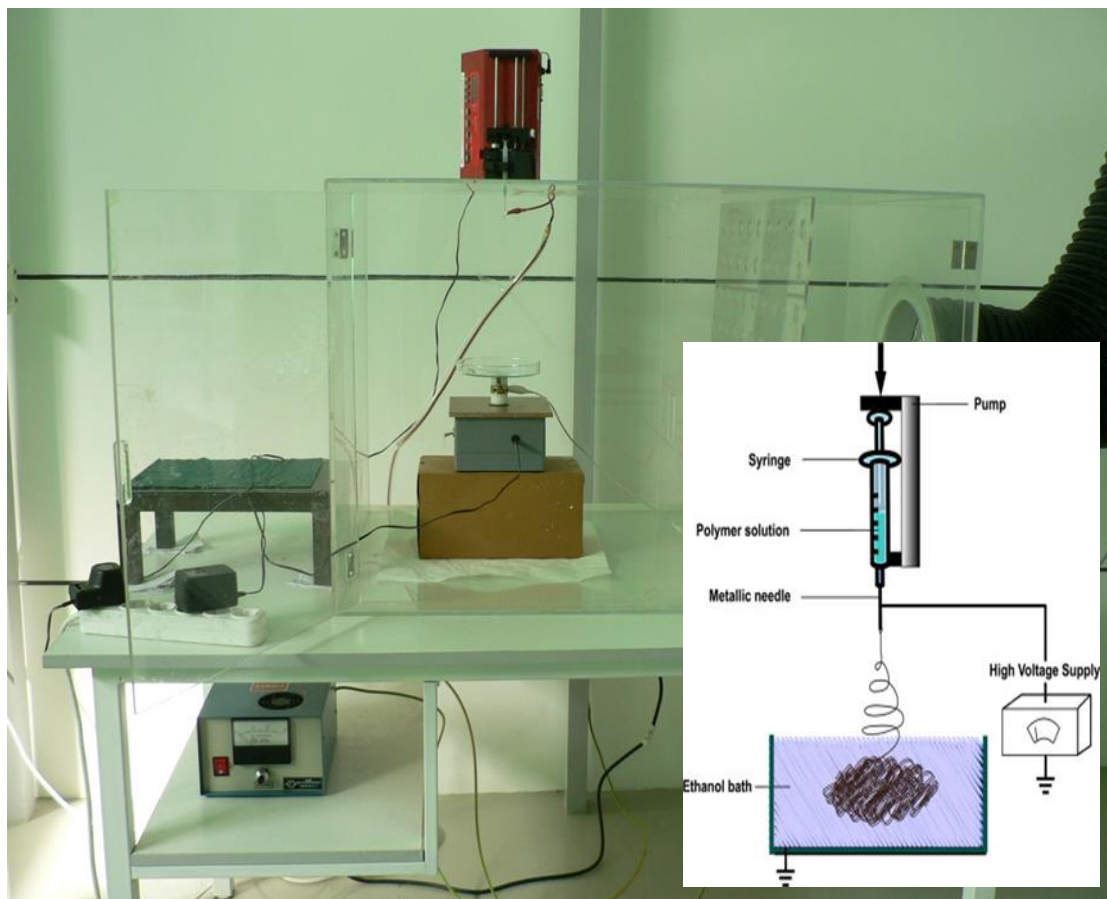


Figure 15. Wet electrospinning set-up and its schematic drawing (insert).

Due to ease of the removal of the electrospun material from the collector filled with liquid and obtaining thicker homogenous scaffolds wet electrospinning was started to be used instead of conventional state electrospinning (Yang et al., 2013). During wet electrospinning, the set-up was converted to vertical position and jet formation was enhanced by the gravitational forces along its way. The rotational collector stand was placed at the bottom of the cabinet. Solution jet was collected in a petri dish filled with absolute ethanol (100%) placed on this collector (Figure 15). Electrospun scaffolds were lyophilized via freeze-drier (*Labconco* Corporation, Kansas City, USA) after freezing at  $-80\text{ }^{\circ}\text{C}$ .

### **2.2.5. Crosslinking of Scaffolds**

Since PULL is a water-soluble material, PULL component of the electrospun scaffolds was cross-linked trisodium trimetaphosphate (STMP). Before crosslinking, all CA/PULL samples were weighed. Amount of STMP was varied according to PULL content of the scaffolds ranging from  $1/10^{\text{th}}$  of PULL to  $5/10^{\text{th}}$ . NaOH was used as initiator of the cross-linking reaction and added as  $1/10^{\text{th}}$  of the amount of STMP in that solution. Different crosslinking durations were tried (2, 8, 15, and 30 minutes) (Jiang et al., 2014).

Crosslinking scheme is shown in Figure 16. In the first step, the opening of cyclic structure of STMP occurred by reaction of alkoxides in strong alkaline media with phosphate groups leading to the formation of a tripolyphosphated polymer. In the second step, the addition of a new polymer chain led to the formation of a crosslinked polymer. The crosslinking reaction was accompanied by the production of pyrophosphate links. Different PULL-phosphates were produced by the reaction between STMP and PULL (Dulong et al., 2011).

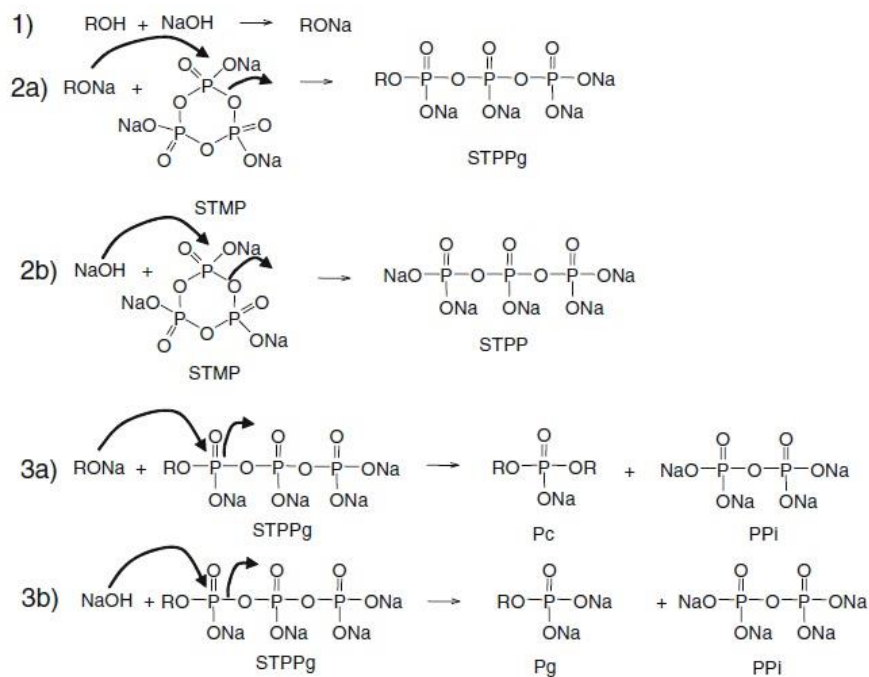


Figure 16. Proposed mechanism for the cross-linking reaction of PULL with STMP (Dulong et al., 2011).

Glutaraldehyde (GTA) crosslinking was used for crosslinking ox-BC/ox-PULL/GEL. A homo-bifunctional reagent, GTA, is reactive towards  $\text{NH}_2$  groups ( $\epsilon$ -amino groups of lysine residues) of proteins and soluble in aqueous solvents. It can form stable inter- and intra-subunit covalent bonds (Migneault et al., 2004). Gelatin (GEL) was added to C–OH group containing ox-BC and ox-PULL for obtaining structurally stable scaffolds by crosslinking (Figure 17).

For crosslinking scaffolds, ox-BC/ox-PULL/GEL were placed in a 25% GTA vapor chamber at room temperature for 2h. To construct the vapor chamber, 2 ml of GTA (New Jersey, U.S.A.) was added into in a small (35 mm diameter) uncapped Petri dish, which was then placed inside of a large (100 mm diameter) Petri dish. The scaffold was also placed within the large Petri dish; the large dish was then covered and sealed with parafilm. After 2h, the cover was removed and the scaffold was allowed to degas for 2h (Sell et al., 2008).

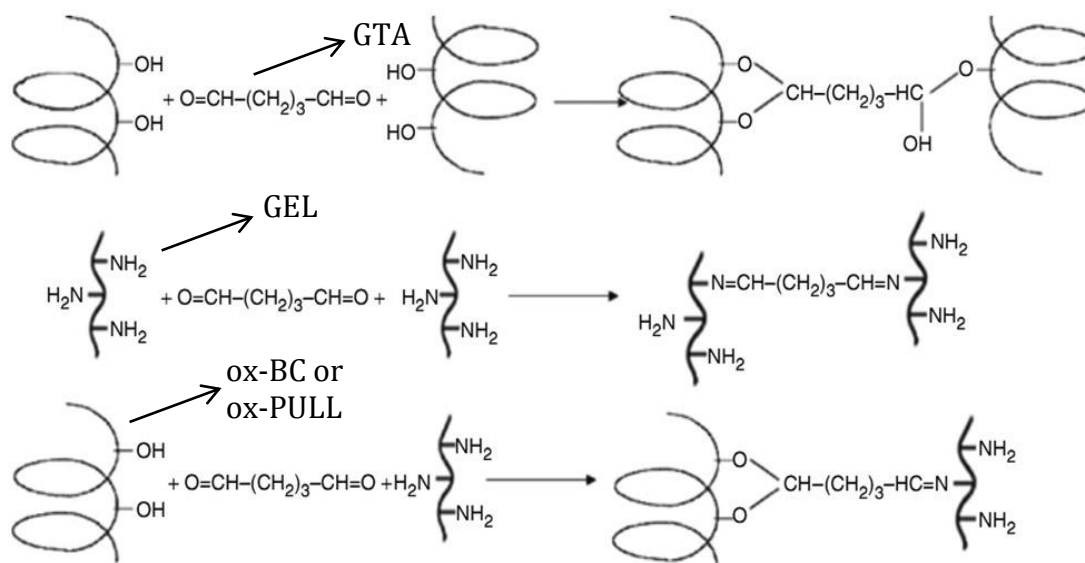


Figure 17. Schematic presentation of GTA cross-linking with oxidized polysaccharides (BC or PULL) and proteins (GEL) (Asma et al., 2014).

After cross-linking, scaffolds were washed with phosphate buffer (PBS, 0.1 M, pH 7.2) at room temperature and their wet-weights were recorded. Then, the cross-linked scaffolds were lyophilized via freeze-drier after freezing at  $-80^{\circ}\text{C}$  and their dry-weights were recorded.

## 2.2.6. Sacrificial Fiber Removal

As an alternative to cross-linking of PULL, CA/PULL 50/50 scaffolds were immersed in PBS (0.1 M, pH 7.2) at  $37^{\circ}\text{C}$  and incubated for 24 hours for remove PULL fibers as sacrificial fibers. Then, scaffolds were lyophilized via freeze-drier after freezing at  $-80^{\circ}\text{C}$ .

## 2.2.6. Characterization of Fibrous Scaffolds

### 2.2.6.1. Scanning Electron Microscopy (SEM)

Surface morphology of electrospun scaffolds were analyzed by scanning electron microscopy. Samples were prepared for analysis by coating with gold using a sputter coating device (Hummer VII, Anatech, Istanbul, Turkey). Fibrous structures were examined by micro and nano SEM devices (Stereoscan S4-10, Cambridge, UK and JSM-6400 Electron Microscope, Jeol Ltd., UK), equipped with NORAN System 6 X-ray Microanalysis System & Semafore Digitizer (Thermo Fisher Scientific Inc.,

USA) in the Department of Metallurgical and Materials Engineering at METU (Ankara, Turkey) and Quanta 400F Field Emission SEM device (FEI, USA) in Central Laboratory at METU in Central Laboratory at METU (Ankara, Turkey). Fiber morphologies and fiber diameter distributions of electrospun scaffolds were examined from various images obtained from different regions on the surface of the samples.

### **2.2.6.2. Fourier Transform Infrared Spectroscopy - Attenuated Total Reflectance (FTIR-ATR) Analyses**

FTIR-ATR analyses were conducted to determine degree of acetylation of BC and degree of cross-linking of PULL via a spectrometer of PerkinElmer L1050002 series (PerkinElmer, Inc., UK) using spectrum 100/100N software program in transmission mode. The analysis was performed within the wavelength range 400-4000  $\text{cm}^{-1}$ , with a resolution of 4  $\text{cm}^{-1}$ , and a total of 50 scans per sample. The spectra of samples were measured by mixing powder of drug components or discs (obtained by crushing in a mortar) with KBr. The spectra of all samples were corrected for background and atmosphere inside the FTIR.

### **2.2.6.3. Degradation Study**

For degradation studies, electrospun scaffolds (n=4) were cut into rectangular pieces with dimensions 3 mm x 5 mm x 4 mm (length x width x height) each was incubated in 4 ml phosphate buffered saline (PBS, 0.1 M, pH 7.2) solution at 37°C in water bath (Nüve Bath NB 5, Turkey) for 35 days. Wet weights of the samples and pH values of PBS were determined at the end of each time period. After then, samples were washed with distilled water and dried in the vertical laminar flow hood (Faster, Italy) for dry weight measurements. Weight loss percentages were calculated according to the below formula.

$$\text{Weight Loss (\%)} = \frac{W_1}{W_0} * 100$$

$W_0$ ; Initial weight of the sample (g)

$W_1$ ; Initial weight of the sample (g)

#### 2.2.6.4. Mechanical Tests

Uniaxial tensile tests were carried out on 5 mm x 10 mm x 2 mm (length x width x thickness) electrospun specimens. Mechanical tests were performed at 4 mm/min to rupture using mechanical tester (Lloyd LR50K, Lloyd Instruments, England) connected to a remote computer including Nexygen software programme (Ametek, U.K.) equipped with a 10 N load cell. Four specimens were used for each electrospun group. The ultimate tensile strength (UTS), Young's modulus and strain values were determined.

For compression tests all samples were cut into pieces with a dimension of 3 mm x 5 mm x 4 mm (length x width x height). They were tested with a mechanical tester (Lloyd LR50K, Lloyd Instruments, England) connected to a remote computer including Nexygen software programme (Ametek, U.K.) equipped with a 10 N load cell at a crosshead speed of 4 mm/min until rupture. The compressive strength, Young's modulus and strain values were determined from stress-strain curves obtained.

#### 2.2.6.5. Porosity Measurements

Pore size distribution and percent porosity of the scaffolds (n=2) were determined by using Coremaster 60 Mercury Porosimeter (Qunatochrome Cooperation, Florida, USA) under low pressure (0-50 psi for 200 - 4  $\mu$ m diameter) and Helium Ultrapycnometer 1000 (Quantachrome Corporation, Florida, USA) in Central Laboratory at METU (Ankara, Turkey). In mercury porosimeter measurements, the relation between applied pressure and pore diameter based on Washburn equation was used given below.

$$D = \frac{-4\gamma \cos\theta}{P}$$

D; Diameter of the pore (cm),

P; Applied pressure (dyne),

$\gamma$ ; Surface tension of mercury (480 dyne/cm) and,

$\theta$ ; Angle between pore surface and mercury (generally 140°).

In helium pycnometer measurements, volume and true density were calculated by using Archimedes' principle of fluid displacement and Boyle's gas law. Helium gas with the size 0.25 nm is suitable for deeper penetration through the pores depending on the polymer type which should not allow the gas pass through itself (Hu et al., 2011).

### **2.2.7. Cell Culture Studies**

After sterilization of the scaffolds with UV and ethanol, scaffolds were immersed in DMEM with 10% FBS, 1% penicillin-streptomycin and incubated at 37°C for 24 hours.

Human osteogenic sarcoma cell line (Saos-2) was used for evaluation of the compatibility of electropun BS/PULL/GEL scaffolds for bone tissue engineering applications. Saos-2 cells were cultured in Dulbecco's modified Eagle medium with high glucose-Glutamine (DMEM) containing 10 v/v% FBS and 10 U/ml penicillin/streptomycin in the 5215 incubator (Shel Lab, USA) providing 5% carbondioxide and 95% moisture at 37°C. Cells were trypsinized with 0.1% trypsin-EDTA for passaging, when their confluency levels reached to at least 80-90 %.

For testing of suitability of SA/PULL electrospun scaffolds for skin tissue engineering applications, mouse fibroblastic cell line (L929) (mouse C3H/An connective tissue cell line) was used.

#### **2.2.7.1. Cell Viability Assays**

Cell attachment and proliferation were determined by Alamar Blue Assay (Invitrogen, USA). Alamar Blue, or 7-hydroxy-3H-phenoxazine-3-one 10-oxetine, is a cell health indicator that is chemically reduced by inner metabolic activities of cells (O'Brien et al., 2000). In principle, cell proliferation stabilizes reduction environment while cell growth inhibition stabilizes oxidation environment. The oxidized form of redox indicator turns from non-fluorescent blue to fluorescent red due to the reduction reaction. Cell viability analyses were performed at the end of 1, 4, 7, and 14 days of incubations (Mishra et al., 2011).

During experiments, scaffolds (n=6) were cut into discs of 9 mm in diameter and placed in 48 well plates after alcohol and UV sterilizations. (An initial seeding

density of  $6 \times 10^6$ /disc was used for cell culture studies.) After seeding scaffolds were incubated in a carbon dioxide incubator (Shel Lab 5215, California, U.S.A.) for 7 days. At different time periods, Alamar Blue cell viability assay was conducted to study the attachment and proliferation of the cells on electrospun scaffolds. For Alamar Blue assay, the medium was removed and the cells were washed with PBS (0.1 M, pH 7.22). 10% Alamar blue solution (10 % alamar blue & 90 % DMEM without phenol red) was added to each well and incubated at dark for 4 hours. The optical densities of reduced solutions were obtained at 570 nm and 600 nm via microplate spectrophotometer ( $\mu$ Ouant<sup>TM</sup>, Biotek Instruments Inc., USA) using the ELISA software programme (Atlanta, USA) and recorded (Li et al., 2005).

*Reduction (%)*

$$= \frac{(\epsilon_{ox})\lambda_2 A \lambda_1 - (\epsilon_{ox})\lambda_1 A \lambda_2 \text{ of test dilution}}{(\epsilon_{red})\lambda_1 A' \lambda_2 - (\epsilon_{ox})\lambda_2 A' \lambda_1 \text{ of untreated positive control}} * 100$$

$\epsilon_{ox}$ ; Molar extinction coefficient of AlamarBlue oxidized form (BLUE),

$\epsilon_{red}$ ; Molar extinction coefficient of AlamarBlue reduced form (RED),

A; Absorbance of test wells,

A'; Absorbance of negative control well,

(The negative control well should contain media + AlamarBlue but no cells.)

$\lambda_1$ ; 570nm and,

$\lambda_2$ ; 600nm.

During determinations of cell viability percentages, cells seeded on tissue culture plates without scaffolds (TCPS) were used as control groups. The wells containing only media and scaffolds without cells served as negative controls for control and cells seeded-scaffolds groups, respectively in the calculations of % reduction.

### **2.2.7.2. Cell Morphology Analyses**

Morphology of cells on electrospun scaffolds was examined after 1 day of incubation with SEM (Quanta 200 FEG, The Netherlands). At the end of each period, cells were fixed in 4% paraformaldehyde solution in PBS. Fixed samples

were washed with PBS, dehydrated with increasing ethanol series (20-100 %), and finally dried in hexamethyldisilazane for 20 minutes prior to storage in desiccator. Before SEM analysis, batches were coated with ultrafine (10 nm) gold layer by precision etching coating system (682 PECS, Gatan, Inc., USA) and then imaged via Scanning Electron Microscopy (Stereoscan S4-10, Cambridge, UK and JSM-6400 Electron Microscope, Jeol Ltd., UK), equipped with NORAN System 6 X-ray Microanalysis System & Semafore Digitizer (Thermo Fisher Scientific Inc., USA).

### **2.2.7.3. Cell Migration Analyses through 3D Scaffolds**

Cell migration studies were conducted using confocal laser scanning microscopy. Cells cultured on scaffolds were fixed with formaldehyde after 35-day of incubation. Fixed scaffolds were stained with PI (Invitrogen, USA) for nuclei and FITC (Invitrogen, USA) for actin (Mandal & Kundu, 2009). Fluorescence images from stained samples were obtained using a confocal laser scanning microscope (Zeiss LSM 510, Germany) equipped with Argon (458-477-488-514 nm), HeNe/1 (543 nm), and HeNe/2 (633 nm) lasers.

## **CHAPTER 3**

### **RESULTS & DISCUSSIONS**

#### **3.1. Part I: Cellulose Acetate – Based Scaffolds**

##### **3.1.1. Electrospinning of CA/PULL**

Various solvents and their different combinations (acetone, d-water, acetic acid, DMAc, DMSO) (Table 2) were used for determining the solvent system for electrospinning CA/PULL polymers.

##### **3.1.1.1. Conventional Electrospinning of CA/PULL**

During optimization studies of electrospinning, applied electrical voltage, flow rate, and distance between the needle tip and the collector surface were changed between the intervals; 5-25 kV, 0.2-8 ml/hr, and 8-35 cm, respectively. Furthermore, the most suitable polymer concentrations and ratios were tuned and determined. CA/PULL (80/20 w/w%) in DMAc/DMSO (55/45 v/v%) with a total polymer concentration of 20wt% was electrospun under 10 kV electrical voltages with 1 ml/hr flow rate at a distance of 25 cm from the collector screen. These scaffolds were photographed on the aluminum surface on the collector (Figure 18). These thin electrospun membranes were found suitable for skin tissue engineering applications regarding to their shape.

Table 2. Solubility of CA/PULL in different solvents or combinations of them.

Polymer	Solvent	Solvent ratio	Solubility	Polymer concentration (w/v %)	Polymer ratio
CA	d-water	–	–	10	
PULL	d-water	–	+	10 & 20	
CA	Acetone/d-water	2:1	+	10 & 20	
PULL	Acetone/d-water	1:1	±	10	
CA	DMAc	–	+	10 & 20	
PULL	Acetone	–	–	10	
CA	DMSO/d-water	1:1	±	10	
PULL	DMSO/d-water	1:1	+	10 & 20	
CA	Acetone/DMAc	2:1	+	10 & 20	
CA/PULL	d-water/acetone/DMAc	2:6:3	–	10	80/20
CA	DMAc/DMSO	1:1	+	10 & 20	
CA/PULL	DMAc/DMSO	1:1	+	10 & 20	50/50
CA	Acetic acid/d-water	3:1	+	10 & 20	
CA/PULL	Acetic acid/d-water	3:1	±	10	80/20

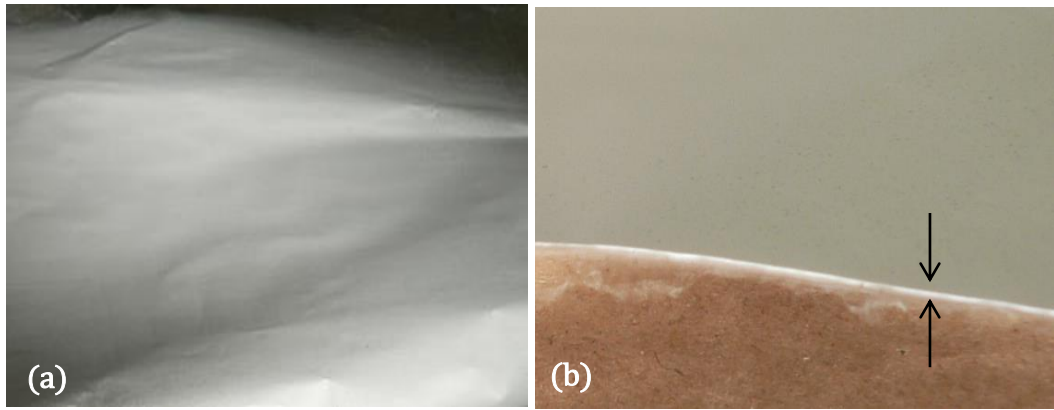


Figure 18. 2D-electrospun CA/PULL scaffolds top (a) and crosssection (b) views.

Bone tissue engineering, however, requires 3D-scaffolds in order to imitate bone ECM more effectively (Jones et al., 2004). Hence, 3D-scaffold fabrication was optimized. CA/PULL (80/20 w/w %) in DMAc/DMSO (55/45 v/v %) with a total polymer concentration 20wt% was electrospun under 15 kV electrical voltages with 1.5 ml/hr flow rate at a distance of 25 cm from the collector screen. Appearances of scaffolds at the initial and final formation steps were photographed (Figure 19).

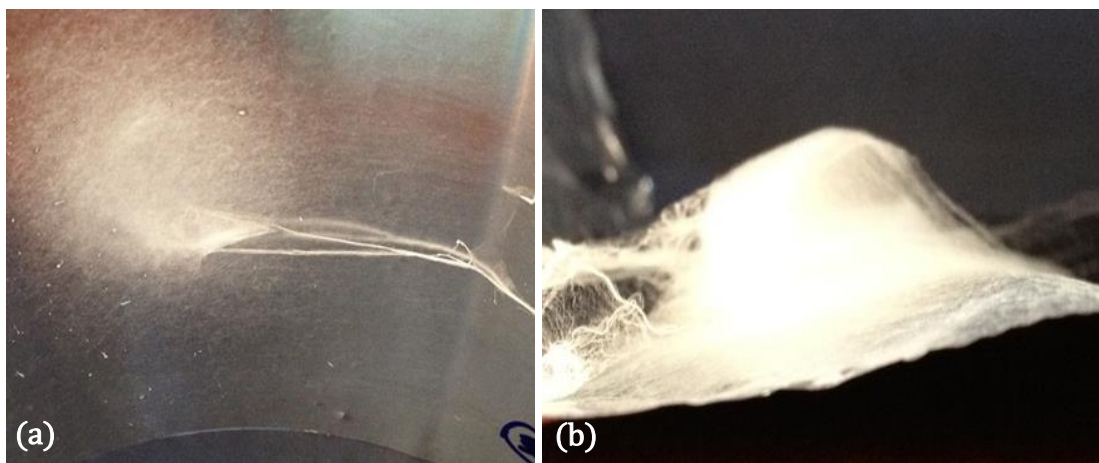


Figure 19. 3D-electrospun CA/PULL scaffolds at the initial (a) and final (b) formation steps.

Electrospun 3D-scaffolds were not produced reproducibly in terms of fiber deposition and layer density on collector screen. Scaffolds should exhibit approximately the same structural pattern with a coherent texture throughout the whole scaffold. In order to achieve this, the surface geometry and configuration of the collector were altered several times holding the same electrospinning parameters;

CA/PULL (80/20 w/w%), DMAc/DMSO (55/45 v/v %), total polymer concentration 20 wt%, 15 kV electrical voltages, 1.5 ml/hr flow rate, and 25 cm distance from the collector screen. More homogeneous electrospun structures were produced and cut into cylindrical geometries (5 mm in diameter and 6 mm in height) (Figure 20).

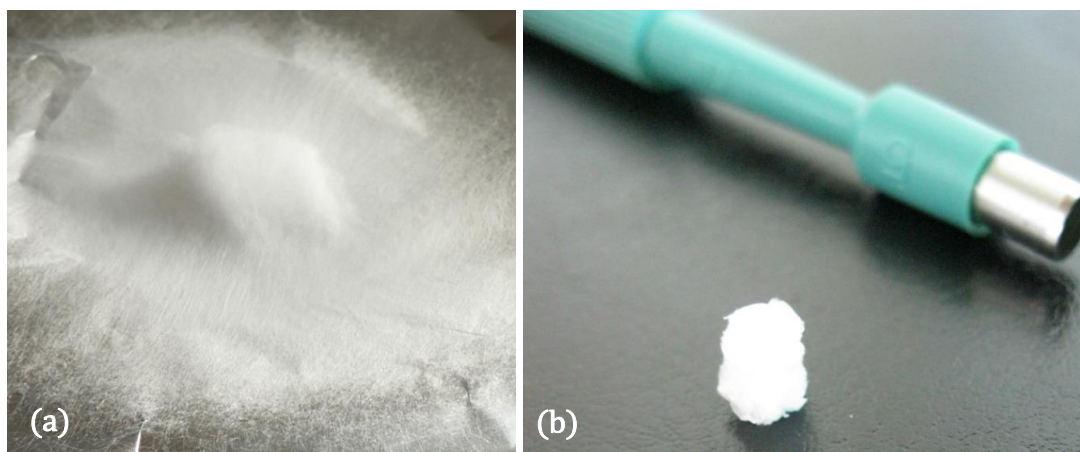


Figure 20. 3D-electrospun CA/PULL scaffolds (a) produced with altered collector geometry on the aluminum surface and (b) disc form obtained with a skin puncher.

Electrospinning of 3D-electrospun CA/PULL scaffolds could not be reproducibly produced because of the obstacles including (i) poor targeting and wide distribution of fibrous mesh to large areas leading to loss of most of the mass of electrospun material, (ii) difficulties during removal of the 3D part accumulated at the center, and (iii) wetting on the collector due to incomplete evaporation of solvents until jets reach to collector, which resulted with fusion of fibers after arriving at collector surface. Then, the technique was changed with wet electrospinning method.

### 3.1.1.2. Wet Electrospinning of CA/PULL

With shift from conventional to wet electrospinning technique could be obtained more homogeneous patterns within the structural orientation of scaffolds (Yang et al., 2013). In addition, polymers electrospun into a nonsolvent bath placed on the collector can easily be removed. Moreover, the residues of solvents within the polymeric solution which were not able to evaporate till it reached to the collector were separated from newly formed fibers by ethanol bath. Therefore, the efficacy of

fiber stabilization was increased by the contact with ethanol immediately after electrospinning.

In wet electrospinning, 100% ethanol was used as immiscible solvent that the mesh was accumulated within such that the fibrous product can be removed without any damage (Li et al., 2003). Ethanol bath was placed on top of a different type of collector. A rotational stand was used in the experimental set-up as a collector screen for providing effective use of fiber collection area. There was no influence of the rotational stand on fiber characteristics. Ratio of DMAc/DMSO was set to 55/45 (v/v) and 20 wt% polymer concentration was chosen as the polymer concentration for 80/20, 50/50, and 20/80 (w/w)% ratio groups of CA/PULL during electrospinning.

The two extremes of CA/PULL ratios, namely 80/20 and 20/80 (w/w)% were mainly analyzed in order to understand the contribution of each component to the scaffold. Structural differences observed revealed that CA caused more flattened structures, whereas PULL resulted in more 3-dimensional forms (Figure 21).

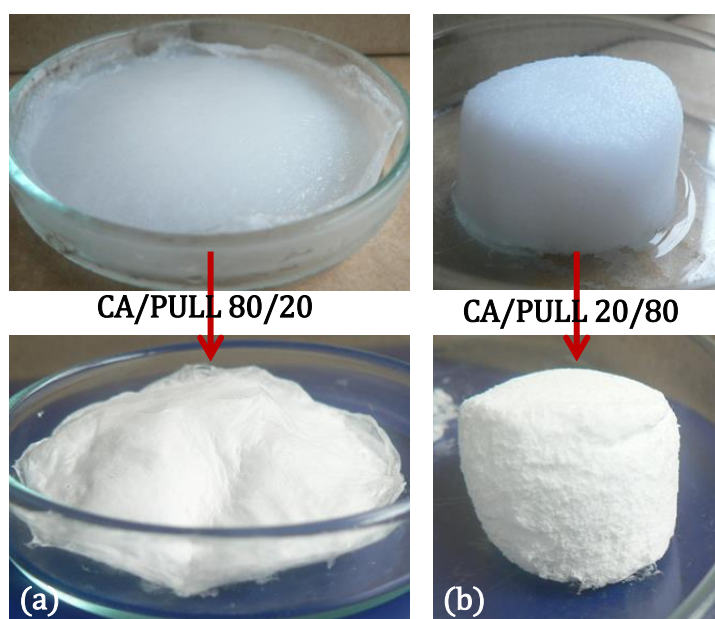


Figure 21. Electrospun CA/PULL scaffolds with 80/20 and 20/80 (w/w)% ratios before (a) & (b) and after (c) & (d) freeze-drying, respectively.

After-freeze drying, CA-dominant scaffolds (80/20 w/w%) separated into layers, while PULL-dominant scaffolds (20/80 w/w%) showed conserved homogeneity and integrity. Hence, this result indicated that PULL was essential polymer that provides 3D-scaffold formation. In addition, CA content was not lowered dramatically not to lose the mechanical properties of the scaffolds.

Considering (i) 3-dimensionality demand, (ii) homogeneity within structural patterns, and (iii) mechanical properties of scaffolds, CA/PULL scaffolds with 50/50 (w/w)% were chosen for electrospinning (Figure 22). When compared with the other CA/PULL scaffolds (80/20 and 20/80 (w/w)%), the electrospun scaffolds of 50/50 (w/w)% exhibited intermediate properties for compactness and softness, which also correlated with porosity and mechanical strength results.

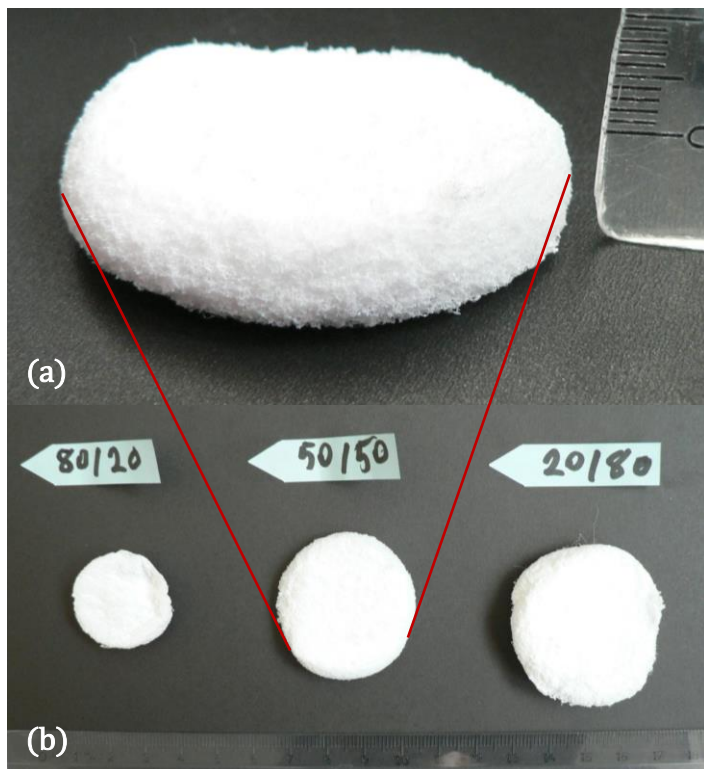


Figure 22. (a) Side view of CA/PULL 50/50 (w/w) % scaffold and (b) Top views of all CA/PULL ratio scaffolds (80/20 and 20/80 w/w %).

### **3.1.2. Characterization of Conventionally Electrospun CA/PULL Scaffolds**

#### **3.1.2.1. Scanning Electron Microscopy (SEM)**

Morphology of fibers is important to provide a suitable environment for cells intended to be grown on them (Sill & Von Recum, 2008) so that the most suitable 3D-fibrous structures with appropriate porosity with high surface to volume ratio were aimed to be electrospun. SEM analyses were done to examine fiber morphologies and fiber diameter distributions of the electrospun scaffolds. Detailed analyses of SEM images were used during optimization of electrospinning parameters.

#### **Effect of Applied Electrical Voltage**

During initial optimization studies, bead formations were observed within fibrous network of CA/PULL (80/20 w/w %) scaffolds. Additionally, SEM examinations revealed influences of electrical voltage on fiber morphology (Figure 23). When the applied voltage was increased from 12 to 14 kV, bead-formation was partially diminished. During electrosopinning, parameters were set as 15wt% total polymer concentrations, 1 ml/hr flow rate, and 25 cm distance after optimization studies.

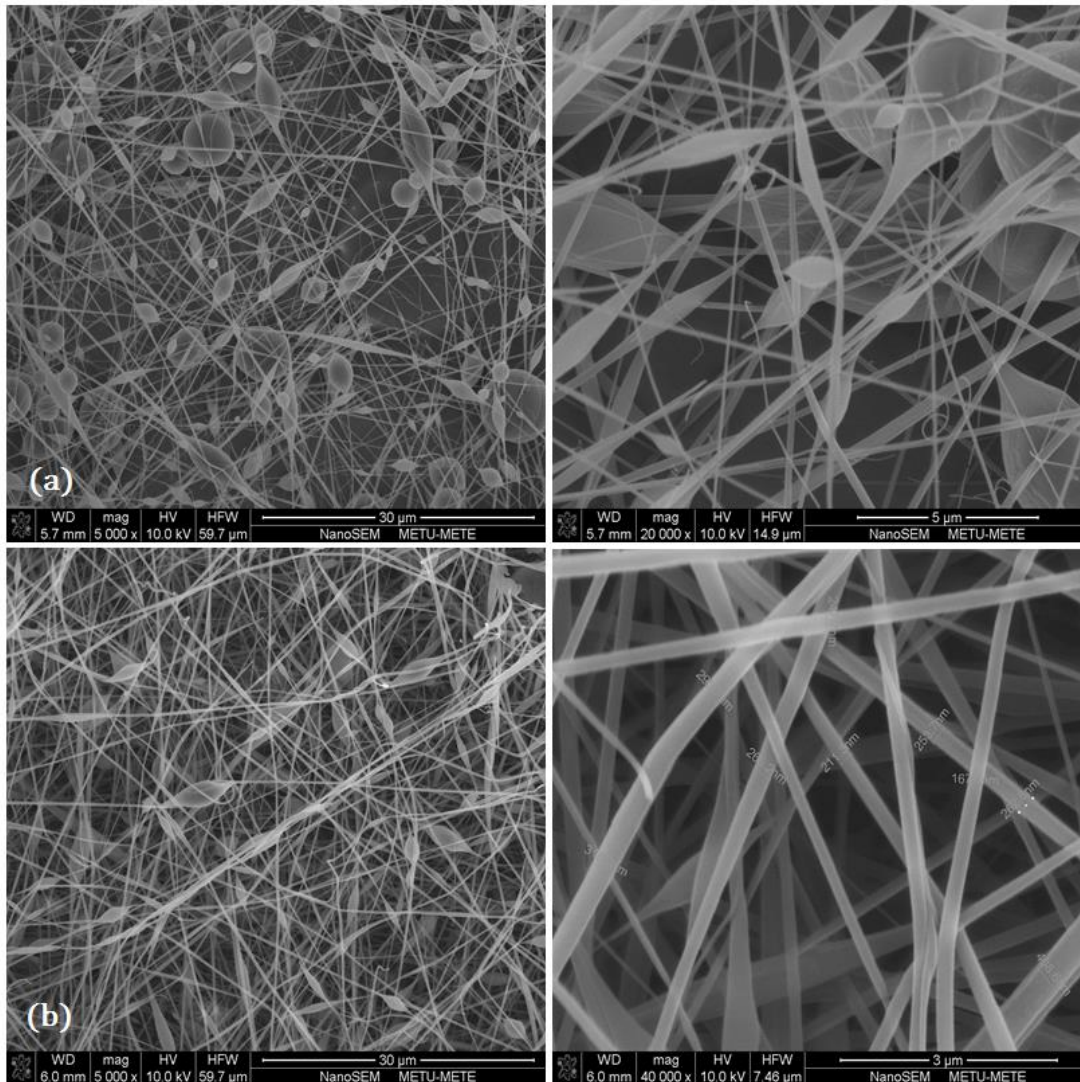


Figure 23. SEM images of CA/PULL (80/20 w/w%) scaffolds electrospun with (a) 12 and (b) 14 kV electrical voltage (15wt% total polymer concentration, 1 ml/hr flow rate, and 25 cm distance).

### **Effect of Total Polymer Concentration**

Apart from the voltage applied, it is also known that low polymer concentration can cause bead formation since higher concentrations leading to higher surface tension values result in lower degrees of bead formation in electrospinning (Liu et al., 2008). SEM images showed that electrospun structures with higher polymer concentrations (20 wt%) were almost bead-free (Figure 24). In those groups, the total polymer concentrations were increased from 15 to 20 wt%, while all other

parameters were kept constant (16 kV electrical voltage, 1 ml/hr flow rate, and 25 cm distance).

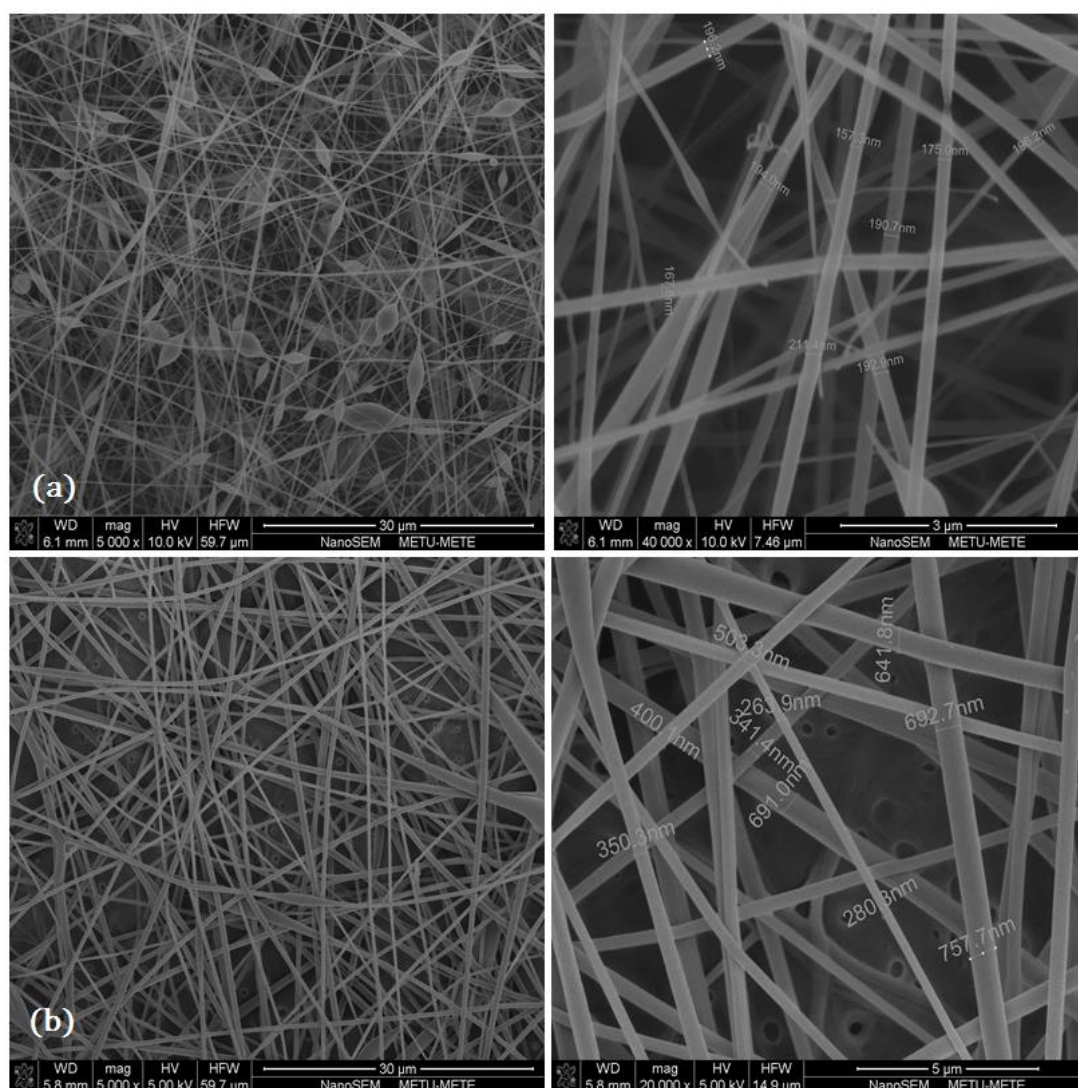


Figure 24. SEM images of CA/PULL (80/20 w/w%) scaffolds electrospun with 16 kV electrical voltage, 1 ml/hr flow rate, 25 cm distance, and total polymer concentrations; (a) 15 and (b) 20 wt %.

### **Effect of Solvent System**

After optimization of polymer concentration the ratio of DMAc/DMSO in the solvent system was tuned. For DMAc/DMSO with 50/50 (v/v%) ratio several large clumps of polymer material within fibrous mesh were observed in SEM

examinations (Figure 25a), which would prevent the cell migration in to the scaffold during tissue culture studies (Mano et al., 2007).

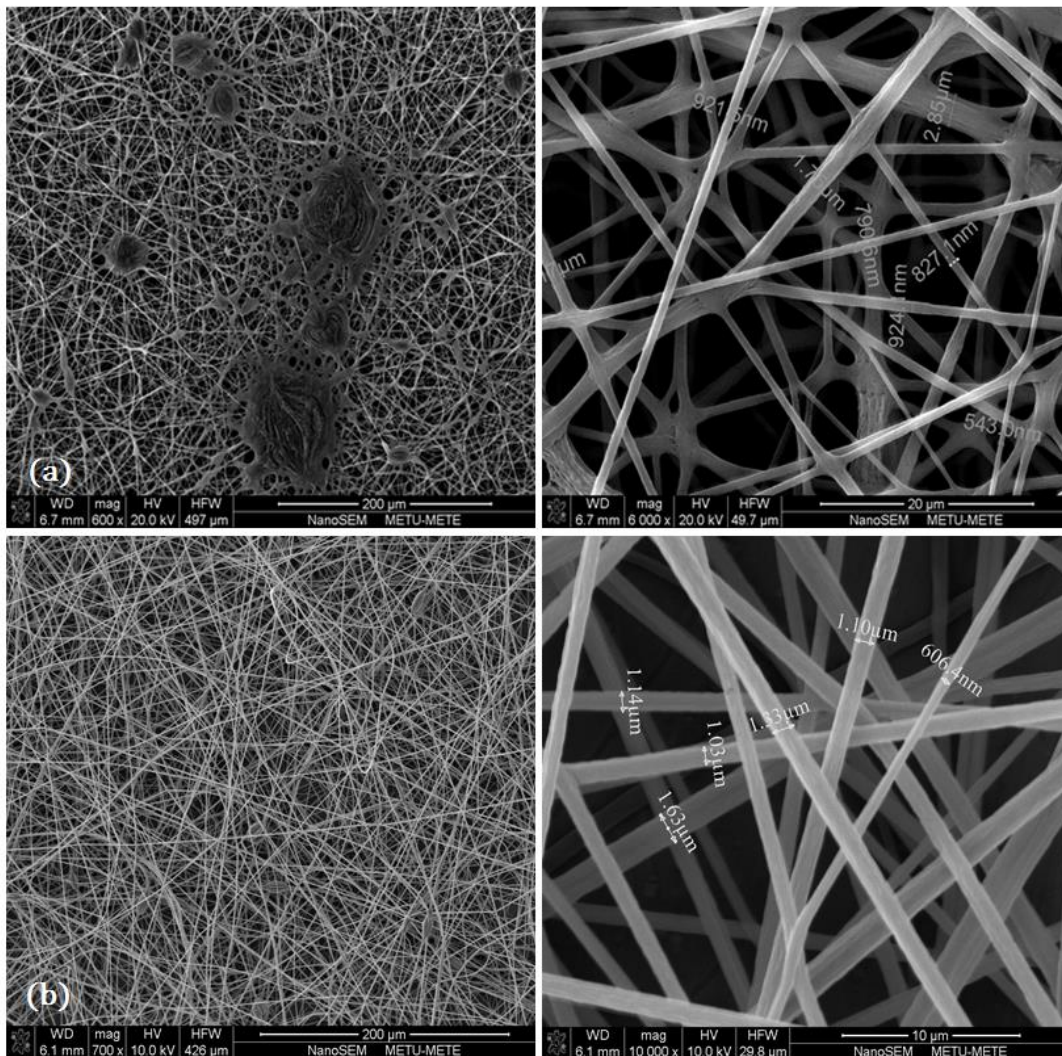


Figure 25. SEM images of CA/PULL (80/20 w/w%) scaffolds electrospun in DMAC/DMSO at v/v% ratios of; (a) 50/50 and (b) 55/45 (other parameters were set as 20 wt% total polymer concentration, 1 ml/hr flow rate, 25 cm distance, electrical voltage 15 kV).

These observed clumps were thought to occur with wetting on the collector depending on properties of the solvent system. DMSO has a dielectric constant of 46.70, which is considered as very high (Choktaweasap et al., 2007). However, solvents with medium dielectric constants are more useful during formation of fibers via electrospinning (Lee et al., 2003). In addition, volatility of the solvent must be

high to overcome ‘the wetting issue’ (Ohkawa et al., 2009). DMAc is more volatile than DMSO and has a slightly lower viscosity. Thus, proportion of DMAc was increased for the adjustment of viscosity, dielectric constant, and volatility. DMAc/DMSO ratio was chosen as 55/45 (v/v%), leading to formation of smooth fibers (Figure 25b). During electrospinning of CA/PULL (80/20 w/w%), parameters were set as 20 wt% total polymer concentration, 1 ml/hr flow rate, 25cm distance, and electrical voltage 15kV.

### **Effect of Collector Geometry**

Electrified jets are oriented by distributions of electrical charges on the collector and this distribution greatly depends on the topography of the collector surface (Konwarh et al., 2013). Therefore, the shift from 2D- to 3D- CA/PULL scaffold fabrication was achieved by altering the geometry of the collector. SEM images of CA/PULL (80/20 w/w%) scaffolds electrospun by using the straight collector screen and curved collector are given in Figure 26.

When straight collector was used, 2D-nanofibrous membranes were obtained (Figure 26a) whereas 3D-nanofibrous structures were obtained with the use of curved collector (Figure 26b). For 2D and 3D-scaffolds, no significant differences in the fiber morphologies were revealed (Figure 26). Only their thicknesses differed since the fiber deposition on the curved collector focused on a narrow area and 3-dimensionality was provided. The depth of the 3D fibrous mesh was recognized in SEM images (Figure 26b). Common parameters were 20 wt% total polymer concentrations, 1.5 ml/hr flow rate, 25 cm distance, and electrical voltage 15 kV.

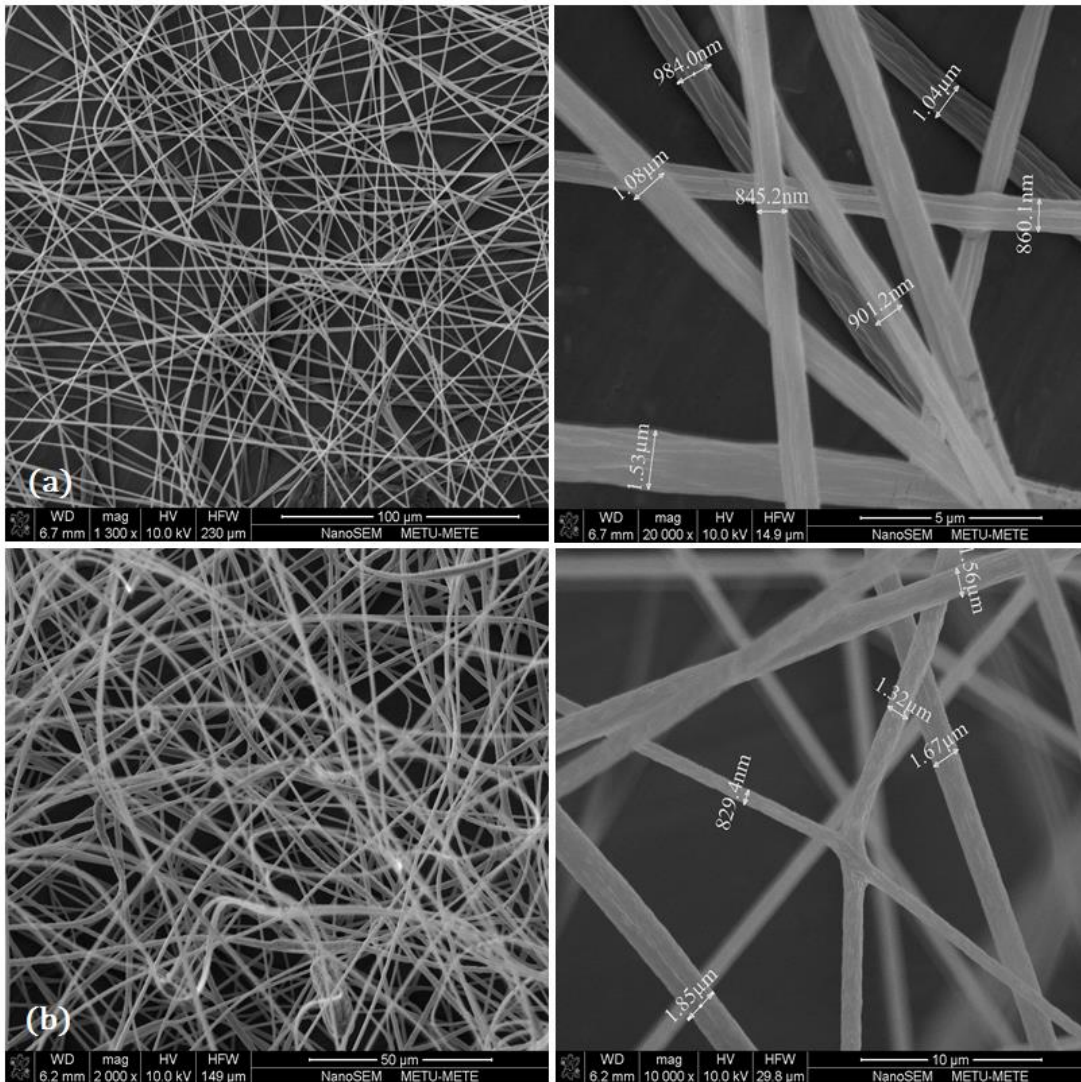


Figure 26. SEM images of electrospun CA/PULL (80/20 w/w %) scaffolds collected on (a) unmodified-flat and (b) modified-curved collectors. (Parameters: 20 wt% total polymer concentration, 1.5 ml/hr flow rate, 25 cm distance, and 15 kV voltage).

Even though electrospun CA/PULL scaffolds can be used in tissue engineering applications, other properties should be met by scaffolds for engineering of bone. Bone has anisotropic mechanical properties with highly oriented ECM and bone cells; therefore aligned fibrous scaffolds mimicking the natural ECM of bone are preferred with sufficient porosity for better cell migration (Jose et al., 2009). Newly designed collector surfaces were prepared to produce aligned CA/PULL (80/20 w/w %) scaffolds. First, double curved aluminum surface with 90° angle to the horizontal axis of the collector base was used and partially aligned fibrous mesh

was obtained between them. Then, single curved aluminum surface with 45° angle to the horizontal axis of the collector base was used. However, CA/PULL fibers were collected on the curve instead of near the curved surfaces as it was in the previous case. Hence, the alignment degree was increased. SEM images showed that aligned 3D CA/PULL (80/20 w/w%) scaffolds were obtained (Figure 27).

The histogram for the fiber diameter distributions of aligned 3D CA/PULL (80/20 w/w %) scaffolds are inserted within the SEM images (Figure 27). Histogram graph was constructed from 100 measurements done at different regions of both samples collected on the two altered collector surfaces since their fiber diameters were measured approximately the same (Figure 27). The fiber diameter distributions ranged between 548 nm-1.795 μm. Mean diameter of electrospun scaffolds was determined as 985.4 nm with a maximum pore size around 10 microns. Average size for human bone cells is approximately 9 μm long along its short axis and 20 μm long along its long axis (Mullender et al., 1996). Thus, the pore size of the scaffold must be greater than the cellular diameter; otherwise, this may cause an insufficient cellular penetration. Wet electrospinning can be used for increasing fiber diameter resulting in larger pores; therefore wet electrospinning was decided to be used for the preparation of three-dimensional CA/PULL electrospun scaffolds.

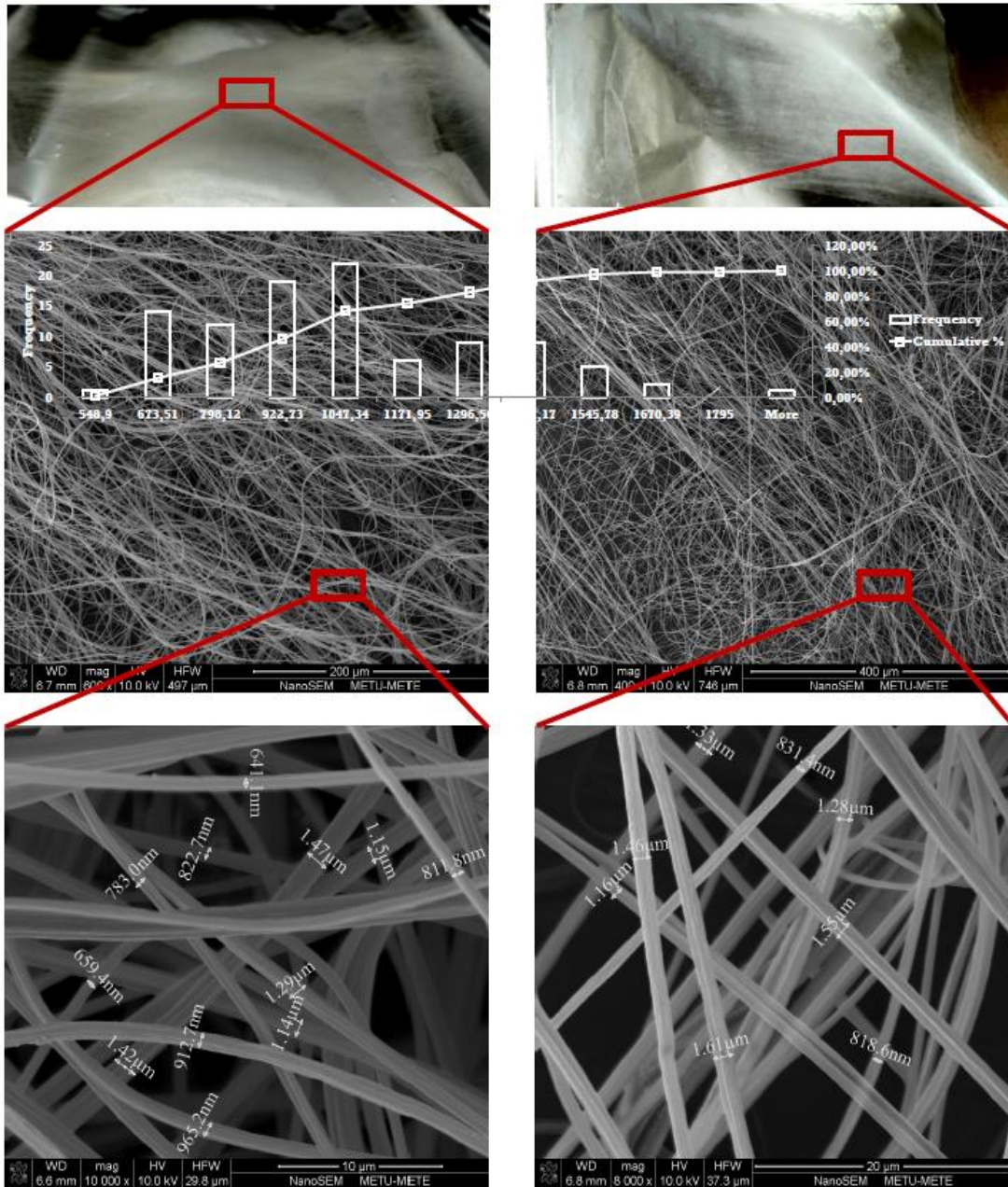


Figure 27. SEM images of aligned 3D CA/PULL (80/20 w/w%) scaffolds electrospun with 20 wt% total polymer concentration, 1 ml/hr flow rate, 30 cm distance, and electrical voltage 14 kV by using set-ups with angles 90° (right) and 45° (left) of aluminum curves to the horizontal axis of the collector base. Histogram for fiber diameter distributions is given as an insert figure.

### 3.1.2.2. Degradation Analyses

Degradation studies showed that the CA/PULL (80/20) scaffolds lost approximately 20% of their weights which indicated that PULL was probably removed and weight loss leveled off (Figure 28).

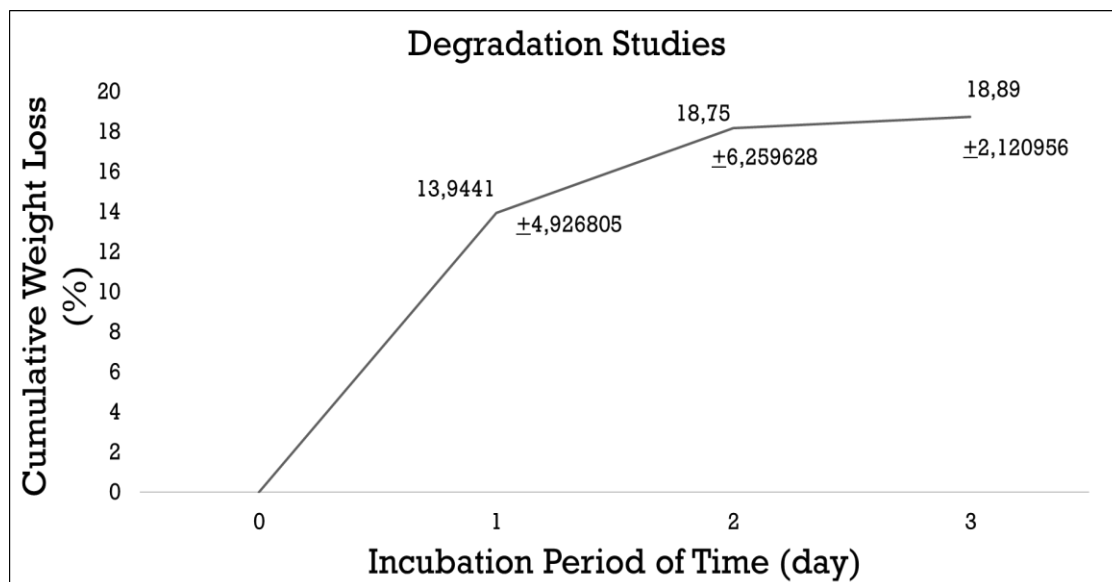


Figure 28. Cumulative weight losses of the scaffolds in PBS (0.1 M, pH 7.2) at 37°C in water bath for 1., 2., and 3. day of incubation with their standard deviations.

### 3.1.3. Characterization of Wet-Electrospun CA/PULL Scaffolds

#### 3.1.3.1. Fourier Transform Infrared Spectroscopy - Attenuated Total Reflectance (FTIR-ATR) Analyses

Polymeric scaffolds are cross-linked to modify their mechanical, thermal, chemical, and degradation properties (Costa-Júnior et al., 2009). Fourier transform infrared (FT-IR) spectroscopy in combination with the attenuated total reflectance (ATR) technique is a simple and fast surface sensitive method to understand whether the cross-linking reaction was successful and specific bonds were formed (Chung et al., 2004).

FTIR-ATR spectra of CA/PULL scaffolds were studied in order to determine sodium trimetaphosphate ( $\text{Na}_3\text{P}_3\text{O}_9$ ) mediated cross-linking of PULL (Figure 35). Peaks at  $1645\text{ cm}^{-1}$  represent the O–C–O stretching region which is characteristic for PULL (Cheng et al., 2010). Accordingly as PULL content of scaffolds increased,

these peaks became sharper (CA/PULL: 20/80>50/50>80/20) and (Dulong et al., 2011). In FTIR-ATR spectra of cross-linked scaffolds, it was observed that peaks at  $1645\text{ cm}^{-1}$  disappeared due to the breakage of O–C–O bonds during crosslinking. Additionally, peak at  $700\text{--}760\text{ cm}^{-1}$  in the FTIR spectra of the cross-linked samples showed the presence of STMP ( $\text{Na}_3\text{P}_3\text{O}_9$ ) (Gunter et al., 1996) which demonstrated that the crosslinking had occurred. The area under the curve at this particular wavelength increased with the increase in the PULL content of the scaffolds.

Single bonds between hydrogen and oxygen atoms are observed at  $3300\text{--}3500\text{ cm}^{-1}$  region representing the O–H stretching (Chung et al., 2004). These peaks were observed in the FTIR spectra of scaffolds with higher PULL content due to its hydrophilicity, pointing out strong hydrogen bonding interactions between water molecules and adjacent surface water molecules (Scatena et al., 2001).

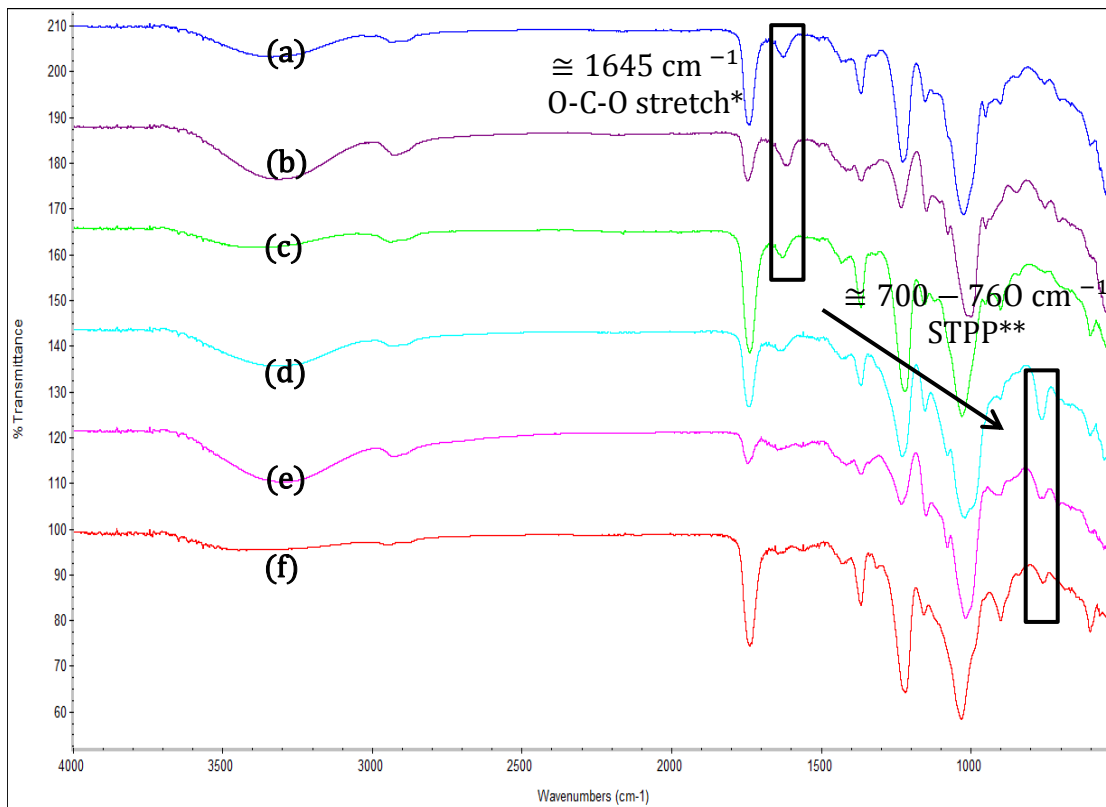


Figure 29. FTIR-ATR spectra of CA/PULL scaffolds a) 50/50, b) 20/80, c) 80/20, d) 50/50, cross-linked, e) 20/80, cross-linked, f) 80/20, cross-linked. \*One of the characteristic bonds of the native PULL. \*\*Sodium tripolyphosphate forming after the crosslinking treatment with STMP.

CA/PULL (50/50 w/w%) scaffolds were incubated in PBS at 37°C in water bath for 30 days and FTIR-ATR spectra were analyzed at the end of incubation period. Red line in Figure 29 represented original CA/PULL scaffolds and exhibited all common transmittance peaks in a typical PULL spectrum; 3430 cm<sup>-1</sup> O–H stretching, 2928 cm<sup>-1</sup> C–H stretching, 1645 cm<sup>-1</sup> O–C–O stretching (Singh et al., 2008; Cheng et al., 2010). In addition, peaks at 755 cm<sup>-1</sup> and 929 cm<sup>-1</sup> showed predominant linkages, namely  $\alpha$  (1,4) and  $\alpha$  (1,6) between glucose units of PULL (Cheng et al., 2010). After 30 days, a decrease in characteristic peaks of PULL was observed, blue line in Figure 30 showed declined levels of main peaks of PULL in the CA/PULL scaffolds, pointing out the fact that most of the of PULL component of fibers were removed from the scaffolds. It can be stated that with the removal of some of PULL fibers, a highly porous 3D electrospun CA/PULL based scaffolds were successfully produced. Therefore, uncross-linked CA/PULL scaffolds were decided to be used after removal of PULL as sacrificial fibers.

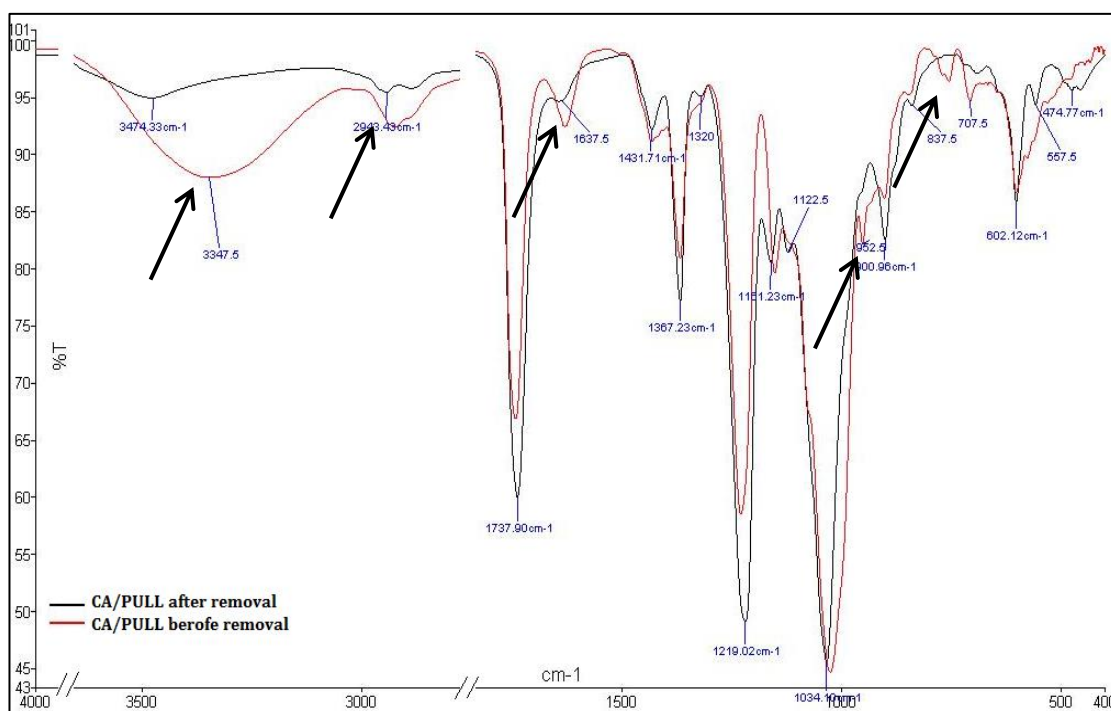


Figure 30. FTIR-ATR spectra of CA/PULL (50/50) scaffolds (red) before and (blue) after removal of sacrificial fibers. Arrows: Characteristic peaks of PULL.

### **3.1.3.2. Scanning Electron Microscopy (SEM)**

#### **Effect of CA/PULL Blend Weight Ratio**

SEM analyses showed that CA/PULL 80/20 w/w% scaffolds contained fibers with the features; (i) smoother and straighter than those of 50/50 w/w% scaffolds and (ii) straighter than those of 20/80 w/w % scaffolds (Figure 31). However, thicker and thinner fibers were observed in SEM images. Thinner fibers are thought to be CA fibers due to their known characteristic morphology (Tungprapa et al., 2007). Such observation points out that a phase separation might have formed due to inequality in the amounts of the two polymers (Bognitzki et al., 2001).

SEM images revealed that CA/PULL 50/50 w/w% scaffolds had slightly wavy fibers rather than straight or curly. Furthermore, each fiber of scaffolds consisted of many smaller fibers like a manila rope. In other words, fusion of nanofibers caused formation of huge fibers at micron level. This observation could not be due to formation of fibers at nanoscale under the applied voltage separately at the site of Taylor cone in a single jet of polymer solution because of the excess amount of electrostatic forces than the surface tension of the solution (Boland et al., 2007). However, these nanofibers of CA/PULL 50/50 w/w% scaffolds remained as fused to each other without any separation while travelling the distance between the tip of the syringe and the collector since PULL was capable of adhering to CA (Singh et al., 2008). 20/80 w/w% CA/PULL, i.e. scaffolds had curly fibers throughout the meshes.

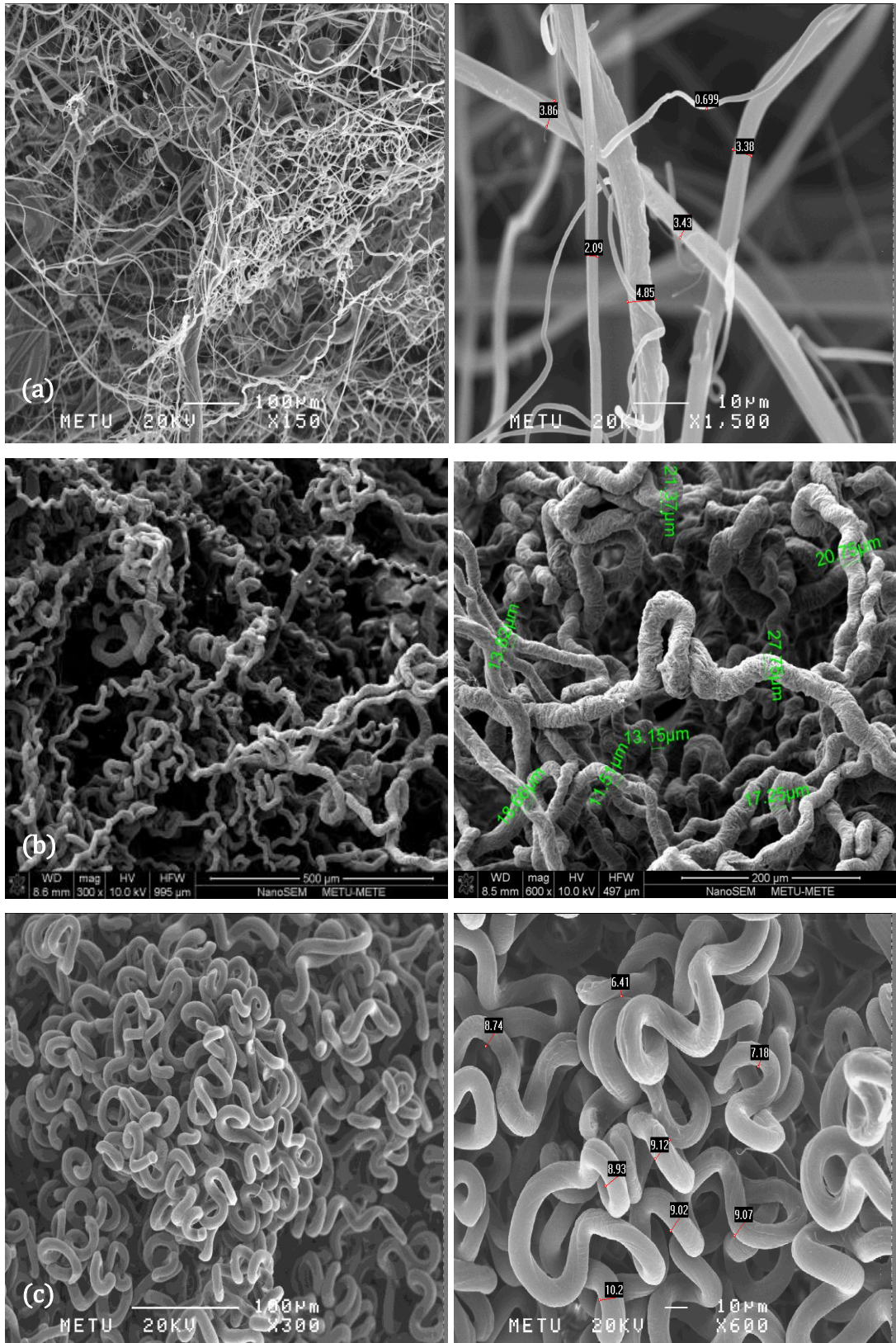


Figure 31. SEM images of CA/PULL (a) 80/20, (b) 50/50, and (c) 20/80 w/w% scaffolds electrospun with 20 wt% total polymer concentration, 8 ml/hr flow rate, 20 cm distance, and 15 kV electrical voltage.

Histogram graphs of fiber diameter distributions of CA/PULL scaffolds were constructed from 100 measurements at different regions of SEM images (Figure 32). It was found that when the amount of CA was significantly increased from 20% to 80%, fiber diameter decreased to half (Mean diameters of CA/PULL 20/80 and 80/20; 8.01  $\mu\text{m}$  and 4.32  $\mu\text{m}$ ). This result can be explained the fact that CA has a lower average molecular weight (30 kDa) compared to PULL (200 kDa). High molecular weight polymers increase the viscosity of the solution which causes an increase in fiber diameter (Sill & von Recum, 2008; Pham et al., 2006). On the other hand, the thickest fiber diameter distribution was obtained for electrospun scaffolds having equal amounts of CA and PULL contents (Mean diameter of CA/PULL 50/50; 14.19  $\mu\text{m}$ ). This result might arise from their unique interlock seen in nature (Singh et al., 2008). The effective CA and PULL attachment is probably due to fitted configurations of their OH groups forming tremendous number of H-bonds among chains.

CA/PULL with 20/80 w/w% electrospun scaffolds had more homogeneous fiber diameter distributions which ranged between 1.17 and 14.74  $\mu\text{m}$  while diameter distributions for CA-dominant (CA/PULL: 80/20) groups had a wider distributions ranging between 0.11 and 31.32  $\mu\text{m}$ . Such wider span values indicate phase separations in CA-dominant polymer solutions. In other words, no phase separation was observed in PULL-dominant solutions while CA-dominant solutions showed an obvious phase separation. The reason could be explained as huge PULL chains cannot merge into smaller CA chains in CA-dominants solutions and stay isolated and thicker fibers while shorter CA chains can merge into longer PULL chains uniformly in PULL-dominant solutions. CA/PULL 50/50 electrospun scaffolds combination showed an intermediate range for fiber diameter between 6.79 and 33.17  $\mu\text{m}$  without any phase separation. This points out that only for solutions with higher CA amount than PULL's end up with phase separation.

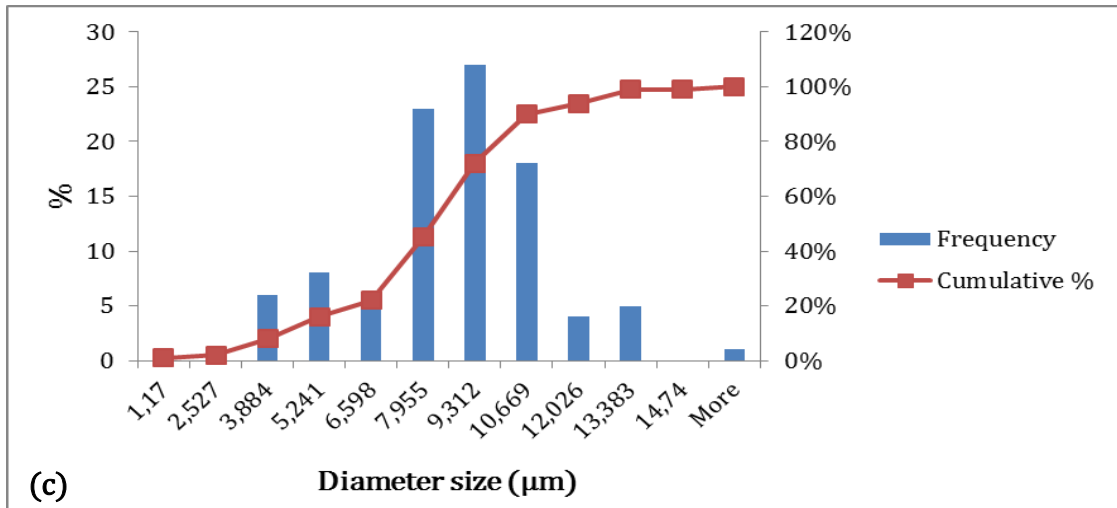
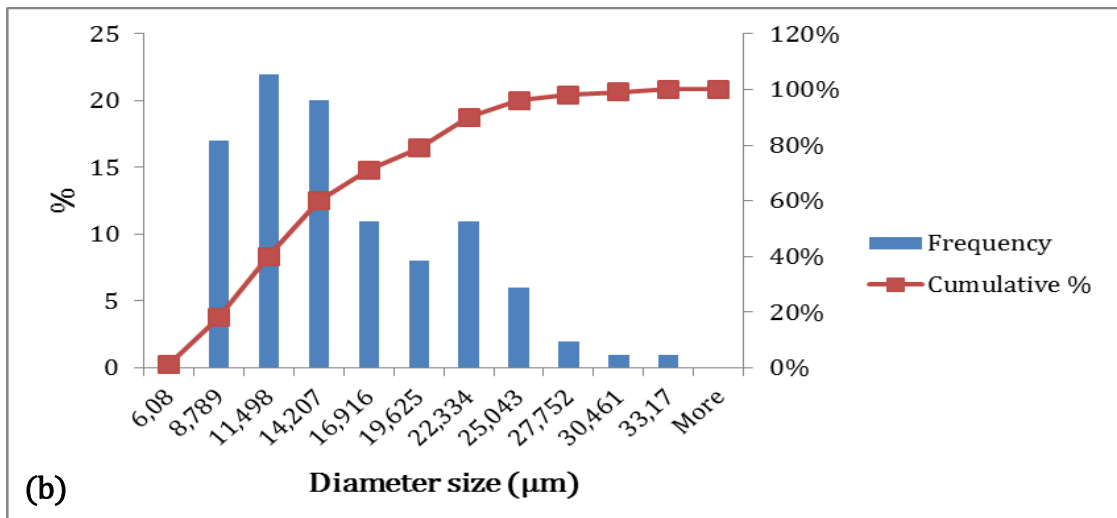
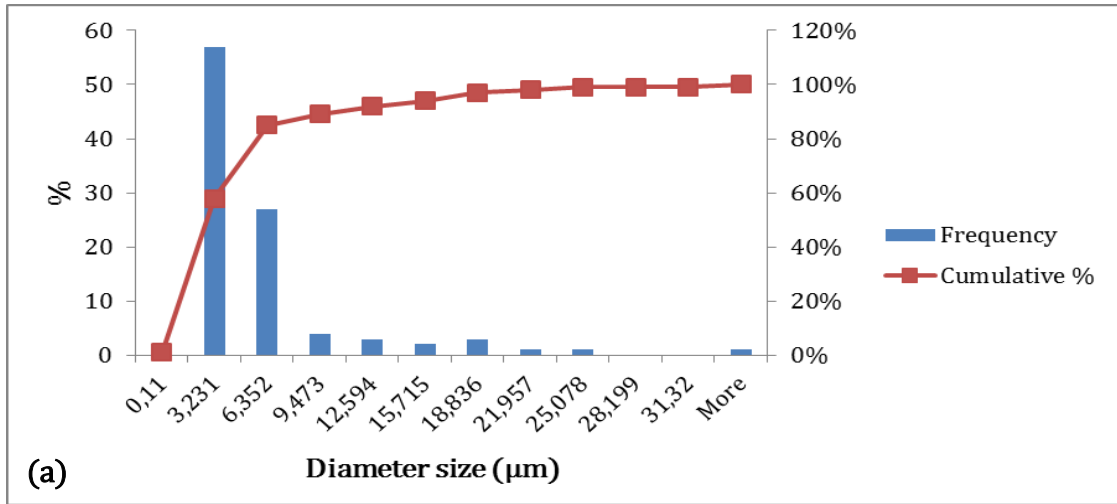


Figure 32. Fiber diameter distribution histograms of CA/PULL scaffolds; (a) 80/20, (b) 50/50, and (c) 20/80 w/w % constructed from 100 fiber measurements from SEM images.

Thus, it has been concluded that the level of homogeneity and coherence of electrospun scaffolds with the most unified CA and PULL contents was aligned as 20/80>50/50>>80/20 ratio of CA/PULL. In brief, all fibers had roughly the same morphology throughout the scaffolds of CA/PULL 20/80 and 50/50 w/w%.

### **Effect of Degradation**

During degradation tests, the optimum level of crosslinking was aimed to be determined. Possible negative effects of crosslinking (chemicals used in crosslinking, fusion of fibers during crosslinking and increased brittleness) were tried to be compensated.

Degradation studies were performed only with CA/PULL 50/50 scaffolds whose properties were the most suitable for tissue engineering applications because:

- (i) Fiber morphologies of CA/PULL 50/50 and 20/80 were more uniform without phase separation.
- (ii) Mechanical properties of CA/PULL 80/20 and 50/50 were found to be more satisfactory for scaffolding.
- (iii) Porosities of CA/PULL 50/50 and 20/80 ( $82.90\pm 6.77\%$  and  $84.04\pm 11.93\%$ ) were higher than that of CA/PULL 80/20 ( $76.19\pm 5.81\%$ ).
- (iv) Only CA/PULL 50/50 and 80/20 could withstand during degradation tests.

Different crosslinker (STMP) ratios were tested for obtaining structurally stable scaffolds. The ratio groups for PULL:STMP were 10:5, 10:3, and 10:1. Two reaction durations were used; 10 and 2 minutes for cross-linking. Dry weights of the samples and pH of incubation media were recorded once a week for 35 days. Uncrosslinked scaffolds were used as control.

Cumulative weight losses (n=4) of CA/PULL (50/50) scaffolds were plotted with respect to weeks (Figure 33). The weight loss observed for scaffolds leveled-off after the third week for most of the groups. The groups cross-linked with PULL:STMP 10:5 and 10:3 ratio for 10 minutes and 2 minutes, respectively degraded slower than all other groups.

Morphology of cross-linked and uncross-linked CA/PULL 50/50, w/w% scaffolds (with PULL/STMP 10/5 ratio for 10 minutes reaction times) was studied by SEM at the end of 35 days of degradation period (Figure 34).

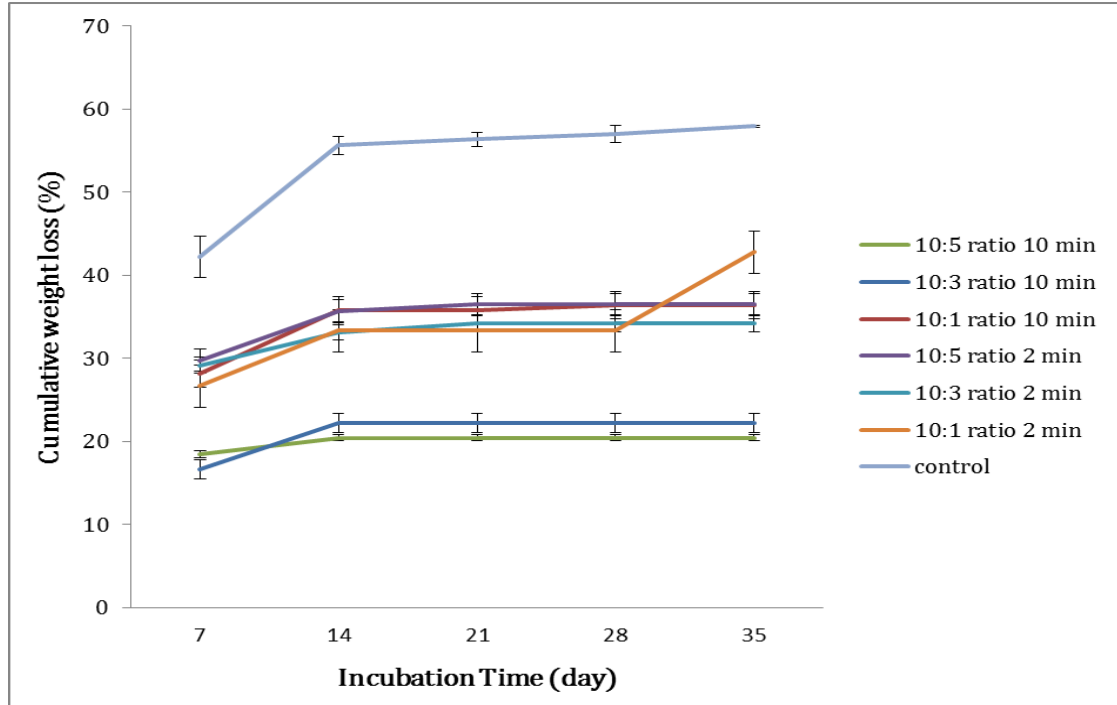


Figure 33. Cumulative percentages of weight loss of CA/PULL (50/50) scaffolds crosslinked with STMP using different reaction times (2 and 10 minutes) and PULL/STMP ratios (10:5, 10:3, 10:1).

It is clearly seen that pore size, shape and their interconnectivity changed. Pores within uncrosslinked scaffolds after degradation were more open and regular compared to the cross-linked samples which had a fused-structure overall. Fiber surfaces of uncross-linked samples after degradation were significantly altered. However, no significant change in morphology of cross-linked scaffolds was observed as it is shown in the magnified images. This observation can be explained in terms of differences in water penetration into scaffolds, thereby the hydrolytic degradation rate and removal of PULL. The cross-linked scaffolds were more likely to maintain their initial shape, and porosity since the hydrophilic PULL component was not lost.

Negative effects of crosslinking procedure might prevent the scaffolds from gaining more resistance after being cross-linked, which were;

- (i) High solubility of the PULL resulted in fusion of fibers due to aqueous environment of crosslinking, which have led to the closure of some of the pores (Singh et al., 2008). Thus, decreased water penetration into scaffolds and hydrolytic degradation took place. High solubility of the PULL also caused removal of uncrosslinked PULL polymer chains.
- (ii) Water penetration through more porous uncrosslinked scaffolds increased the hydrolytic degradation and removal of PULL component of the fibers.
- (iii) CA might be affected due to excess amount of NaOH (initiator molecule of crosslinking) treatment during cross-linking, which in fact breaks some of the hydrogen bonds that holds the cellulose structure together (Malmström & Carlmark, 2012).
- (iv) Mechanical properties of the scaffold altered. As the cross-link density increases, the fibers become more brittle (Buehler, 2008), which was not suitable for tissue engineering fields that require more flexible scaffolds in accordance with the tissue characteristics.

Crosslinking the scaffolds with STMP caused a change in the fiber morphology, porosity, and mechanical properties of the scaffolds. Therefore, it was decided to use PULL as the sacrificial component which would increase the pore size, porosity and interconnectivity in the scaffolds for tissue engineering applications.

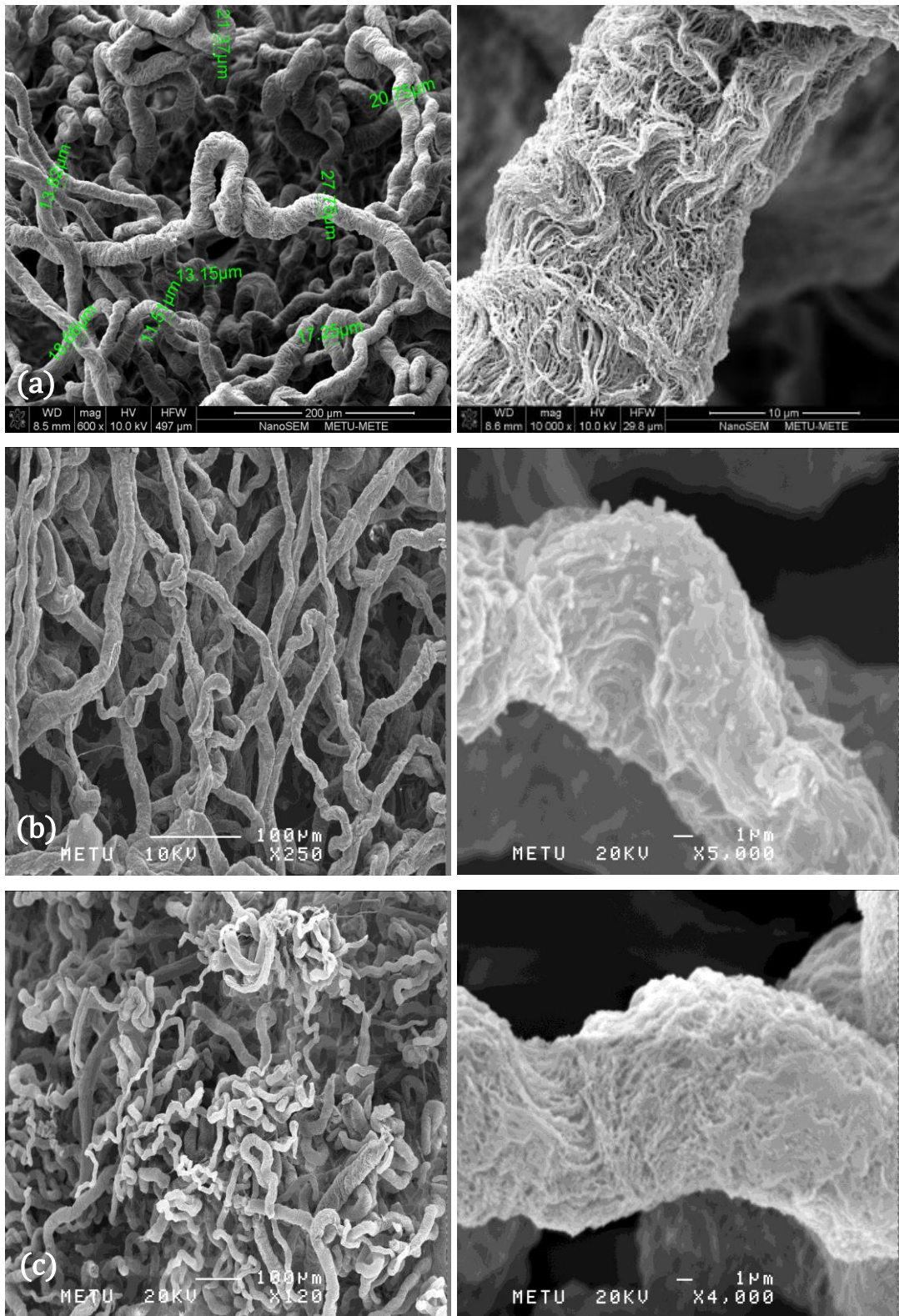


Figure 34. SEM images of CA/PULL scaffolds (50/50) (a) before degradation, (b) after degradation without crosslinking, and (c) with crosslinking. Right hand side show high magnification images of single fibers.

### Effect of Cross-linking

All scaffolds were crosslinked with PULL:STMP 10:5 for 10 minutes in order to increase the stability of structures. SEM analyses were done to understand structural changes. CA/PULL 80/20 electrospun fibers had both thicker PULL fibers and thinner CA fibers (Figure 35). After cross-linking with STMP, these scaffolds had irregular bunches of melts and bundles of fibers with a lower degree of porosity which is non-favorable for ingrowth of cells within the scaffolds (Figure 35). The thicker PULL-based fibers were melted and deformed during cross-linking. Since STMP crosslinks PULL which constitutes only 20% of these scaffolds, the fiber morphology of the scaffolds was not affected.

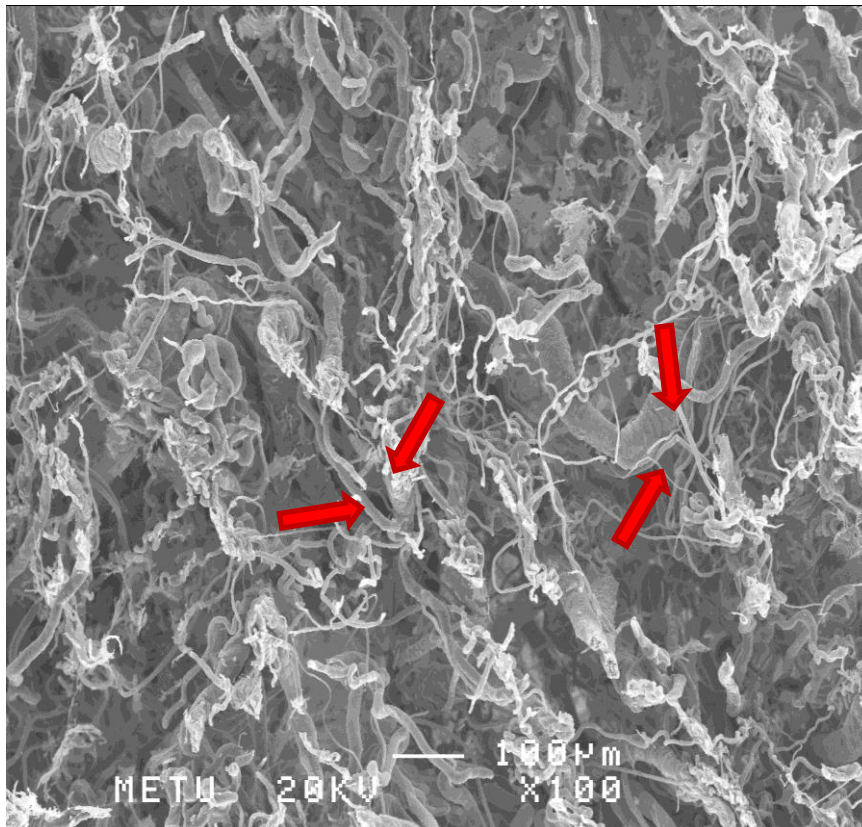


Figure 35. SEM images of CA/PULL 80/20 w/w% scaffolds after crosslinking with STMP (Arrows: thicker PULL fibers).

For CA/PULL 50/50 group, cross-linking reaction occurred more effectively. CA portion of CA/PULL (50/50) scaffolds without phase separation did not allow PULL to melt excessively with cross-linking agent there were no huge PULL regions

as in Figure 36. Wavy fibrous structures changed into more straight morphology after cross-linking. Moreover, several deformed fibers were also recognized and considered as defects indicated with arrows (Figure 36).

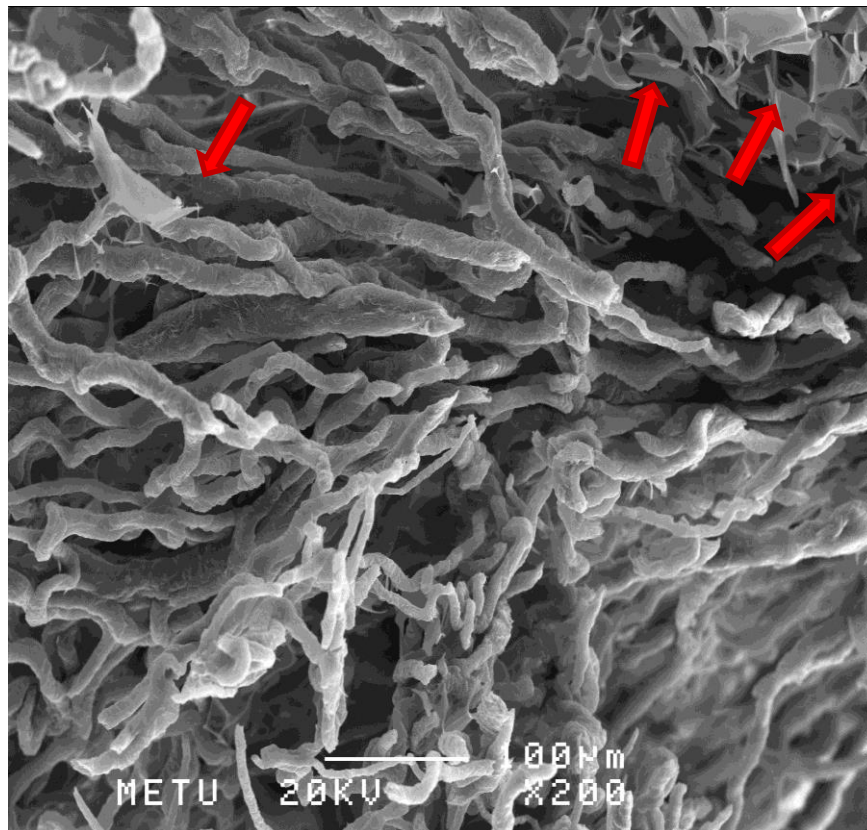


Figure 36. SEM images of CA/PULL 50/50 w/w% after crosslinking (Arrows: deformed fibers due to cross-linking).

After cross-linking, no change in the morphology of CA/PULL 20/80 scaffolds was observed inside on the 3D structure (Figure 37). These scaffolds had melt surfaces (data not shown), caused by PULL erosion on surfaces because of (i) initial contact with excess amount of water on scaffold surface during cross-linking leading to sudden melting of PULL and (ii) initial cross-linker (STMP) exposure leading to immediate cross-linking of PULL-melt causing gelation of PULL on the surface of scaffold. Therefore, cross-linked PULL-melt formed coverage on the surface of 3D scaffold which serves as a barrier for water and cross-linker entrance, sustaining the helices of PULL in the inner portions. Figure 37 shows that the inner portion of these scaffolds was not affected from crosslinking. Only some spots

pointed with arrows (Figure 37) were deformed due to water and cross-linker contact. Melt surfaces of them could be seen by naked eye.

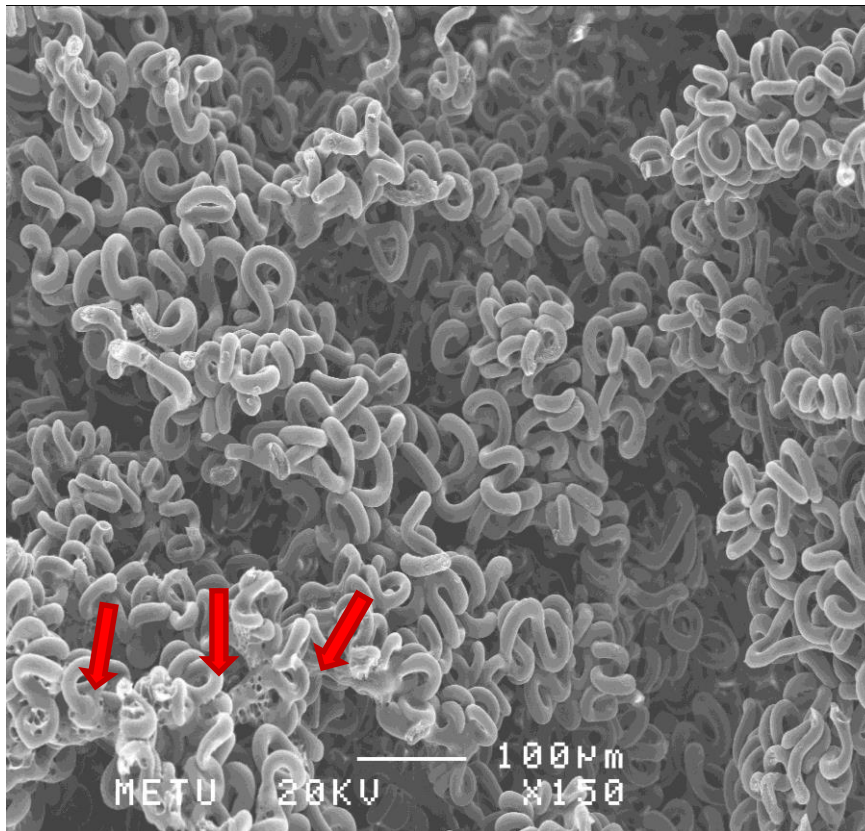


Figure 37. SEM images of cross-section view of CA/PULL 20/80 w/w% after crosslinking (Arrows: deformed fibers due to water and cross-linker contact).

In conclusion, cross-linking of PULL in CA/PULL 80/20 electrospun scaffolds was not appropriate because of thicker PULL fibers formed due to phase separation (Figure 35). For CA/PULL 50/50 scaffolds, cross-linking was achieved to some extent in spite of defects formed after crosslinking (Figure 36). Cross-linking of PULL in CA/PULL 20/80 electrospun scaffolds was not feasible and could not effectively be achieved in all regions of the scaffold (Figure 37). These scaffolds could not hold their structural integrity in PBS. Even though PULL gels can be fabricated via cross-linking as reported (Dulong et al., 2011), cross-linked PULL-dominant scaffolds could not be formed so that their fibrous structures cannot be maintained during degradation period.

### 3.1.3.3. Porosity Measurements

CA/PULL 80/20, 50/50, and 20/80 scaffolds were found to have  $76.19 \pm 5.81$ ,  $82.90 \pm 6.77$ , and  $84.04 \pm 11.93\%$  porosities via Mercury Porosimeter and Helium Pycnometer. Histograms representing pore size distributions are given in Figure 38. Despite having the lowest pore diameter values, CA/PULL 50/50 (w/w %) had the intermediate level of porosity (82.90%) among the other groups, making it still suitable for cell seeding.

The presence of the big pores, between 100 and 400  $\mu\text{m}$ , is important for bone cell penetration (Machado et al., 2007) so that CA/PULL: 20/80 scaffolds were not very ideal for bone tissue regenerations because their largest pore diameters were around 97.91  $\mu\text{m}$ . However the other ratios of CA/PULL (80/20 and 50/50) was found to be suitable with the largest pore diameters of 237.1 and 183.1  $\mu\text{m}$ , respectively.

For soft tissues, preferential pore size distributions differ according to tissue and/or material used. Endothelial cells (<80  $\mu\text{m}$ ) and vascular smooth muscle cells (63–150  $\mu\text{m}$ ) have different pore size requirements (O'Brien et al., 2005). Cell can have different pore size preferences on different materials. For example, fibroblasts preferring pores >90  $\mu\text{m}$  on silicon nitride scaffolds can also prefer pore sizes of a different range (38–150  $\mu\text{m}$ ) on different polymeric material (PLLA) (O'Brien et al., 2005). Therefore, CA/PULL 80/20, 50/50, and 20/80 scaffolds could be used for tissue engineering applications for different soft tissues according to needs of mentioned tissues.

After sacrificial fibers were removed, pore size distribution histograms were constructed for CA/PULL 80/20 and 50/50 scaffolds (Figure 39) since PULL-dominant scaffolds (CA/PULL 20/80) could not maintain their structural stability upon incubation in PBS (0.1 M, pH 7.2) at 37°C for removal of sacrificial fibers. Histograms showed that pores of CA/PULL 80/20 and 50/50 scaffolds became larger (mostly between 50-200  $\mu\text{m}$ ), which make them versatile scaffolds for tissue engineering applications from hard to soft tissues. Porosity values could not be determined due to technical problems related with mercury porosimeter and helium pycnometer.

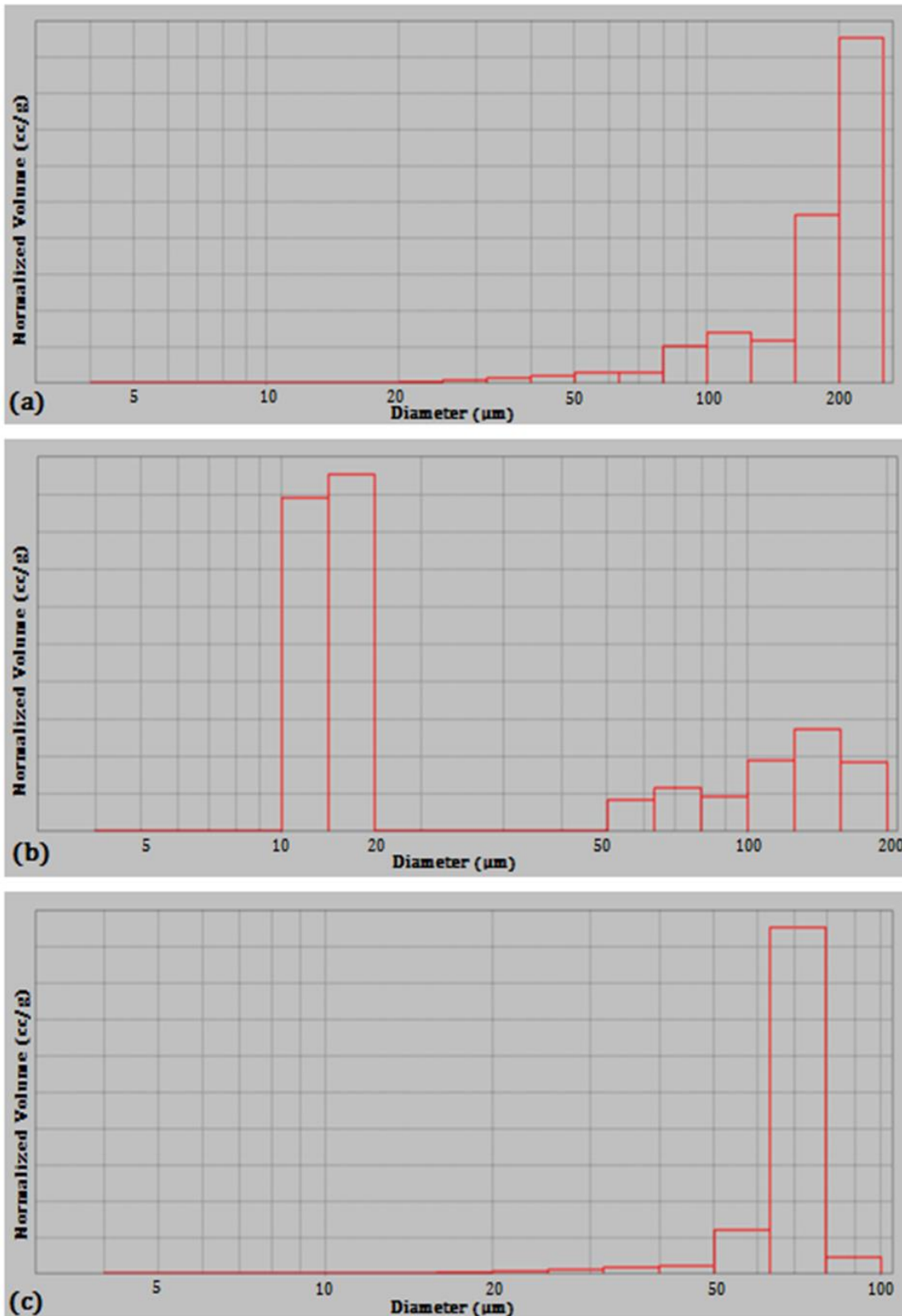


Figure 38. Histograms of pore size distributions of CA/PULL (a) 80/20, (b) 50/50, and (c) 20/80 (w/w %) scaffolds obtained by using mercury porosimeter and helium pycnometer results.

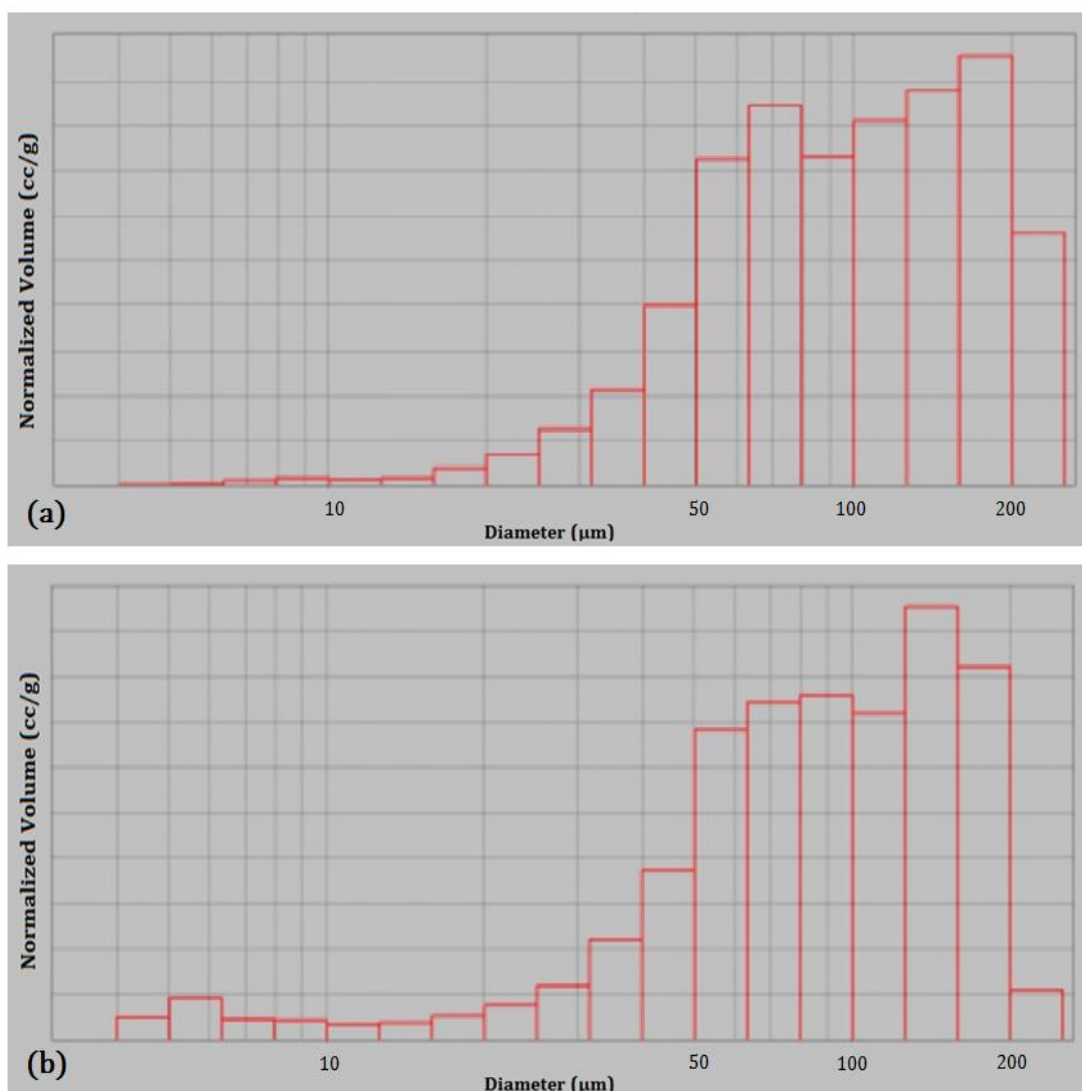


Figure 39. Histograms of pore size distributions of CA/PULL (a) 80/20 and (b) 50/50 (w/w%) scaffolds after sacrificial fiber removal in PBS at 37°C.

#### 3.1.3.4. Mechanical Testing

Mechanical properties of CA/PULL scaffolds and their cross-linked (PULL/STMP ratio 10:5) counterparts were investigated by performing compression and tensile strength tests ( $n=4$ ). In addition, CA/PULL scaffolds after sacrificial fiber removal were tested to understand which of the modifications (cross-linking or sacrificial fiber removal) makes structures mechanically more stable.

For compression tests, stress-strain curves of CA/PULL scaffolds before and after cross-linking were plotted (Figure 40). Cross-linked CA/PULL: 20/80 scaffolds

had a Young's modulus of around 2.95 MPa; however they became more brittle, which means their strain was decreased 3-folds after cross-linking. On the other hand, unlike the others having higher PULL ratio (50/50 and 20/80 w/w %) compressive strain of the cross-linked meshes of CA/PULL: 80/20 scaffolds was higher than that of their non-cross-linked ones. Furthermore, these scaffolds exhibited the highest decrease in Young's Modulus among the groups when cross-linked. It was expected that CA/PULL: 80/20 scaffolds had the highest modulus values ( $20.80 \pm 1.46$  MPa) due to its highest CA content. Moreover, its stress-strain curve showed that CA/PULL: 80/20 scaffolds were tougher (area under the curve), the ability of the material to absorb energy while plastic deformation without fracturing. Compressive properties of CA/PULL: 50/50 scaffolds were similar to those of CA/PULL: 20/80 ones.

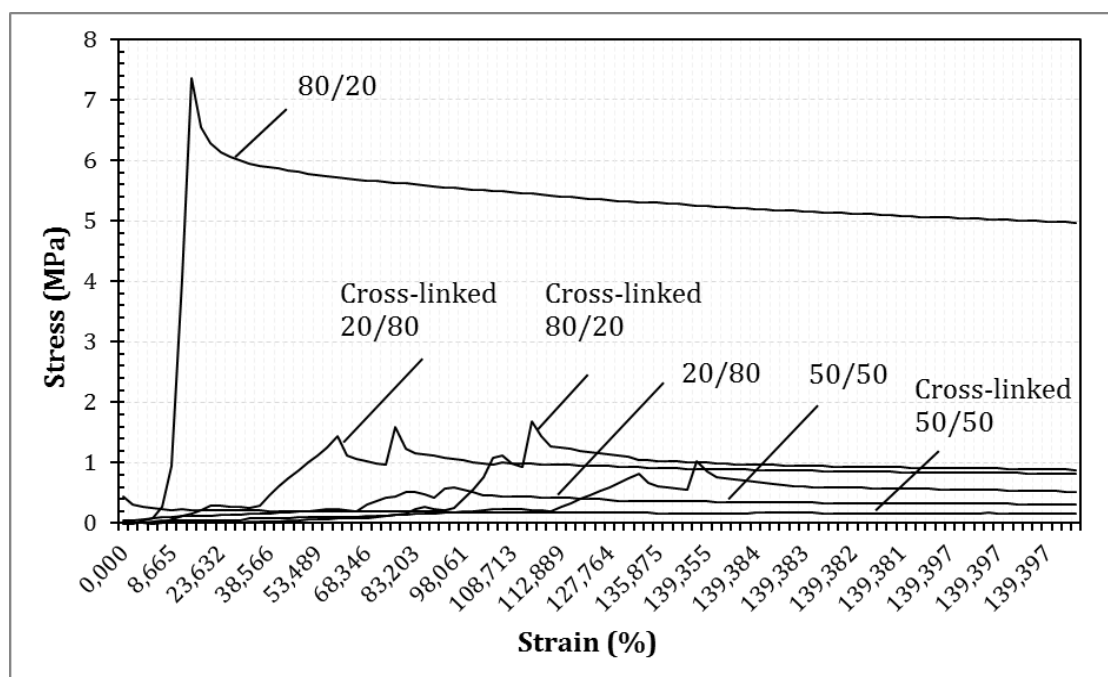


Figure 40. Compression test diagrams of CA/PULL scaffolds illustrating stress-strain curves before and after cross-linking.

Stress-strain curves obtained for tensile tests are given for CA/PULL scaffolds before and after cross-linking (Figure 41). Cross-linked CA/PULL 20/80 seemed to have the highest Young's modulus ( $5.38 \pm 0.09$  MPa). However, their surface was cross-linked only, not the inner regions. Since their cross-linked surfaces

were in melt form, their fibrous and porous structures were deformed. Thus, they were not proper as tissue engineered-scaffolds. This result only proved that cross-linked PULL makes the structure strong against tensile forces. Apart from cross-linked CA/PULL 20/80, CA/PULL 50/50 scaffolds had the highest elastic modulus ( $2.91\pm 0.21$  MPa) among all and also retained their porous form after being cross-linked. Furthermore, strain values of cross-linked CA/PULL 50/50 scaffolds were improved from  $22.2\pm 0.01\%$  to  $33.93\pm 2.18\%$ . Other CA/PULL scaffolds, in particularly 20/80 and 80/20 ratio groups, were split almost fiber by fiber indicated as multiple peaks, not like a well-integrated and united fibrous structure.

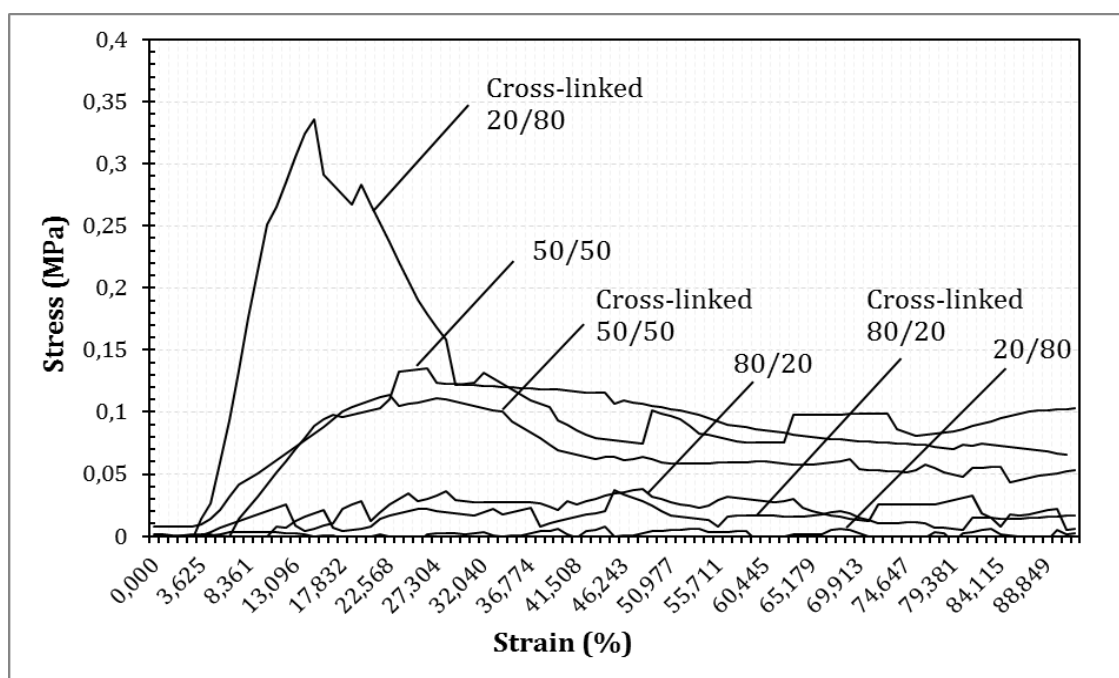


Figure 41. Tension test diagrams of CA/PULL scaffolds illustrating stress-strain curves before and after cross-linking.

Instead of cross-linking treatment, sacrificial fiber removal was used as an alternative solution for obtaining mechanically stronger scaffolds. After sacrificial fiber removal in PBS (0.1 M, pH 7.2), mechanical tests were performed for CA/PULL 80/20 and 50/50 scaffolds since CA/PULL 20/80 scaffolds could not be maintained in PBS. The stress-strain curves showed that CA/PULL 80/20 scaffolds after removal of sacrificial fibers were stronger than 50/50's in compression and tension profiles (Figure 42).

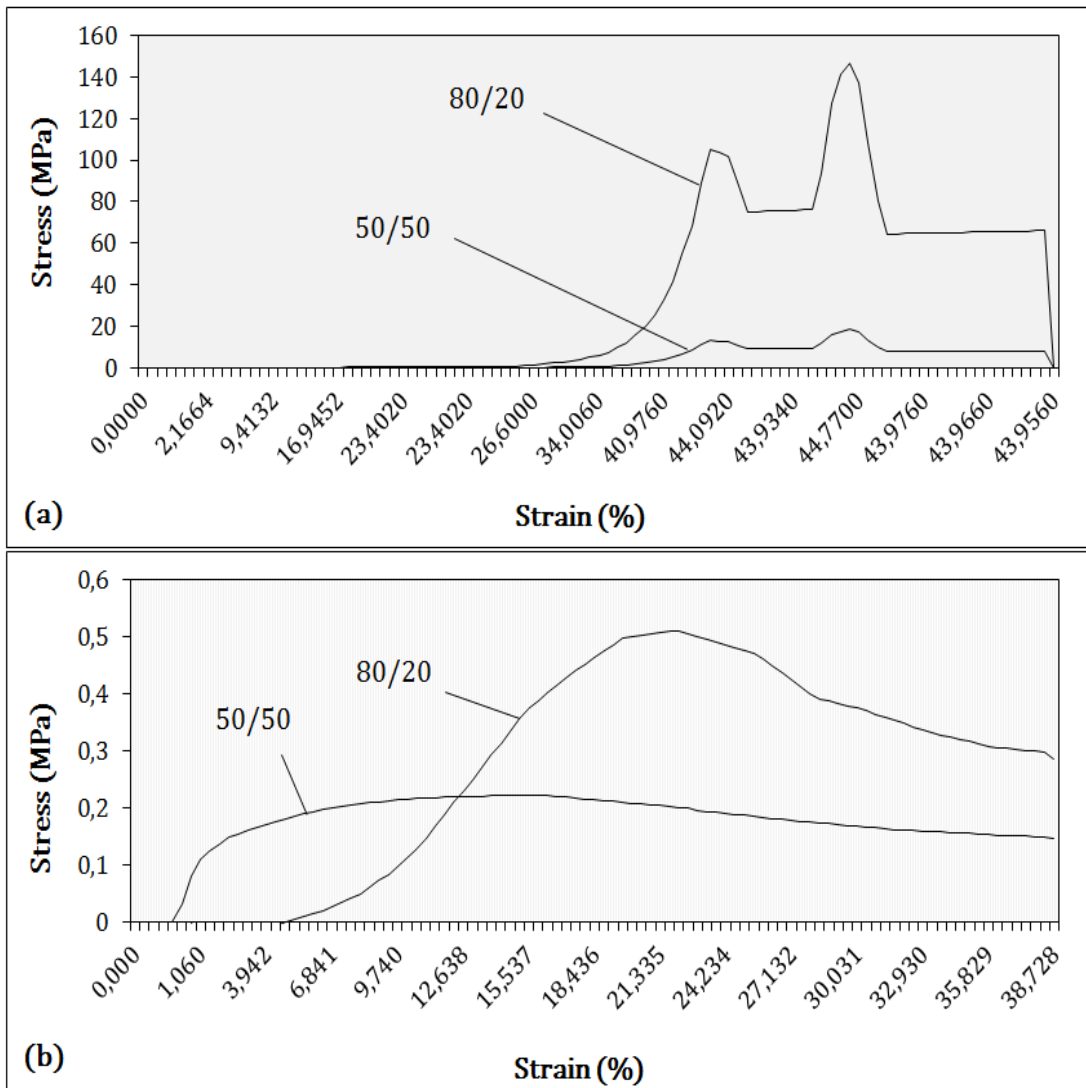


Figure 42. (a) Compression and (b) Tension test diagrams of CA/PULL scaffolds illustrating stress-strain curves before and after cross-linking.

Both compression and tension tests showed that all tested CA/PULL groups after removal of fibers had significantly improved compression strength and UTS values when compared to either unmodified or cross-linked counterparts (Table 3). Young's moduli of CA/PULL 80/20 scaffolds after sacrificial fiber removal were found as  $11.18 \pm 0.36$  MPa which is in between that of cross-linked 80/20 scaffolds ( $5.50 \pm 0.79$  MPa) and that of unmodified 80/20 ones ( $20.80 \pm 1.46$  MPa).

Table 3. Mechanical properties of CA/PULL scaffolds.

CA/PULL (w/w %)	Compression Test			Tension Test		
	Compressive Strength (MPa)	Elastic modulus (MPa)	Strain (%)	UTS (MPa)	Elastic modulus (MPa)	Strain (%)
CA/PULL						
80/20	7.36±0.61	20.80±1.46	92.55±7.91	0.04±0.17	0.43±0.06	55.56±7.05
50/50	0.60±0.07	4.96±0.91	86.45±4.15	0.13±0.08	2.91±0.21	22.2±0.01
20/80	1.03±0.20	2.94±0.01	92.93±5.08	0.008±0.0	0.15±0.04	91.69±2.69
Cross-linked CA/PULL						
80/20	1.68±0.09	5.50±0.79	95.85±1.56	0.04±0.56	0.40±0.06	63.85±5.01
50/50	0.43±0.01	4.13±0.68	27.64±2.89	0.11±0.02	1.54±0.13	33.93±2.18
20/80	1.59±0.36	2.97±0.09	22.00±4.96	0.34±0.24	5.38±0.09	48.38±3.96
CA/PULL after Sacrificial Fiber Removal						
80/20	146.9±9.24	11.18±0.36	44.87±3.16	0.51±0.01	0.02±0.00	12.07±1.21
50/50	18.36±2.35	1.17±0.02	8.97±0.65	0.22±0.00	0.03±0.01	38.73±5.46
20/80	-	-	-	-	-	-

To sum up compression tests, compressive strength of scaffolds increased with increase in CA/PULL ratio (elastic moduli: 20/80<50/50<80/20) and CA/PULL 80/20 scaffolds after sacrificial fiber removal were determined as the strongest scaffolds during tests (146.9±9.24 MPa). Compressive strength values of all groups were ranged between 0.43 and 146.9 MPa which provide required strength for spongy bone, cortical bone, cartilage and skin (Rezwan et al., 2006). On the other hand, CA/PULL 80/20 scaffolds without any modifications showed the outstanding elastic modulus value (20.80±1.46 MPa) during compression tests. This could be explained by the fusion of PULL fibers due to PULL solubility during cross-linking

in aqueous environment that damaged the fibrous structure, which made the scaffold weaker (Singh et al., 2008). Second reason could be breakage of some of the hydrogen bonds that holds the cellulose structure together due to NaOH exposure during cross-linking (Malmström & Carlmark, 2012).

To sum up tension tests, CA/PULL 80/20 and 50/50 scaffolds after sacrificial fiber removal had the highest UTSs, respectively. Secondly, unmodified CA/PULL 50/50 scaffolds can be stated that they resisted tensile stress best. When they were cross-linked, UTS value decreased slightly and half of elastic modulus was lost. This means that cross-linking process somehow weakened the scaffolds mechanically. Therefore, the cross-linked CA/PULL scaffolds may not be advantageous for the areas with the expectations of dual superiorities because the strain and brittleness are opposite properties. Alternatively, CA/PULL scaffolds were suitable for use after removal of sacrificial fibers (PULL mass) otherwise the unwanted consequences of cross-linking should be compensated.

### **3.1.4. Cell Culture Studies**

#### **3.1.4.1. Cell Viability Measurements**

At different time periods, Alamar Blue cell viability assay was conducted to study the attachment and proliferation of the cells on electrospun scaffolds. Cells were seeded at an initial cell seeding density of 80000/cm<sup>2</sup> and were incubated for 1<sup>st</sup>, 4<sup>th</sup>, 7<sup>th</sup>, and 14<sup>th</sup> days. Reduction percentages of alamar blue indicating cell viability were graphed (Figure 43). Cells plated on polystyrene culture wells (TCPS) served as controls.

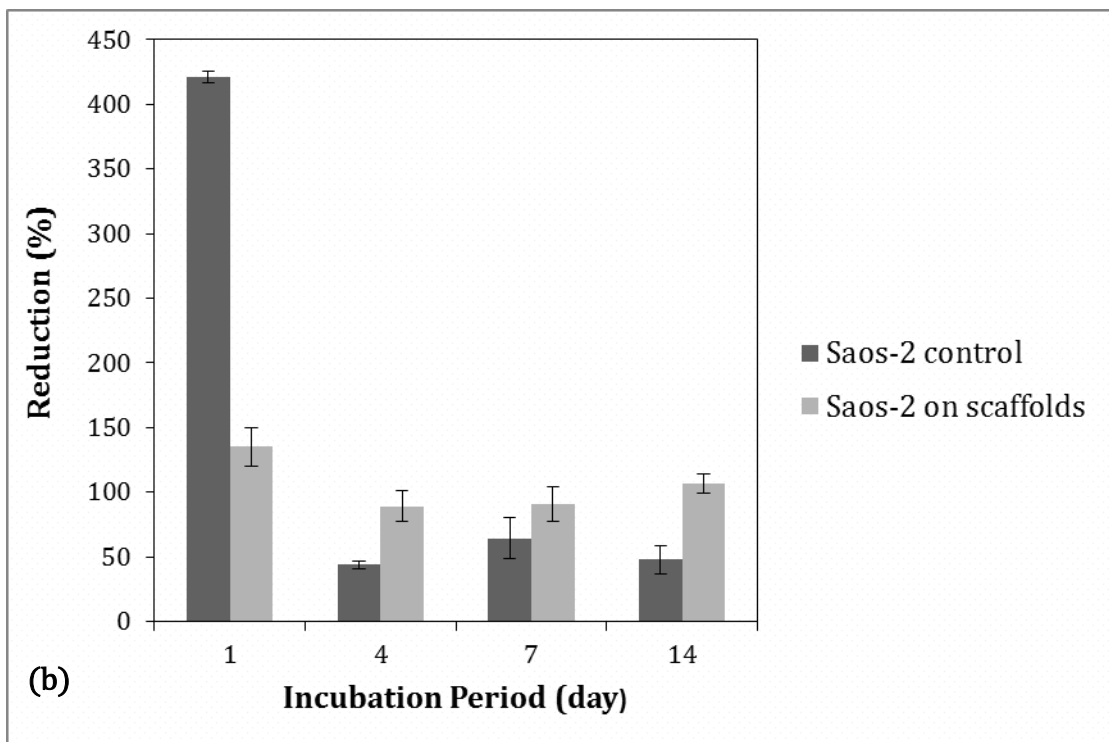
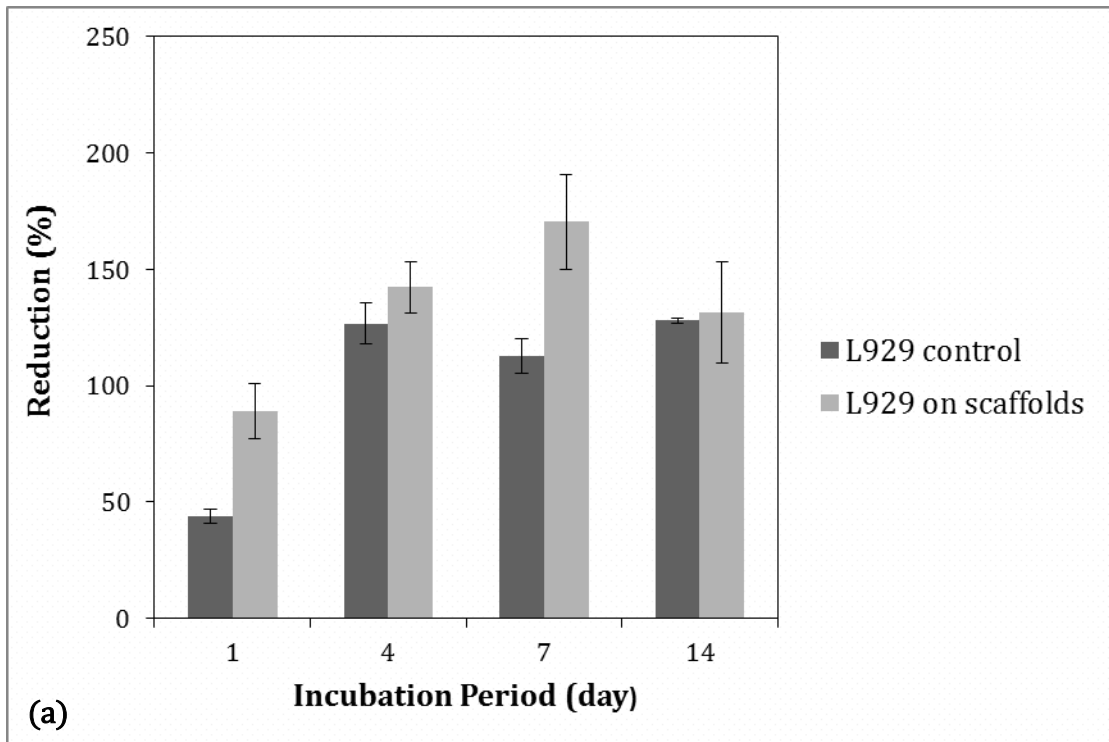


Figure 43. Alamar Blue-reduction levels of CA/PULL 50/50 w/w % scaffolds with cells of (a) L929 and (b) Saos-2 for specific incubation times (n=3).

L929 seeded on TCPS had similar reduction levels for 4<sup>th</sup>, 7<sup>th</sup>, and 14<sup>th</sup> days. This shows confluency period of wells. On the test wells, reduction percentages of Alamar Blue showed that proliferation of L929 increased until 7 days then decreased slightly. L929 seeded on TCPS exhibited no decline after 7<sup>th</sup> day. This decline might be caused by limited cell migration through pores of the scaffold. In other words, cells probably proliferated on the surface of the scaffold. After 7 days, they might not continue to grow and began to die due to the inadequate space on the surface of the scaffold.

Saos-2 seeded on TCPS had higher reduction level on 1<sup>st</sup> day and similar reduction levels for 4<sup>th</sup>, 7<sup>th</sup>, and 14<sup>th</sup> days. After 1<sup>st</sup> day, Saos-2 cells might need place to grow. On the test wells, reduction percentages of Alamar Blue showed that proliferation of Saos-2 was maintained until 14<sup>th</sup> day. This result was probably due to Saos-2 cells could penetrate inside the 3D-scaffold and grow within.

Reduction percentages showed that all cells on the scaffolds proliferated more than the cells on control wells except for the results of Saos-2 groups at 1<sup>st</sup> day (Figure 43). This exception might arise from pipetting errors during cell seeding.

The cell viability percentages were calculated by considering proliferation of control wells as 100% (Figure 44). It shows that both types of cells were proliferating on the scaffolds. However, L929 cell line exhibited a decreased profile of cell viability after the 1<sup>st</sup> day whereas that of Saos-2 cell line increased during following days.

It can be explained with tissue type-difference of cells (L929 and Saos-2) mentioned before. Since L929 is a cell line of 2D skin tissue, it grew on the 2D surface of the scaffold and probably became confluent at 4<sup>th</sup> day. On the 4<sup>th</sup> and 7<sup>th</sup> days, they could not proliferate because there was no place left on the surface sites of the scaffolds. On the other hand, Saos-2 is a cell line of 3D bone tissue thus they could migrate through the pores of the 3D scaffolds and grow inside.

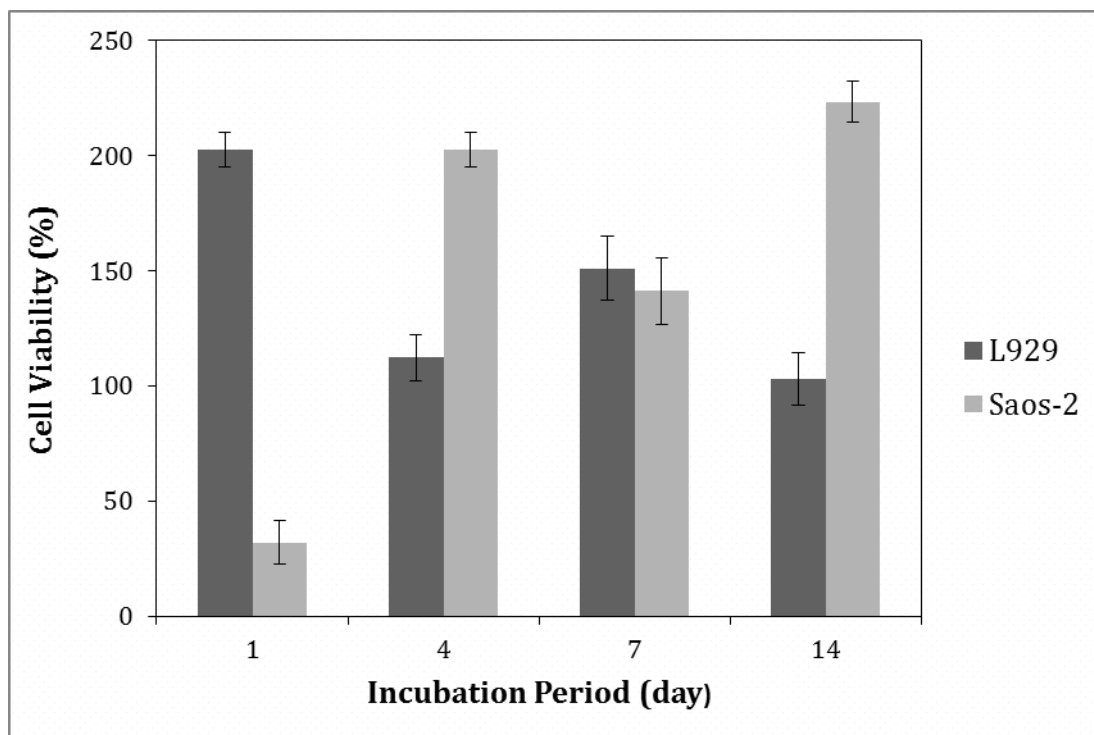


Figure 44. Cell viability levels of CA/PULL 50/50 (w/w) scaffolds with cells of L929 and Saos-2 for specific incubation times (Control groups: 100%).

The cell viability results can also be explained with different doubling times of cells L929: 32 h and Saos-2: 45.7 h (Karakecili et al., 2007; Jia et al., 1999). Shorter doubling time of L929 might cause cells to reach their confluency condition faster so that cells could not proliferate and some even died, leading to further proliferation of cells towards the place left from death cells. On the other hand, longer doubling time of Saos-2 probably caused a gradual increase in cell number of Saos-2 groups shown in Figure 44.

#### 3.1.4.2. Cell Morphology Analysis

Morphology of fixed Saos-2 cells on electrospun scaffolds was examined after 1 day of incubation with SEM. Figure 45 showed that there was no recognizable cells on the unmodified CA/PULL 50/50 scaffolds at the 1<sup>st</sup> day of incubation while cells proliferated on cross-linked scaffolds. Magnified image of the cross-linked scaffold indicated that cells extended from one fiber to another.

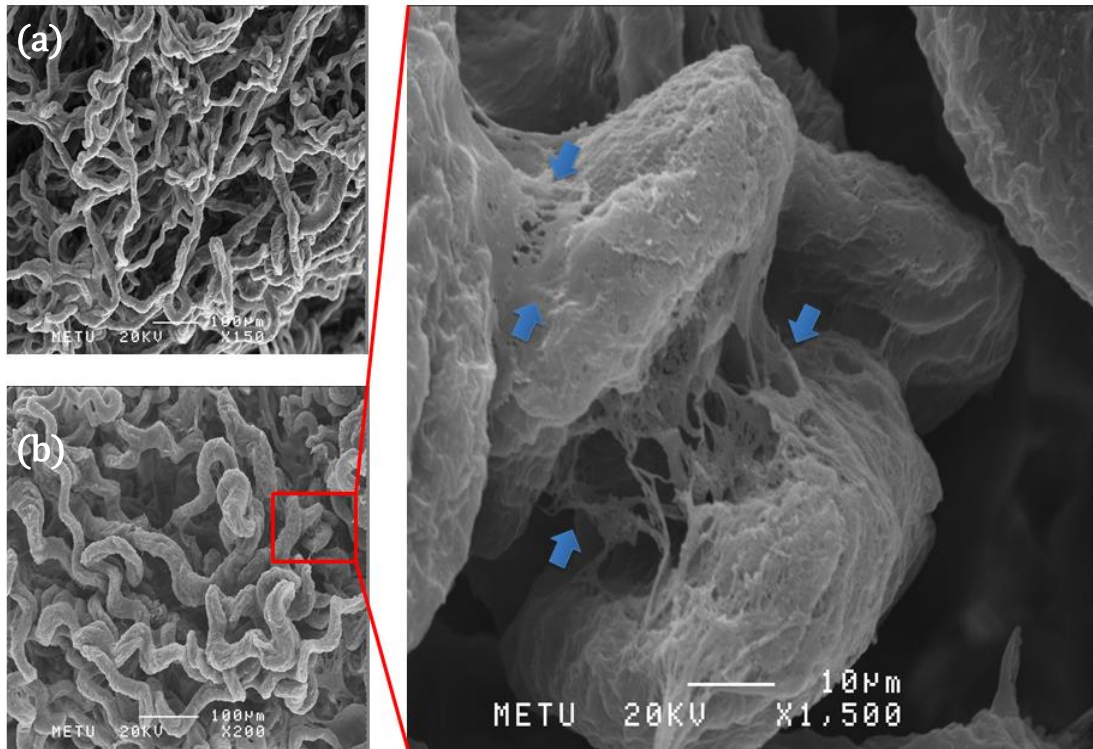


Figure 45. SEM images of (a) unmodified and (b) cross-linked CA/PULL 50/50 scaffolds at 1<sup>st</sup> day after Saos-2 cell seeding. Arrows: Cells extending from one fiber to another fiber.

### 3.1.4.3. Cell Migration Analyses through 3D Scaffolds

Cell migration studies were conducted using confocal laser scanning microscopy. Saos-2 cells cultured on scaffolds were fixed with formaldehyde after 35 day of incubation. Fixed scaffolds were stained with PI (Invitrogen, USA) for nuclei and FITC (Invitrogen, USA) for actin filaments of the cells (Mandal & Kundu, 2009). Cell-nuclei were stained successfully in red (Figure 46). However, counterstaining of actin with FITC also affected background fibers nonspecifically, thus fibers were shown green. Result showed that cells were able to live on the scaffolds for 35 days and penetrate inside of the scaffolds.

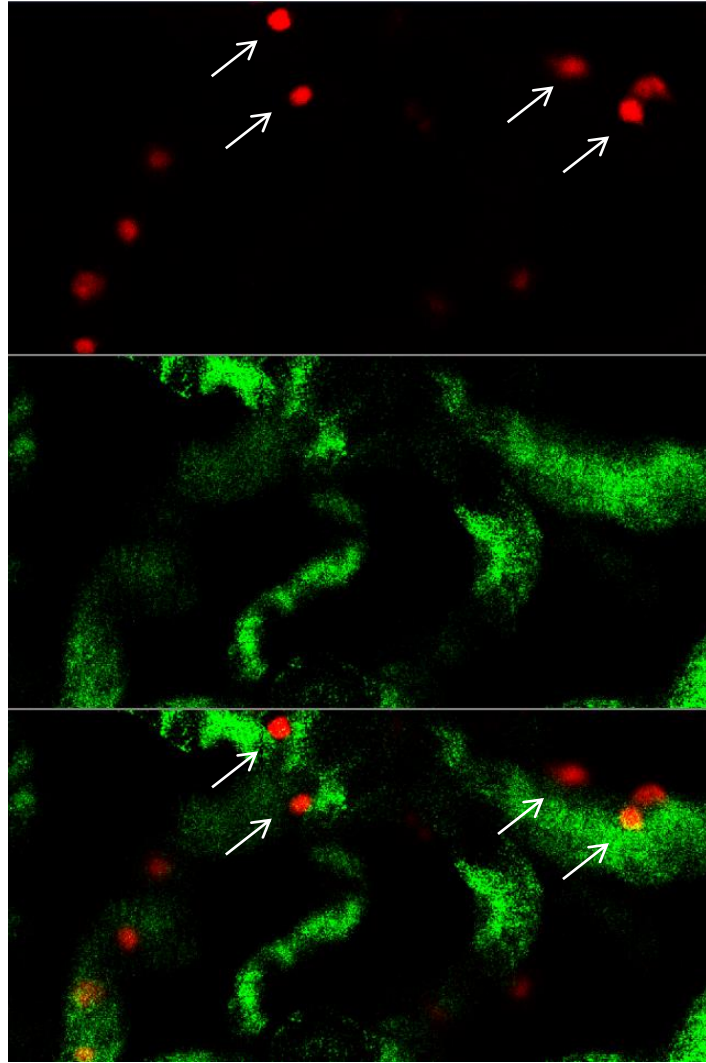


Figure 46. Confocal Laser Scanning Microscope images of cross-linked CA/PULL (50/50) scaffolds with Saos-2 cells 35-day after cell seeding (Arrows: Cells adhere to fibers). RED: Cell nuclei stained with PI. GREEN: Fibers of scaffold counter stained with FITC.

## **3.2. Part II: Bacterial Cellulose – Based Scaffolds**

### **3.2.1. BC Production**

During BC production from *G. xylinum* species, 0.06 g bacteria cells seeded at the beginning yielded 1 g cellulose each time.

### **3.2.2. Pretreatments on BC**

Cellulose is a stiff molecule and has close chain packing with numerous intermolecular and intramolecular hydrogen bonds (Wu et al., 2004). Therefore, it is not easily-processible for solubilization. Prior to electrospinning, BC needs further modification because of its crystalline regions in the polymeric chains. These regions render BC highly resistant to dissolution by preventing necessary chemical interactions such as solvent-polymer interactions. In addition, some researchers claimed that chemical modification is needed for biodegradation (Samios et al., 1997). Therefore, several treatments, namely acetylation, powder size reduction by mixer milling and autoclave treatments, and sulfuric acid exposure of BC were performed in this study.

Acetylation was the first chemical modification on BC pellicles. Since commercial CA is ready to dissolve in DMAc/DMSO solvent system, BC was acetylated to produce CA for different degrees of substitution. For acetylation of BC, ratios of acetic anhydride to acetic acid used were 1:10, 2:10, and 3:10. In other researches, it was demonstrated that the degree of substitution (DS) ranges from 1.5 to 3.0 when the ratio of acetic anhydride to acetic acid was varied between 1:10 and 10:10 (Kim et al., 2002). In that point of view, our aim in was to acetylate BC at DS: 2.5 because CA purchased with a DS of 2.49 is soluble in common solvents (Puls et al., 2010).

Acetylation treatments were completed. Average number of acetyl groups per anhydro-D-glucose unit of cellulose, i.e. DS, was calculated via the back titration method (Samios et al., 1997) (Figure 47) and compared with literature. DS values of our BC series after acetylation lied between 0.2 and 2.9 in agreement with literature findings (Kim et al., 2002). However, the addition of acetic anhydride more than 2

ml was not correlated to the values of literature showing the DS must stay around 3 (Kim et al., 2002). In our study, DS values decreased as the amount of acetic anhydride increased. This result might arise from the breakage of polymer chains due to excessive exposure. Cellulose acetates having a DS value of between 0.64–2.74 (corresponding to 21–91% acetylation) were produced using this system (Abbott et al., 2005).

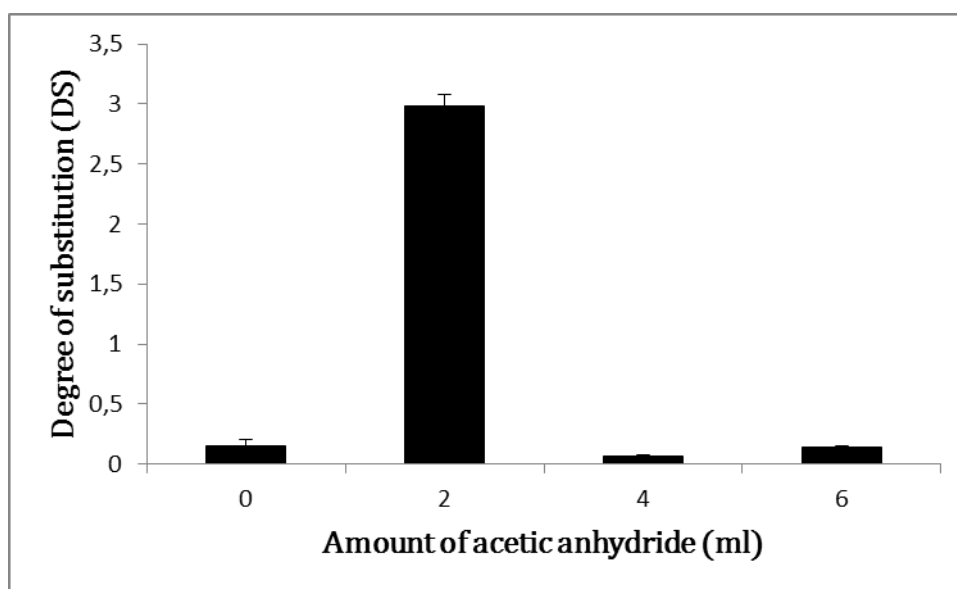


Figure 47. DS values of acetylated BC groups treated with different amounts of acetic anhydride.

To validate acetylation, FTIR-ATR analysis was conducted and spectra of acetylated BC groups were compared to spectrum of native BC (Figure 48). Three newly emerged peaks of samples were characteristics of acetylated BC; (i) the carbonyl C=O stretching vibration at  $1735\text{--}1755\text{ cm}^{-1}$  (C=O), (ii) the methyl in-plane bending in  $\text{--O(C=O)CH}_3$  at  $1374\text{ cm}^{-1}$  (C–H), and (iii) the C–O stretching of acetyl group at  $1235\text{--}1250\text{ cm}^{-1}$  (C–O) (Hu et al., 2011; Tang et al., 2013; Tomé et al., 2011; Xu et al., 2013). On the other hand, non-acetylated BC with zero DS exhibited no peak in the same regions as a negative control. Furthermore, areas under the peaks belonging to all acetylated groups of BC (2, 4, and 6 ml) were measured as approximately the same pointing out the fact that all acetylated groups had the similar DS values. Hence, FTIR-ATR results indicated that the titration results with the dramatic decreases in DS values of groups above 2 ml acetic anhydride addition

were inconsistent with the identified FTIR-ATR spectra of them. It was probably caused by experimental errors during back titrations.

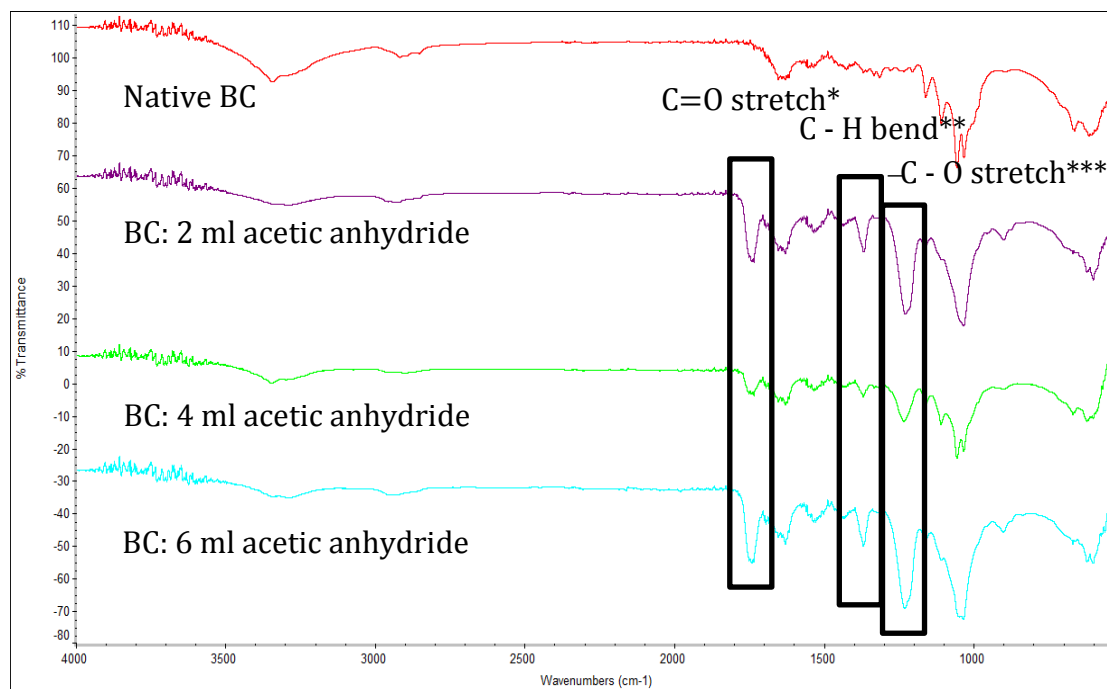


Figure 48. FTIR-ATR spectra of native BC and BC acetylated with 2 ml, 4 ml, and 6 ml acetic anhydride (\*carbonyl stretching, \*\*methyl in plane bending, and \*\*\*acetyl group stretching).

Finally, BC samples acetylated with 2 ml acetic anhydride which had the highest DS were used for electrospinning; however, the solutions could not be electrospun due to inadequate dissolution of BC powders and limited fiber formation under applied voltage. Therefore, other ways to improve processability of BC pellicles were tried like powder size reduction by mixer milling and autoclave treatments, and/or sulfuric acid exposure of BC and then freeze dried.

### 3.2.3. Electrospinning of BC/PULL

Due to presence of crystalline regions in BC, electrospinnability of BC/PULL solutions was difficult. After sulphuric acid treatment, BC was electrospun with PULL. Different ratios of BC/PULL (1/1 w/w %) solutions were prepared for electrospinning (Table 4). BC/PULL (50/50 w/w %) dissolved in NMMO/DMAc/DMSO (2:1:1, volume ratio) were electrospun using 10-14% of

polymer concentrations via wet electrospinning method. The applied voltage, tip-to-collector distance, and flow rate were fixed as 20 kV, 12 cm, and 1 ml/hr. Produced scaffolds were removed from the ethanol bath, freeze-dried and analyzed (Figure 49).

Table 4. Electrospinning behavior of BC/PULL (1/1 w/w %) solutions.

NMMO/DMAc/DMSO (Volume Ratio)	Total Polymer Concentration (%)	Solution Property	Electro-spinning Behavior
1/0/0	5	Highly translucent & Highly viscous	–
8/1/1	5 & 6		–
2/1/1	5, 10, 12, & 14	Translucent & Viscous	+
1/2/2	5, 7, & 10	Transparent w/BC particles & Slightly viscous	±
0/1/1	5, 7, & 10		± (wetting)

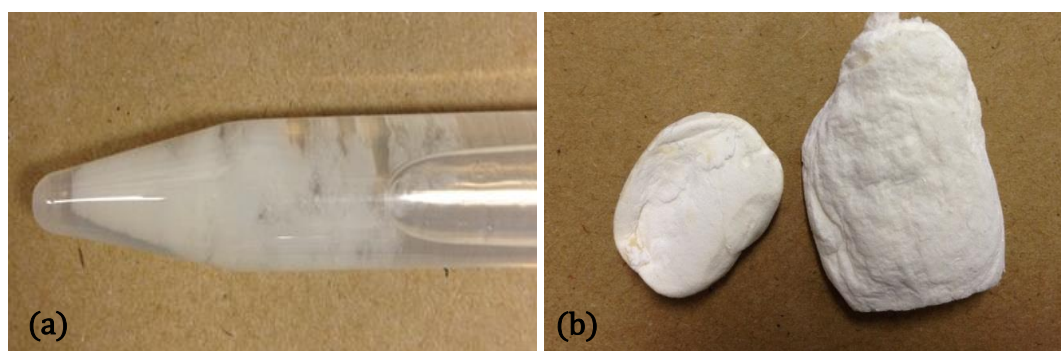


Figure 49. Electrospun BC/PULL scaffolds (a) collected in etOH bath and (b) after freeze-drying.

When high percentage of PULL (50%) was used because of its superior electrospinnability, collapse of the scaffolds in aqueous media even after cross-linking with STMP occurred. Therefore, gelatin (GEL) was added to the polymer

composition oxidized-BC/oxidized-PULL/GEL at various ratios (Table 5) were used as polymer composition. The solvents for dissolving both gelatin (GEL) and oxidized PULL (ox-PULL) were the same; NMMO/DMAc/DMSO (2:1:1, volume ratio). Apart from ox-PULL and GEL, solubility of ox-BC was not considered during making a choice for the solvent because ox-BC powders were always found as suspension.

Table 5. Electrospinning behavior of BC/PULL/GEL polymer solutions in NMMO/DMAc/DMSO 2/1/1 (volume ratio).

BC/PULL/GEL Weight Ratio	Total Polymer Concentration (%)	Solution Property	Electrospinning Behavior
1/1/1	5	Opaque & Highly viscous	–
1/2/2	5 and 7.5	Opaque & Highly viscous	–
1/2/4	5 and 7.5	Translucent & Viscous	–
1/10/10	5, 7.5, and 10	Transparent w/BC particles & Viscous	±
1/10/20	5, 7.5, and 10		±

First, 5-10% ox-PULL/GEL 50/50 (w/w) solutions in NMMO/DMAc/DMSO (2:1:1, volume ratio) were used for optimization of electrospinning parameters. They were electrospun under 11-16 kV electrical voltages with 2-10 ml/hr flow rates from 12 cm distance to ethanol bath. Then, the solutions of ox-BC/ox-PULL/GEL (1/10/10, weight ratio) at different polymer concentrations (5-10%) in NMMO/DMAc/DMSO (2:1:1, volume ratio) were tried to be electrospun using different electrical voltages, flow rates, and distances to ethanol bath. Although jet formation from those solutions was observed under 12-16 kV electrical voltage and collected as fibrous meshes, they were not considered as successful electrospun

structures due to discontinuous and instable fiber formation. Moreover, BC powders in the solution were accumulated at the bottom of the syringe in a short period of time, preventing the solution from passing through the needle completely.

### **3.2.4. Characterization of BC/PULL Scaffolds**

#### **3.2.4.1. Scanning Electron Microscopy (SEM)**

SEM analysis were conducted for electrospun BC/PULL (50/50 w/w %) scaffolds dissolved in NMMO/DMAc/DMSO (2:1:1, volume ratio) with 10, 12, and 14 % of polymer concentrations (Figure 50). The applied voltage, tip-to-collector distance, and flow rate were fixed as 20 kV, 12 cm, and 1 ml/hr, respectively. Fiber diameters of the electrospun structures increased as the total polymer concentration was increased. On the other hand, the images showed that BC particles were found in suspension in the electrospinning solution and bead formation (if there were any) during electrospinning were not distinguished from each other. However, BC powders were supposed to be enclosed with PULL and integrated within fibrous architecture having thicker fiber diameters ( $> 8\mu\text{m}$ ) since those of cellulose acetate-based scaffolds were around  $11\mu\text{m}$ .

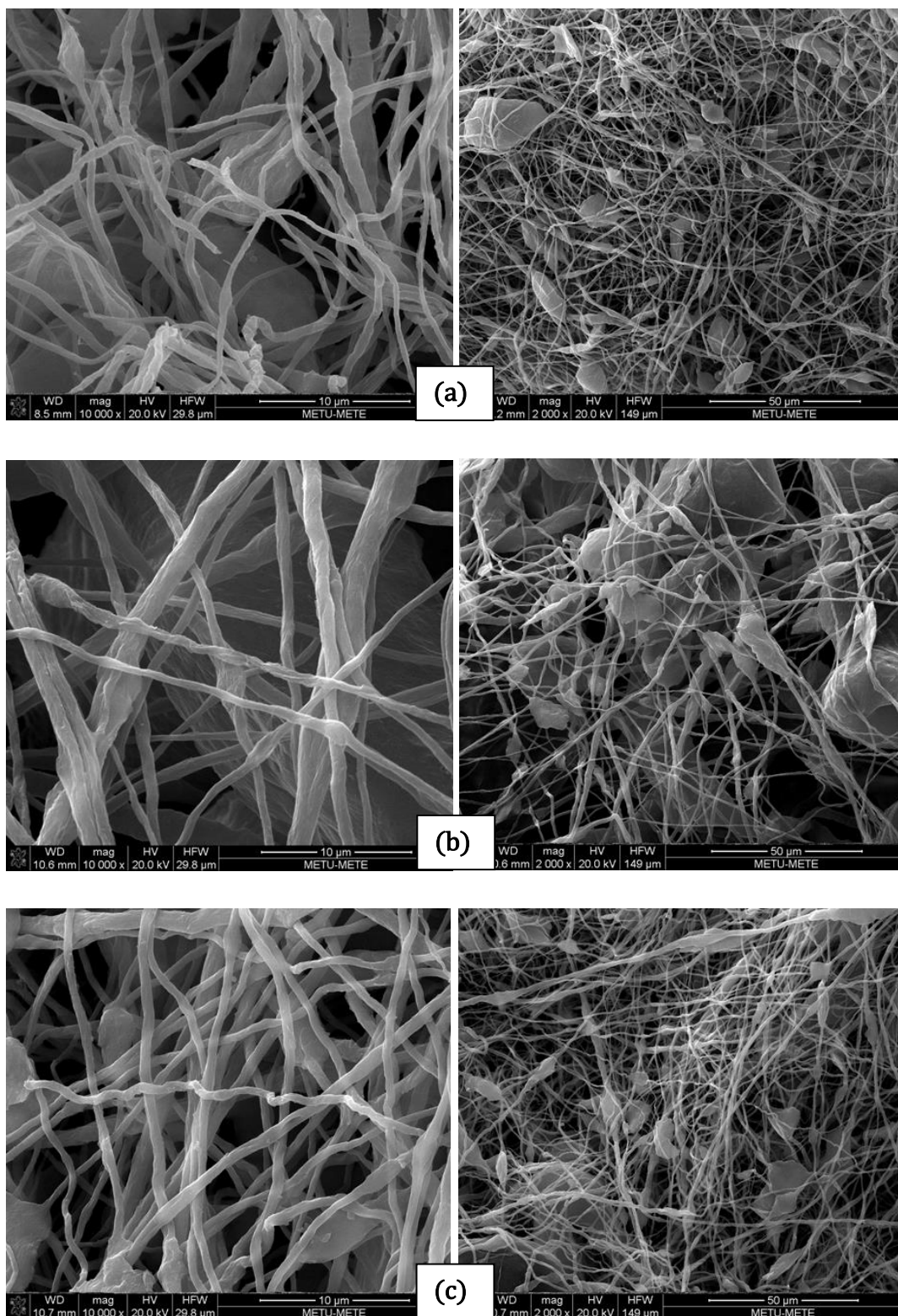


Figure 50. SEM images of electrospun BC/PULL (50/50 w/w %) scaffolds with (a) 10, (b) 12, and (c) 14 % of polymer concentrations. Scale bars: 10 μm (left) and 50 μm (right).

## CHAPTER 4

### CONCLUSION

Electrospinning is a simple and applicable method produce fibrous and porous meshes mimicking the natural ECMs of tissues. Cellulose acetate (CA), bacterial cellulose (BC), pullulan (PULL), and gelatin (GEL) were electrospun in various combinations to satisfy the needs of the tissue construct. CA based scaffolds in combination with PULL were produced successfully. CA/PULL solutions with 80/20, 50/50, and 20/80 (w/w)% contents in DMAc/DMSO 55/45 (v/v) solvent systems with 20 wt% polymer concentration were electrospun for the first time in literature to produce scaffolds. Both conventional and wet electrospinning techniques were performed with altered designs. Porous structures with adjustable 2D and 3D architectures were achieved to be produced for tissue engineering applications. Two modifications namely cross-linking and sacrificial fiber removal were performed to improve the mechanical properties of CA/PULL scaffolds. SEM images indicated that fibers became straighter and scaffolds became much 2-dimensional with increased CA contents. Hence, PULL was determined as a component leading to 3-dimensionality. To increase PULL content more than 20% in the CA/PULL scaffolds and thus produce 3D scaffolds much easily with higher flow rates, conventional electrospinning method was changed with wet electrospinning. The dominant use of CA or PULL influences the fiber diameter size oppositely. Fiber diameter thickness increased with an increased PULL content. However, codominance of CA and PULL resulted in the thickest fibers. This surprising finding has been associated with the unique attachment between PULL and cellulosic materials seen in nature. SEM images also indicated that cross-linked scaffolds had fused fibers in PULL-dominant

scaffolds. Increased PULL content within the CA/PULL scaffolds caused fast degradation (from 13.94% to ~100% i.e. disintegration of the scaffold) for the 1<sup>st</sup> day of incubation in PBS (0.1 M, pH 7.2). Cross-linked CA/PULL 50/50 scaffolds showed 20% mass loss after 35-day of degradation. Porosity measurements showed that porosity of CA/PULL scaffolds increased with increase in PULL content. Pore sizes were enlarged after sacrificial fiber removal. Pore diameter of CA/PULL 50/50 increased from 10-20  $\mu\text{m}$  to 50-200  $\mu\text{m}$ . Mechanical test showed that CA/PULL 80/20 scaffolds had the highest compression strength and UTS after sacrificial fiber removal. Unmodified CA/PULL 80/20 scaffolds had the highest Young's modulus (20.80 $\pm$ 1.46 MPa) against compressive forces and cross-linked CA/PULL 20/80 had the highest Young's modulus (5.38 $\pm$ 0.09 MPa) against tensile forces. Cell viability assay done with Alamar Blue Assay showed that L929 and Saos-2 cells were able to proliferate within the CA/PULL 50/50 scaffolds after sacrificial fiber removal. Confocal laser microscopy also showed that Saos-2 cells were proliferating on the cross-linked CA/PULL 50/50 scaffolds during 35 day of incubation.

In this study, BC based scaffolds were also electrospun. Firstly, BC produced by bacteria species *Glucanoacetobacter xylinum*, were modified in order to be electrospun with the addition of pullulan or/and gelatin. Acetylation, powder size reduction by mixer milling and autoclave treatments, and sulfuric acid exposure of BC were performed. However, crystalline BC was not easily processable for electrospinning due to poor solubility in the solvent systems suitable for plant origin cellulose. Future studies on development of BC/PULL/GEL based scaffolds will continue with the use of more BC degraded longer with sulfuric acid treatment.

In conclusion, CA/PULL solutions with 80/20, 50/50, and 20/80 ratios were electrospun in 2D and 3D forms for the first time. CA and BC were used for mechanical strength while PULL was used for 3-dimensionality. Crosslinking and sacrificial fiber removal were used to stabilize structures. Cell culture studies showed that CA/PULL scaffolds are suitable for skin and bone tissue engineering applications. BC/PULL 50/50 (w/w)% was electrospun for the first time. Future studies on development of BC/PULL/GEL based scaffolds will continue.

## REFERENCES

- Abbott, A. P., Bell, T. J., Handa, S., & Stoddart, B. (2005). O-Acetylation of cellulose and monosaccharides using a zinc based ionic liquid. *Green Chemistry*, 7(10), 705.
- Abed, A., Assoul, N., Ba, M., Derkaoui, S. M., Portes, P., Louedec, L., Flaud, P., Bataille, I., Letourneur, D., & Meddahi-Pellé, A. (2011). Influence of polysaccharide composition on the biocompatibility of pullulan/dextran-based hydrogels. *Journal of Biomedical Materials Research. Part A*, 96(3), 535–42.
- Alonso, L., & Fuchs, E. (2003). Stem cells in the skin: waste not, Wnt not. *Genes & Development*, 17(10), 1189–200.
- Asma, C., Meriem, E., Mahmoud, B., & Djafer, B. (2014). Physicochemical characterization of gelatin-CMC composite edibles films from polyion-complex hydrogels. *Journal of the Chilean Chemical Society*, 59(1), 2279–83.
- Aubin, J. E., & Triffitt, J. T. (2002). Mesenchymal stem cells and osteoblast differentiation. In: J. P. Bilezikian, L. G. Raisz, & G. A. Rodan (Eds.), *Principles of Bone Biology*, 2<sup>nd</sup> edn.; San Diego: Academic Press; p 59–81.
- Bačáková, L., Novotná, K., & Pařízek, M. (2014). Polysaccharides as cell carriers for tissue engineering: the use of cellulose in vascular wall reconstruction. *Physiological Research / Academia Scientiarum Bohemoslovaca*, 63 Suppl 1, 29–47.
- Baker, B. M., Gee, A. O., Metter, R. B., Nathan, A. S., Marklein, R. A., Burdick, J. A., & Mauck, R. L. (2008). The potential to improve cell infiltration in composite fiber-aligned electrospun scaffolds by the selective removal of sacrificial fibers. *Biomaterials*, 29(15), 2348–58.

- Balmayor, E. R., Baran, E. T., Azevedo, H. S., & Reis, R. L., (2012). Injectable biodegradable starch/chitosan delivery system for the sustained release of gentamicin to treat bone infections. *Carbohydrate Polymers*, 87(1), 32-9.
- Basar, B., Tezcaner, A., Keskin, D., & Evis, Z. (2010). Improvements in microstructural, mechanical, and biocompatibility properties of nano-sized hydroxyapatites doped with yttrium and fluoride. *Ceramics International*, 36(5), 1633–43.
- Bhardwaj, N., & Kundu, S. C. (2011). Silk fibroin protein and chitosan polyelectrolyte complex porous scaffolds for tissue engineering applications. *Carbohydrate Polymers*, 85(2), 325–333.
- Blackwood, K., McKean, R., Canton, I., Freeman, C., Franklin, K., Cole, A., Brook, I., Farthing, P., Rimmer, S., Haycock, J., Ryan, A., & MacNeil, S. (2008). Development of biodegradable electrospun scaffolds for dermal replacement. *Biomaterials*, 29, 3091-3104.
- Bognitzki, M., Czado, W., Frese, T., Schaper, A., Hellwig, M., Steinhart, M., Greiner, A., & Wendorff, J. H. (2001). Nanostructured Fibers via Electrospinning. *Advanced Materials*, 13(1), 70–2.
- Boland, E. D., Wnek, G. E., Simpson, D. G., Pawlowski, K. J., & Bowlin, G. L. (2007). Tailoring tissue engineering scaffolds using electrostatic processing techniques: A study of poly (glycolic acid) electrospinning, *Journal of Macromolecular Science, Part A: Pure and Applied Chemistry*, 38, 1231–43.
- Böttcher-Haberzeth, S., Biedermann, T., & Reichmann, E. (2010). Tissue engineering of skin. *Burns: Journal of the International Society for Burn Injuries*, 36(4), 450–60.
- Buehler, M. J. (2008). Nanomechanics of collagen fibrils under varying cross-link densities: atomistic and continuum studies. *Journal of the Mechanical Behavior of Biomedical Materials*, 1(1), 59–67.

- Burg, K. J., Porter, S., & Kellam, J. F. (2000). Biomaterial developments for bone tissue engineering. *Biomaterials*, *21*(23), 2347-59.
- Callegari, G., Tyomkin, I., Kornev, K. G., Neimark, A. V., & Hsieh, Y. (2011). Absorption and transport properties of ultra-fine cellulose webs. *Journal of Colloid and Interface Science*, *353*(1), 290–293.
- Canton, I., McKean, R., Charnley, M., Blackwood, K., Fiorica, C., Ryan, A., & MacNeil, S. (2010). Development of an Ibuprofen-releasing biodegradable PLA/PGA electrospun scaffold for tissue regeneration. *Biotechnology and Bioengineering*, *105*, 396-408.
- Chan, G., & Mooney, D. J. (2008). New materials for tissue engineering: towards greater control over the biological response. *Trends in Biotechnology*, *26*(7), 382-92.
- Chen, L., Bromberg, L., Hatton, T. A., & Rutledge, G. C. (2008). Electrospun cellulose acetate fibers containing chlorhexidine as a bactericide. *Polymer*, *49*(5), 1266–75.
- Chen, Y. M. (2009). In vitro cytotoxicity of bacterial cellulose scaffolds used for tissue-engineered bone. *Journal of Bioactive and Compatible Polymers*, *24*(1 Suppl), 137-45.
- Cheng, K.-C., Demirci, A., & Catchmark, J. M. (2010). Effects of plastic composite support and pH profiles on pullulan production in a biofilm reactor. *Applied Microbiology and Biotechnology*, *86*(3), 853–61.
- Choktaweessap, N., Arayanarakul, K., Aht-ong, D., Meechaisue, C., & Supaphol, P. (2007). Electrospun gelatin fibers: Effect of solvent system on morphology and fiber diameters. *Polymer Journal*, *39*(6), 622-31.
- Chung, C., Lee, M., & Choe, E. (2004). Characterization of cotton fabric scouring by FT-IR ATR spectroscopy. *Carbohydrate Polymers*, *58*(4), 417–20.

- Cooper, A., Bhattarai, N., & Zhang, M. (2011). Fabrication and cellular compatibility of aligned chitosan–PCL fibers for nerve tissue regeneration. *Carbohydrate Polymers*, 85(1), 149–56.
- Costa-Júnior, E. S., Barbosa-Stancioli, E. F., Mansur, A. A. P., Vasconcelos, W. L., & Mansur, H. S. (2009). Preparation and characterization of chitosan/poly(vinyl alcohol) chemically crosslinked blends for biomedical applications. *Carbohydrate Polymers*, 76, 472–81.
- Coxon, J. P., Oades, G. M., Colston, K. W., & Kirby, R. S. (2004). Advances in the use of bisphosphonates in the prostate cancer setting. *Prostate Cancer and Prostatic Diseases*, 7(2), 99–104.
- Dawson, E., Mapili, G., Erickson, K., Taqvi, S., & Roy, K. (2008). Biomaterials for stem cell differentiation. *Advanced Drug Delivery Reviews*, 60(2), 215–228.
- Dammaschke, T., Gerth, H. U. V., Züchner, H., & Schäfer, E. (2005). Chemical and physical surface and bulk material characterization of white ProRoot MTA and two Portland cements. *Dental Materials : Official Publication of the Academy of Dental Materials*, 21(8), 731–8.
- Dulong, V., Forbice, R., Condamine, E., Le Cerf, D., & Picton, L. (2011). Pullulan–STMP hydrogels: a way to correlate crosslinking mechanism, structure and physicochemical properties. *Polymer Bulletin*, 67, 455–66.
- Ekholm, E., Tommila, M., Forsback, A.-P., Märtson, M., Holmbom, J., Aäritalo, V., Finnberg, C., Kuusilehto, A., Salonen, J., Yli-Urpo, A., & Penttinen, R. (2005). Hydroxyapatite coating of cellulose sponge does not improve its osteogenic potency in rat bone. *Acta Biomaterialia*, 1(5), 535–44.
- Engel, E., Michiardi, A., Navarro, M., Lacroix, D., & Planell, J. A. (2008). Nanotechnology in regenerative medicine: The materials side. *Trends in Biotechnology*, 26(1), 39–47.

- Fang, B., Wan, Y., Tang, T., Gao, C., & Dai, K. (2009). Proliferation and osteoblastic differentiation of human bone marrow stromal cells on hydroxyapatite/bacterial cellulose nanocomposite scaffolds, *Tissue Engineering Part A*, 15(5), 1091–8.
- Fatimi, A., Axelos, M. A. V., Tassin, J. F., & Weiss, P. (2008). Rheological characterization of self-hardening hydrogel for tissue engineering applications: Gel point determination and viscoelastic properties. *Macromolecular Symposia*, 266(1), 12–6.
- Fricain, J. C., Schlaubitz, S., Le Visage, C., Arnault, I., Derkaoui, S. M., Siadous, R., Catros, S., et al. (2013). A nano-hydroxyapatite--pullulan/dextran polysaccharide composite macroporous material for bone tissue engineering. *Biomaterials*, 34(12), 2947–59.
- Glaesemann, B. P., Whittington, A. R., Aning, A. O., & Corcoran, S. G. (2011). Ovalbumin-based scaffolds reinforced with cellulose nanocrystals for bone tissue engineering, Thesis, Virginia Tech, Blacksburg, VA.
- Gómez-Mascaraque, L. G., Méndez, J. A., Fernández-Gutiérrez, M., Vázquez, B., & San Román, J. (2014). Oxidized dextrans as alternative crosslinking agents for polysaccharides: Application to hydrogels of agarose-chitosan. *Acta Biomaterialia*, 10(2), 798–811.
- Gouma, P., Xue, R., Goldbeck, C. P., Perrotta, P., & Balázs, C. (2012). Nano-hydroxyapatite—Cellulose acetate composites for growing of bone cells. *Materials Science and Engineering: C*, 32(3), 607–612.
- Griffith, L. G., & Naughton, G. (2002). Tissue engineering--current challenges and expanding opportunities. *Science (New York, N.Y.)*, 295(5557), 1009–14.
- Groeber, F., Holeiter, M., Hampel, M., Hinderer, S., & Schenke-Layland, K. (2011). Skin tissue engineering--in vivo and in vitro applications. *Advanced Drug Delivery Reviews*, 63(4-5), 352–66.

- Gulrez, S. K. H., Al-assaf, S., & Phillips, G. O (2011). *Hydrogels: Methods of Preparation, Characterisation and Applications*. In: Angelo Carpi (Ed.), *Progress in Molecular and Environmental Bioengineering - From Analysis and Modeling to Technology Applications*, Croatia: In Tech; p 117-50.
- Gunter, G. C., Craciun, R., Tam, M. S., Jackson, J. E., & Miller, D. J. (1996). FTIR and <sup>31</sup>P-NMR spectroscopic analyses of surface species in phosphate-catalyzed lactic acid conversion. *Journal of Catalysis*, *164*, 207–19.
- Helenius, G., Bäckdahl, H., Bodin, A., Nannmark, U., Gatenholm, P., & Risberg, B. (2006). In vivo biocompatibility of bacterial cellulose. *Journal of Biomedical Materials Research. Part A*, *76*(2), 431–8.
- Hermanson, G. T., (1997). *Bioconjugate techniques*. San Diego: Academic Press, (General Pharmacology: The Vascular System).pp
- Holzwarth, J. M., & Ma, P. X. (2011). Biomimetic nanofibrous scaffolds for bone tissue engineering. *Biomaterials*, *32*(36), 9622–9.
- Horner, E. A., Kirkham, J., Wood, D., Curran, S., Smith, M., Thomson, B., & Yang, X. B. (2010). Long bone defect models for tissue engineering applications: criteria for choice. *Tissue Engineering. Part B, Reviews*, *16*(2), 263–71.
- Höglund, A., Målberg, S., & Albertsson, A.-C. (2012). Assessing the degradation profile of functional aliphatic polyesters with precise control of the degradation products. *Macromolecular Bioscience*, *12*(2), 260–8.
- Hutmacher, D. W. (2000). Scaffolds in tissue engineering bone and cartilage. *Biomaterials*, *21*(24), 2529–43.
- Hu, W., Chen, S., Xu, Q., & Wang, H. (2011). Solvent-free acetylation of bacterial cellulose under moderate conditions. *Carbohydrate Polymers*, *83*, 1575–81.
- Ikada, Y., & Tsuji, H. (2000). Biodegradable polyesters for medical and ecological applications. *Macromolecular Rapid Communications*, *21*(3), 117–132.

- Izadifar, Z., Chen, X., & Kulyk, W. (2012). Strategic design and fabrication of engineered scaffolds for articular cartilage repair. *Journal of Functional Biomaterials*, 3(4), 799–838.
- Jang, J.-H., Castano, O., & Kim, H.-W. (2009). Electrospun materials as potential platforms for bone tissue engineering. *Advanced Drug Delivery Reviews*, 61(12), 1065–83.
- Jhon, M. J., & Thomas, S. (2008). Biofibres and biocomposites. *Carbohydrate Polymers*, 71(3), 343-364.
- Jia, S. F., Worth, L. L., & Kleinerman, E. S. (1999). A nude mouse model of human osteosarcoma lung metastases for evaluating new therapeutic strategies. *Clinical & Experimental Metastasis*, 17(6), 501–6.
- Jiang, X., Nai, M. H., Lim, C. T., Le Visage, C., Chan, J. K. Y., & Chew, S. Y. (2014). Polysaccharide nanofibers with variable compliance for directing cell fate. *Journal of Biomedical Materials Research. Part A*, 1, 1–10.
- Jonoobi, M., Harun, J., Mathew, A. P., Hussein, M. Z. B., & Oksman, K. (2009). Preparation of cellulose nanofibers with hydrophobic surface characteristics. *Cellulose*, 17(2), 299–307.
- Jones, A. C., Milthorpe, B., Averdunk, H., Limaye, A., Senden, T. J., Sakellariou, A., Sheppard, A. P., Sok, R. M., Knackstedt, M. A., Brandwood, A., Rohner, D., & Huttmacher, D. W. (2004). Analysis of 3D bone ingrowth into polymer scaffolds via micro-computed tomography imaging. *Biomaterials*, 25(20), 4947–54.
- Jose, M.V, Thomas, V., Johnson, K.T., Dean, D.R.,& Nyairo, E. (2009). Aligned PLGA/HA nanofibrous nanocomposite scaffolds for bone tissue engineering. *Acta Biomaterialia*, 5(1), 305–15.
- Karakecili, A. G., Demirtas, T. T., Satriano, C., Gümüsderelioglu, M., & Marletta, G. (2007). Evaluation of L929 fibroblast attachment and proliferation on Arg-Gly-

- Asp-Ser (RGDS)-immobilized chitosan in serum-containing/serum-free cultures. *Journal of Bioscience and Bioengineering*, 104(1), 69–77.
- Karp, J. M., Dalton, P. D., Shoichet, M. S., & Cahn, F. (2003). Scaffolds for Tissue Engineering. *MRS Bulletin*, (April), 301–6.
- Kerschnitzki, M., Wagermaier, W., Roschger, P., Seto, J., Shahar, R., Duda, G. N., Mundlos S., & Fratzl, P. (2011). The organization of the osteocyte network mirrors the extracellular matrix orientation in bone. *Journal of Structural Biology*, 173(2), 303–11.
- Kim, D., Nishiyama, Y., & Kuga, S. (2002). Surface acetylation of bacterial cellulose, *Cellulose*, 9, 361–7.
- Konwarh, R., Karak, N., & Misra, M. (2013). Electrospun cellulose acetate nanofibers: the present status and gamut of biotechnological applications. *Biotechnology Advances*, 31(4), 421–37.
- Lalande, C., Miraux, S., Derkaoui, S. M., Mornet, S., Bareille, R., Fricain, J. C., Franconi, J. M., et al. (2011). Magnetic resonance imaging tracking of human adipose derived stromal cells within three-dimensional scaffolds for bone tissue engineering. *European Cells & Materials*, 21, 341–54.
- Leathers, T. D. (2003). Biotechnological production and applications of pullulan. *Applied Microbiology and Biotechnology*, 62, 468–73.
- Lee, K. H., Kim, H. Y., Khil, M. S., Ra, Y. M., & Lee, D. R. (2003). Characterization of nanostructured poly(1-caprolactone) nonwoven mats via electrospinning. *Polymer*, 44, 1287-94.
- Lee, S. J., & Atala, A. (2013). Scaffold technologies for controlling cell behavior in tissue engineering. *Biomedical Materials (Bristol, England)*, 8(1), 010201.
- Li, D., Wang, Y., & Xia, Y. (2003). Electrospinning of Polymeric and Ceramic Nanofibers as Uniaxially Aligned Arrays. *Nano Letters*, 3(8), 1167–71.

- Li, J., Connell, S., & Shi, R. (2009). *Biomimetic Architectures for Tissue Engineering*. In: Amitava Mukherjee (Ed.), *Biomimetics, Learning from Nature*, Croatia: In Tech; p 487–507.
- Li, M. G., Tian, X. Y., & Chen, X. B. (2009). A brief review of dispensing-based rapid prototyping techniques in tissue scaffold fabrication: role of modeling on scaffold properties prediction. *Biofabrication*, *1*(3), 1-10.
- Li, W.-J., Laurencin, C. T., Caterson, E. J., Tuan, R. S., & Ko, F. K. (2002). Electrospun nanofibrous structure: a novel scaffold for tissue engineering. *Journal of Biomedical Materials Research*, *60*(4), 613–21.
- Liu, L., He, D., Wang, G., & Yu, S. (2011). Bioinspired crystallization of CaCO<sub>3</sub> coatings on electrospun cellulose acetate fiber scaffolds and corresponding CaCO<sub>3</sub> microtube networks, *Langmuir*, *27*(11), 199–7206.
- Liu, P., Deng, Z., Han, S., Liu, T., Wen, N., Lu, W., Geng, X., Huang, S., & Jin, Y. (2008). Tissue-engineered skin containing mesenchymal stem cells improves burn wounds. *Artificial Organs*, *32*(12), 925–31.
- Liu, Y., He, J.-huan, Yu, J.-yong, & Zeng, H.-mei. (2008). Controlling numbers and sizes of beads in electrospun nanofibers. *Polymer International*, *636* (August 2007), 632-6.
- Loss, M., Wedler, V., Ku, W., & Meyer, V. E. (2000). Artificial skin, split-thickness autograft and cultured autologous keratinocytes combined to treat a severe burn injury of 93 % of TBSA, *Burns*, *26*(7), 644-52.
- Machado, C. B., Ventura, J. M. G., Lemos, a F., Ferreira, J. M. F., Leite, M. F., & Goes, a M. (2007). 3D chitosan-gelatin-chondroitin porous scaffold improves osteogenic differentiation of mesenchymal stem cells. *Biomedical Materials (Bristol, England)*, *2*(2), 124–31.
- MacNeil, S. (2007). Progress and opportunities for tissue-engineered skin. *Nature*, *445*(7130), 874–80.

- Malmström, E., & Carlmark, A. (2012). Controlled grafting of cellulose fibres – an outlook beyond paper and cardboard. *Polymer Chemistry*, 3(7), 1702-13.
- Mano, J. F., Silva, G. A., Azevedo, H. S., Malafaya, P. B., Sousa, R. A., Silva, S. S., Boesel, L. F., Oliveira, J. M., Santos, T. C., Marques, A. P., Neves, N. M., & Reis, R. L. (2007). Natural origin biodegradable systems in tissue engineering and regenerative medicine: present status and some moving trends. *Journal of the Royal Society, Interface / the Royal Society*, 4(17), 999–1030.
- Mandal, B. B., & Kundu, S. C. (2009). Cell proliferation and migration in silk fibroin 3D scaffolds. *Biomaterials*, 30(15), 2956–65.
- Märtson, M., Viljanto, J., Hurme, T., Laippala, P., & Saukko, P. (1999). Is cellulose sponge degradable or stable as implantation material? An in vivo subcutaneous study in the rat. *Biomaterials*, 20(21), 1989–95.
- Martínez-Sanz, M., Olsson, R. T., Lopez-Rubio, A., & Lagaron, J. M. (2010). Development of electrospun EVOH fibres reinforced with bacterial cellulose nanowhiskers. Part I: Characterization and method optimization. *Cellulose*, 18(2), 335–47.
- Megelski, S., Stephens, J. S., Chase, D. B., & Rabolt, J. F. (2002). Micro- and nanostructured surface morphology on electrospun polymer fibers. *Macromolecules*, 35(22), 8456–66.
- Melchels, F. P. W., Bertoldi, K., Gabbrielli, R., Velders, A. H., Feijen, J., & Grijpma, D. W. (2010). Mathematically defined tissue engineering scaffold architectures prepared by stereolithography. *Biomaterials*, 31(27), 6909–16.
- Metcalfe, A. D., & Ferguson, M. W. J. (2007). Tissue engineering of replacement skin: the crossroads of biomaterials, wound healing, embryonic development, stem cells and regeneration. *Journal of the Royal Society, Interface / the Royal Society*, 4(14), 413–37.

- Miao, J., Pangulea, R.C., Paskalevaa, E.E., Hwangh, E.E., Kanea, R.S., Linhardta, R.J., & Dordicka, J.S., (2011). Lysostaphin-functionalized cellulose fibers with antistaphylococcal activity for wound healing applications. *Biomaterials*, 32(36), 9557-67.
- Migneault, I., Dartiguenave, C., Bertrand, M. J., & Waldron, K. C. (2004). Glutaraldehyde: behavior in aqueous solution, reaction with proteins, and application to enzyme crosslinking. *BioTechniques*, 37(5), 790–6, 798–802.
- Mishra, B., Vuppu, S., & Rath, K. (2011). The role of microbial pullulan, a biopolymer in pharmaceutical approaches: A review, *Journal of Applied Pharmaceutical Sciences*, 01(06), 45-50.
- Murakami, M., Kaneko, Y., & Kadokawa, J. (2007). Preparation of cellulose-polymerized ionic liquid composite by in-situ polymerization of polymerizable ionic liquid in cellulose-dissolving solution. *Carbohydrate Polymers*, 69(2), 378–381.
- Müller, F. A., Müller, L., Hofmann, I., Greil, P., Wenzel, M. M., & Staudenmaier, R. (2006). Cellulose-based scaffold materials for cartilage tissue engineering. *Biomaterials*, 27(21), 3955–63.
- Mullender, M.G., van der Meer, D.D., Huiskes, R., & Lips, P., (1996). Osteocyte density changes in aging and osteoporosis. *Bone*, 18(2), 109-13.
- Nguyen, H., Ostendorf, A. P., Satz, J. S., Westra, S., Ross-Barta, S. E., Campbell, K. P., & Moore, S. A. (2013). Glial scaffold required for cerebellar granule cell migration is dependent on dystroglycan function as a receptor for basement membrane proteins. *Acta Neuropathologica Communications*, 1(1), 58.
- O'Brien, F. J., Harley, B. A, Yannas, I. V, & Gibson, L. J. (2005). The effect of pore size on cell adhesion in collagen-GAG scaffolds. *Biomaterials*, 26(4), 433–41.

- O'Brien, J., Wilson, I., Orton, T., & Pognan, F. (2000). Investigation of the Alamar Blue (resazurin) fluorescent dye for the assessment of mammalian cell cytotoxicity. *European Journal of Biochemistry / FEBS*, 267(17), 5421–6.
- Ohkawa, K., Hayashi, S., Nishida, A., Yamamoto, H., & Ducreux, J. (2009). Preparation of pure cellulose nanofiber via electrospinning. *Textile Research Journal*, 79(15), 1396-401.
- Olszta, M. J., Cheng, X., Jee, S. S., Kumar, R., Kim, Y.-Y., Kaufman, M. J., Douglas, E. P., & Gower, L. B. (2007). Bone structure and formation: A new perspective. *Materials Science and Engineering: R: Reports*, 58(3-5), 77-116.
- Oshima, T., Taguchi, S., Ohe, K., & Baba, Y. (2011). Phosphorylated bacterial cellulose for adsorption of proteins. *Carbohydrate Polymers*, 83(2), 953–58.
- Park, W.-I., Kang, M., Kim, H.-S., & Jin, H.-J. (2007). Electrospinning of Poly(ethylene oxide) with Bacterial Cellulose Whiskers. *Macromolecular Symposia*, 249-250(1), 289–94.
- Palmer, L. C., Newcomb, C. J., Kaltz, S. R., Spoerke, E. D., & Stupp, S. I. (2008). Biomimetic systems for hydroxyapatite mineralization inspired by bone and enamel. *Chemical Reviews*, 108(11), 4754–83.
- Petersson, U., Somogyi, E., Reinholt, F. P., Karlsson, T., Sugars, R. V., & Wendel, M. (2004). Nucleobindin is produced by bone cells and secreted into the osteoid, with a potential role as a modulator of matrix maturation. *Bone*, 34(6), 949–60.
- Pham, Q. P., Sharma, U., & Mikos, A. G. (2006). Electrospinning of polymeric nanofibers for tissue engineering applications: A review. *Tissue Engineering*, 12(5), 1197–211.
- Priya, S. G., Jungvid, H., & Kumar, A. (2008). Skin tissue engineering for tissue repair and regeneration. *Tissue Engineering. Part B, Reviews*, 14(1), 105–18.

- Puls, J., Wilson, S. A., & Hölder, D. (2010). Degradation of Cellulose Acetate-Based Materials: A Review. *Journal of Polymers and the Environment*, 19(1), 152–65.
- Rezwan, K., Chen, Q. Z., Blaker, J. J., & Boccaccini, A. R. (2006). Biodegradable and bioactive porous polymer/inorganic composite scaffolds for bone tissue engineering. *Biomaterials*, 27(18), 3413–31.
- Rambo, C. R., Recouvreux, D. O. S., Carminatti, C. A., Pitlovanciv, A. K., Antônio, R. V., & Porto, L. M. (2008). Template assisted synthesis of porous nanofibrous cellulose membranes for tissue engineering. *Materials Science and Engineering: C*, 28(4), 549–54.
- Rekha, M. R., & Sharma, C. P. (2007). Pullulan as a Promising Biomaterial for Biomedical Applications : A Perspective, *Trends in Biomaterials and Artificial Organs*, 20(2), 116-21.
- Reneker, D. H., & Yarin, A. L. (2008). Electrospinning jets and polymer nanofibers. *Polymer*, 49(10), 2387–425.
- Rodan (Eds.), *Principles of bone biology*, 2nd edn.; San Diego: Academic Press; p 59–81.
- Rosen, C. J., Compston, J. E., & Lian, J. B. (2009). *Primer on the Metabolic Bone Diseases and Disorders of Mineral Metabolism*. (7<sup>th</sup> ed.). Washington: The Sheridan Press, (Section1).
- Sell, S. A, Francis, M. P., Garg, K., McClure, M. J., Simpson, D. G., & Bowlin, G. L. (2008). Cross-linking methods of electrospun fibrinogen scaffolds for tissue engineering applications. *Biomedical Materials*, 3(4), 045001.
- Sachlos, E., & Czernuszka, J. T. (2003). Making tissue engineering scaffolds work. Review: the application of solid freeform fabrication technology to the production of tissue engineering scaffolds. *European Cells & Materials*, 5, 29–39; discussion 39–40.

- Sahoo, S. K., Parveen, S., & Panda, J. J. (2007). The present and future of nanotechnology in human health care. *Nanomedicine: Nanotechnology, Biology, and Medicine*, 3(1), 20–31.
- Sakai, R., John, B., Okamoto, M., Seppälä, J. V., Vaithilingam, J., Hussein, H., & Goodridge, R. (2013). Fabrication of Polylactide-Based Biodegradable Thermoset Scaffolds for Tissue Engineering Applications. *Macromolecular Materials and Engineering*, 298(1), 45–52.
- Salgado, A. J., Coutinho, O. P., Reis, R. L., & Davies, J. E. (2006). In vivo response to starch-based scaffolds designed for bone tissue engineering applications. *Journal of Biomedical Materials Research Part A*, 80(4), 983–9.
- Samios, E., Dart, R. K., & Dawkins, J. V. (1997). Preparation, characterization and biodegradation studies on cellulose acetates with varying degrees of substitution. *Polymer*, 38(12), 3045–54.
- Scatena, L. F., Brown, M. G., & Richmond, G. L. (2001). Water at hydrophobic surfaces: Weak hydrogen bonding and strong orientation effects. *Science (New York, N.Y.)*, 292, 908–12.
- Shekaran, A., & García, A. J. (2011). Extracellular matrix-mimetic adhesive biomaterials for bone repair. *Journal of Biomedical Materials Research. Part A*, 96(1), 261–72.
- Sill, T. J., & von Recum, H. A. (2008). Electrospinning: applications in drug delivery and tissue engineering. *Biomaterials*, 29(13), 1989–2006.
- Silva, A., Silva-Freitas, É., Carvalho, J., Pontes, T., Araújo-Neto, R., Silva, K., Carriço, A., & Egito, E. (2012). *Magnetic Particles in Biotechnology: From Drug Targeting to Tissue Engineering*. In: Marian Petre (Ed.), *Advances in Applied Biotechnology*, Croatia: In Tech; p 237-56.
- Singh, R. S., Saini, G. K., & Kennedy, J. F. (2008). Pullulan: Microbial sources, production and applications. *Carbohydrate Polymers*, 73(4), 515–31.

- Sirvio, J., Hyvakko, U., Liimatainen, H., Niinimäki, J., & Hormi, O. (2011). Periodate oxidation of cellulose at elevated temperatures using metal salts as cellulose activators. *Carbohydrate Polymers*, 83(3), 1293–7.
- Sombatmankhong, K., Sanchavanakit, N., Pavasant, P., & Supaphol, P. (2007). Bone scaffolds from electrospun fiber mats of poly(3-hydroxybutyrate), poly(3-hydroxybutyrate-co-3-hydroxyvalerate) and their blend. *Polymer*, 48, 1419–27.
- Spector, Myron, and Fu-Zhai Cui. HST.535 Principles and Practice of Tissue Engineering, Fall 2004. (MIT OpenCourseWare: Massachusetts Institute of Technology), <http://ocw.mit.edu/courses/health-sciences-and-technology/hst-535-principles-and-practice-of-tissue-engineering-fall-2004> (Accessed 12 Jun, 2014). License: Creative Commons BY-NC-SA.
- Stevens, M. M. (2008). Biomaterials for bone tissue engineering, *Materials Today*, 11(5), 18-25.
- Stijnman, A. C., Bodnar, I., & Hans Tromp, R. (2011). Electrospinning of food-grade polysaccharides. *Food Hydrocolloids*, 25(5), 1393–398.
- Subbiah, T., Bhat, G. S., Tock, R. W., Parameswaran, S., & Ramkumar, S. S. (2005). Electrospinning of nanofibers. *Journal of Applied Polymer Science*, 96(2), 557-69.
- Svensson, A., Nicklasson, E., Harrah, T., Panilaitis, B., Kaplan, D. L., Brittberg, M., & Gatenholm, P. (2005). Bacterial cellulose as a potential scaffold for tissue engineering of cartilage. *Biomaterials*, 26(4), 419-31.
- Swetha, M., Sahithi, K., Moorthi, A., Srinivasan, N., Ramasamy, K., & Selvamurugan, N. (2010). Biocomposites containing natural polymers and hydroxyapatite for bone tissue engineering. *International Journal of Biological Macromolecules*, 47(1), 1–4.
- Toker, S. M., Tezcaner, A., & Evis, Z., (2011). Microstructure, microhardness, and biocompatibility characteristics of yttrium hydroxyapatite doped with fluoride,

*Journal of Biomedical Materials Research B: Applied Biomaterials*, 9(2), 207-17.

Tungprapa, S., Puangparn, T., Weerasombut, M., Jangchud, I., Fakum, P., Semongkhon, S., Meechaisue, C., & Supaphol, P. (2007). Electrospun cellulose acetate fibers: effect of solvent system on morphology and fiber diameter. *Cellulose*, 14(6), 563–575.

Tuzlakoglu, K., Bolgen, N., Salgado, a J., Gomes, M. E., Piskin, E., & Reis, R. L. (2005). Nano- and micro-fiber combined scaffolds: A new architecture for bone tissue engineering. *Journal of Materials Science. Materials in Medicine*, 16(12), 1099-104.

Wan, Y., Hong, L., Jia, S., Huang, Y., Zhu, Y., Wang, Y., & Jiang, H. (2006). Synthesis and characterization of hydroxyapatite–bacterial cellulose nanocomposites. *Composites Science and Technology*, 66(11-12), 1825–832.

Wan, Y. Z., Huang, Y., Yuan, C. D., Raman, S., Zhu, Y., Jiang, H. J., He, F., & Gao, C. (2007). Biomimetic synthesis of hydroxyapatite/bacterial cellulose nanocomposites for biomedical applications. *Materials Science and Engineering*, 27(4), 855-64.

Wei, G., & Ma, P. X. (2004). Structure and properties of nano-hydroxyapatite/polymer composite scaffolds for bone tissue engineering. *Biomaterials*, 25(19), 4749–57.

Wittaya-areekul, S., & Prahsarn, C. (2006). Development and in vitro evaluation of chitosanpolysaccharides composite wound dressings. *International Journal of Pharmaceutics*, 313, 123–8.

Wong, V. W., Rustad, K. C., Galvez, M. G., Neofytou, E., Glotzbach, J. P., Januszyk, M., Major, M. R., Sorkin, M., Longaker, M. T., Rajadas, J., & Gurtner, G. C. (2011). Engineered pullulan – collagen compositedermal hydrogels improve early cutaneous wound healing, *Tissue Engineering. Part A*, 17(5-6), 631-44.

- Wu, J., Zhang, J., Zhang, H., He, J., Ren, Q., & Guo, M. (2004). Homogeneous acetylation of cellulose in a new ionic liquid. *Biomacromolecules*, 5(2), 266–8.
- Xu, X., Zhou, J., Jiang, L., Lubineau, G., Chen, Y., Wu, X.-F., & Piere, R. (2013). Porous core-shell carbon fibers derived from lignin and cellulose nanofibrils. *Materials Letters*, 109, 175–8.
- Yang, W., Yang, F., Wang, Y., Both, S. K., & Jansen, J. A. (2013). In vivo bone generation via the endochondral pathway on three-dimensional electrospun fibers. *Acta Biomaterialia*, 9(1), 4505–12.
- Yang, F., Murugan, R., Wang, S., & Ramakrishna, S. (2005). Electrospinning of nano/micro scale poly(L-lactic acid) aligned fibers and their potential in neural tissue engineering. *Biomaterials*, 26(15), 2603–10.
- Zhou, H., & Lee, J. (2011). Nanoscale hydroxyapatite particles for bone tissue engineering. *Acta Biomaterialia*, 7(7), 2769–81.